Investigation of Ionic and Flexible Metal-organic Frameworks and Derived Materials

A Thesis Submitted for the Degree of

MASTER OF SCIENCE

as a part of the

Integrated Ph.D Programme

(Materials Science)

By

Sohini Bhattacharyya

Chemistry and Physics of Materials Unit (CPMU)
Jawaharlal Nehru Centre for Advanced Scientific Research
(A Deemed University)
Bangalore – 560064

Dedicated

to My Parents

DECLARATION

I hereby declare that the matter embodied in the thesis entitled "***Investigation of Ionic and Flexible Metal-organic Frameworks and Derived Materials***" is the result of investigations carried out by me at the Chemistry and Physics of Materials Unit, Jawaharlal Nehru Centre for Advanced Scientific Research, India under the supervision of Prof. Tapas Kumar Maji and that it has not been submitted elsewhere for the award of any degree or diploma.

In keeping with the general practice in reporting the scientific observations, due acknowledgement has been made whenever the work described is based on the findings of other investigators. Any omission that might have occurred due to oversight or error in judgement is regretted.

Sohini Bhattacharyya

CERTIFICATE

I hereby certify that the work described in this thesis entitled "***Investigation of Ionic and Flexible Metal-organic Frameworks and Derived Materials***" has been carried out by Sohini Bhattacharyya under my supervision at the Chemistry and Physics of Materials Unit, Jawaharlal Nehru Centre for Advanced Scientific Research, India and that it has not been submitted elsewhere for the award of any degree or diploma.

Prof. Tapas Kumar Maji
CPMU, JNCASR
(Research Supervisor)

Acknowledgements

I wish to express my heartfelt gratitude to my research supervisor Prof. Tapas Kumar Maji for his constant support, guidance and encouragement. While his invaluable suggestions and ideas have always motivated me, he has always provided enough freedom to incorporate my own ideas. I am greatly indebted to him for mentoring me with infinite patience as I take my initial steps in the world of research.

Prof. C. N. R. Rao has always been a source of inspiration. Being in JNCASR gives one the wonderful privilege to observe an iconic figure like him closely, listen to his delightful motivational words and draw constant inspiration from him.

I express my sincere thanks to Prof. Balasubramanian Sundaram, the Chairman of CPMU, for allowing me to avail the facilities of the Centre and also for motivating me all through.

I am thankful to the faculty members of JNCASR for the great courses that have enriched my basic knowledge, which is valuable for going ahead in research. Particularly, I would like to thank Prof. S. Balasubramanian, Prof. M. Eswaramoorthy, Prof. N.S. Vidyadhiraja, Dr. Sridhar Rajaram, Dr. Rajesh Ganapathy, Dr. Ranjan Dutta, Prof. C. Narayana, Prof. K. S. Narayana, Prof. S. Narasimhan, Prof. A. Sundaresan, Prof. H. Ila, Prof. U. V. Waghmare, Prof. S. M. Shivaprasad, Dr. Kanishka Biswas, Prof. G. U. Kulkarni and Prof. T. K. Maji of JNCASR and Prof. Aloknath Chakraborty of IISc for their enlightening courseworks.

I am also greatly thankful to the technical staff members of JNCASR, namely, Mr. Anil, Mr. Vasu, Ms. Bhavya, Mr. Mahesh, Mr. Ala Srinivas Rao and Mr. Shivakumar for their help with instruments and measurements.

I thank JNCASR library, Comp Lab, Hostel, Dhanwantary, Academic Section and Administrative staff for providing and maintaining the great facilities of the centre, which have made my life comfortable and easy in many ways during the journey of past two and half years.

I want to convey my profound gratitude to my lab seniors Arpan, Ritesh, Suresh, Anindita, Nivedita, Syamantak, Papri and Komal, each one of whom have guided and supported me in my work in their own ways. They are a group of amazing enthusiastic people who share

a common love for their work, fun and food alike and always provide a vibrant working atmosphere full of positivity. I also want to thank my past lab member Dr. Kolleboyina Jayaramulu for his help in my work.

I want to convey my gratitude to Mrs. Supreeti Maji for the wonderful muffins, cheesecakes and the enjoyable dinners. I am also thankful to the little angels Neel and Sonai, whose unbridled energy and imagination never fail to amaze me.

I want to thank my integrated PhD batchmates for the wonderful time we have spent during the coursework and particularly during the practical classes.

No one can get by or get high without a little help from their friends! I want to express my deepest gratitude to Soumyabrata, Syamantak, Ananya, Chandradhish and Dipanwita for being my family in Bangalore and for always being there for me. I could not have survived in an unknown city without their unfailing support. I also want to thank Saurav Islam and Arka Bakshi for being such wonderful friends and my younger cousin Atreya, who has almost been my local guardian in Bangalore! I also wish to thank my closest friends Saranya, Swatilekha, Barsha, Ritwika and Abhishek, who have always been just a phone call away. I want to thank my dear old friend Broto profusely for being my pillar of strength and support and for always being with me, no matter what.

Lastly, words are insufficient to express my gratitude to my parents who are my source of strength and energy. Ma and Baba have showered me with unconditional love, taken care of my every need and endured all my tantrums and have always encouraged me to strive harder. They are the sole reason that I have been able to dream and think positively, even in the hardest of times.

Preface

This thesis comprises five chapters and elaborates on various properties and applications of different Metal-organic frameworks (MOFs).

Chapter 1 describes the characteristics of porous coordination polymers, their structure, synthesis and various applications. It further touches on the topics of post-synthetic modification, anionic MOFs and flexibility in MOFs.

Chapter 2 describes the design, synthesis and characterisation of a Mg^{II} based anionic MOF (AMOF). The guest cations present in the framework can be exchanged with different cations to get various applications and in this case its applications in selective Cu^{II} sensing and specific Eu^{III} sensitization has been upheld.

Chapter 3 deals with the dual synthesis of nanoporous carbon and graphitic carbon nitride from the AMOF described in Chapter 2. Further, the nanoporous carbon and graphitic carbon nitride thus synthesized have been characterized and their adsorption properties have been checked.

Chapter 4 describes the room temperature synthesis and characterization of two tetracarboxylate based Cu^{II} MOFs with different structural aspects. The adsorption properties of the MOFs based on their flexibility and structural properties have been characterized and analysed.

Chapter 5 contains the synthesis and characterization of a bimetallic cationic MOF with guest anions residing in its pores. The adsorption properties of this cationic MOF have been studied. Also the anion exchange and Iodine capture properties of this cationic framework have been studied.

Table of Contents

DECLARATION iii

CERTIFICATE v

Acknowledgements vii

Preface ix

Chapter 1: Introduction 1

1.1 Metal-organic Frameworks: An Introduction 3

1.1.1 Synthesis 5

1.1.2 Classification of MOFs 9

1.1.3 Applications of MOFs 10

1.2 Flexible MOFs 14

1.2.1 Breathing, swelling, linker rotation and subnetwork displacement 15

1.2.2 Photoresponsivity 15

1.2.3 Thermoresponsivity 16

1.2.4 Mechanical properties, elasticity 16

1.3 Postsynthetic Modification in MOFs 17

1.4 Anionic MOFs 18

1.5 Cationic MOFs 20

1.6 MOF Derived Carbonaceous Materials 22

1.5 References 26

Chapter 2: A bimodal Anionic MOF: Selective Cu^{II} Sensing and Specific Eu^{III} Sensitization 31

Abstract 33

2.1 Introduction 34

2.2 Experimental Section 35

2.2.1 Materials 35

2.2.2 Synthesis of $[Mg_3(ndc)_{2.5}(HCO_2)_2(H_2O)(NH_2Me_2)]\cdot 2H_2O\cdot DMF$ (1) 36

2.2.3 Preparation of M^{II}@1' and Ln^{III}@1' 36

2.2.4 Physical Measurements 36

2.2.5 Crystallography 37

2.2.6 Preparation of Sample for Adsorption 37

2.2.7 Characterization 37
2.3 Results and Discussion 39
2.3.1 Crystal Structure Description 39
2.3.2 Adsorption Properties 42
2.3.3 Cation Exchange 43
2.3.3.1 Selective Cu^{II} Sensing 44
2.3.3.2 Selective Eu^{III} Sensitization 48
2.4 Conclusion 50
2.5 References 51
Chapter 3: Two from one: Synthesis of Nanoporous Carbon and Carbon nitride Nanodots from an Anionic MOF 53
Abstract 55
3.1 Introduction 56
3.2 Experimental Section 59
3.2.1 Materials 59
3.2.2 Synthesis of $[Mg_3(ndc)_{2.5}(HCO_2)_2(H_2O)]\cdot[NH_2Me_2]\cdot 2H_2O\cdot DMF$ (1) 59
3.2.3 Carbonization of 1 59
3.2.4 Synthesis of PC_1 59
3.2.5 Synthesis of CN _1 59
3.2.6 Physical Measurements 59
3.2.7 Preparation of Sample for Adsorption 60
3.3 Results and Discussion 61
3.3.1 Morphology 61
3.3.2 PXRD analysis 63
3.3.3 XPS and Elemental analysis 63
3.3.4 IR and Raman Spectroscopy 64
3.3.5 Surface Area and Storage Properties 65
3.4 Conclusion 67
3.5 References 68
Chapter 4: Tetracarboxylate Ligand Based Flexible Cu^{II} Frameworks with Selective CO_2 Uptake and Solvent Adsorption Properties 71

Abstract 73

4.1 Introduction 74

4.2 Experimental Section 76

4.2.1 Materials 76

4.2.2 Synthesis of L1 & L2 77

4.2.3 Synthesis of 1 $\{[Cu_2(bpp)_3(L2)]\cdot(bpp)\cdot(5H_2O)\}$ 77

4.2.4 Synthesis of 2 $\{[Cu_2(L1)(H_2O)_2(bipy)_2]\cdot(bipy)\cdot(5H_2O)\}$ 78

4.2.5 Physical measurements 78

4.2.6 X-ray Crystallography 78

4.2.7 Adsorption Study 79

4.2.8 Characterization 79

4.3 Results and Discussion 82

4.3.1 Crystal Structure Description 82

4.3.2 Gas and Solvent Vapour Adsorption 87

4.4 Conclusion 90

4.5 References 91

Chapter 5: Anionic Exchange and Iodine Capture in a Cationic MOF 93

Abstract 95

5.1 Introduction 96

5.2 Experimental Section 97

5.2.1 Materials 97

5.2.2 Synthesis of 4-(1H-imidazole-1-yl)-ethyl ester (HIEE) 98

5.2.3 Synthesis of 4-(1H-imidazole-1-yl) benzoic acid (HIBA) 98

5.2.4 Synthesis of $[KCd_3(HIB)_6(H_2O)_3]\cdot(NO_3)\cdot 7H_2O$ (1) 98

5.2.5 Preparation of A^-@1' 99

5.2.6 Physical Measurements 99

5.2.7 Crystallography 99

5.2.8 Preparation of Sample for Adsorption 100

5.2.9 Characterization 100

5.3 Results and Discussion 101

5.3.1 Structural Description 101

5.3.2 Framework Stability and Adsorption properties.....105
5.3.3 Encapsulation of Anions.....106
5.3.4 I_2 Capture.....107
5.4 Conclusion.....109
5.5 References.....110
List of Publications.....113

Chapter 1

Introduction

1.1 Metal-organic Frameworks: An Introduction

In recent times, Metal-organic frameworks (MOFs) have fascinated chemists for their versatile applications as well as rational crystal structure design. Porous coordination polymers (PCPs) or MOFs are porous and polymeric infinite one, two or three dimensional networks held together by the coordination bonds between metal centres and organic ligands.[1] Porous compounds have been of interest to scientists because the creation of nanometer sized spaces give rise to many interesting applications, e.g., gas storage, separation, catalysis, sensing, etc. Traditionally, porous compounds were classified as inorganic (e.g., zeolites, aluminosilicates, etc.) and carbon based materials (**Fig. 1**).

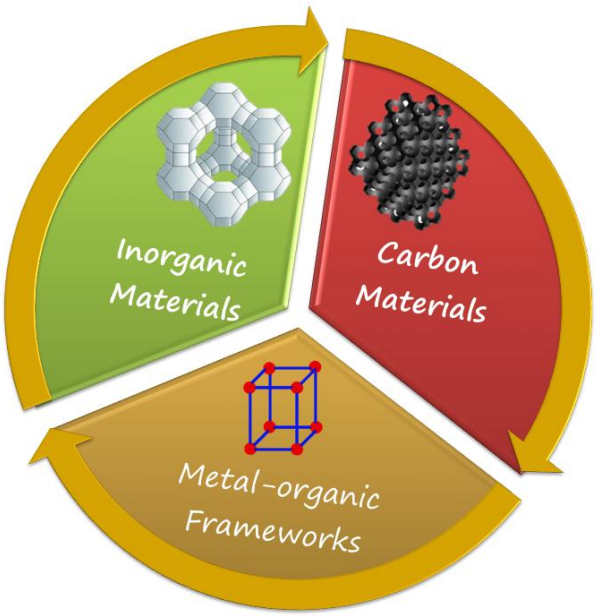

Fig. 1 Three classes of porous materials.

Zeolites are the front runners of inorganic porous materials, and have been used extensively as microporous materials for gas adsorption and ion-exchangers owing to their extra-framework cation.[2] However, zeolites are rather rigid in nature and do not allow functionalization of the pore surface and hence selective sequestration and signalling is not possible in them. Aluminosilicates,[3] aluminophosphates,[4] metalloaluminophosphates, metallosilicates,[5] etc., are also other inorganic porous materials which have been studied extensively.

Although activated carbons[6] have open porous structures with high surface area, the structure is essentially disordered. The salient structural features involve a network of defective hexagonal carbon layers, cross-linked by aliphatic bridging groups.

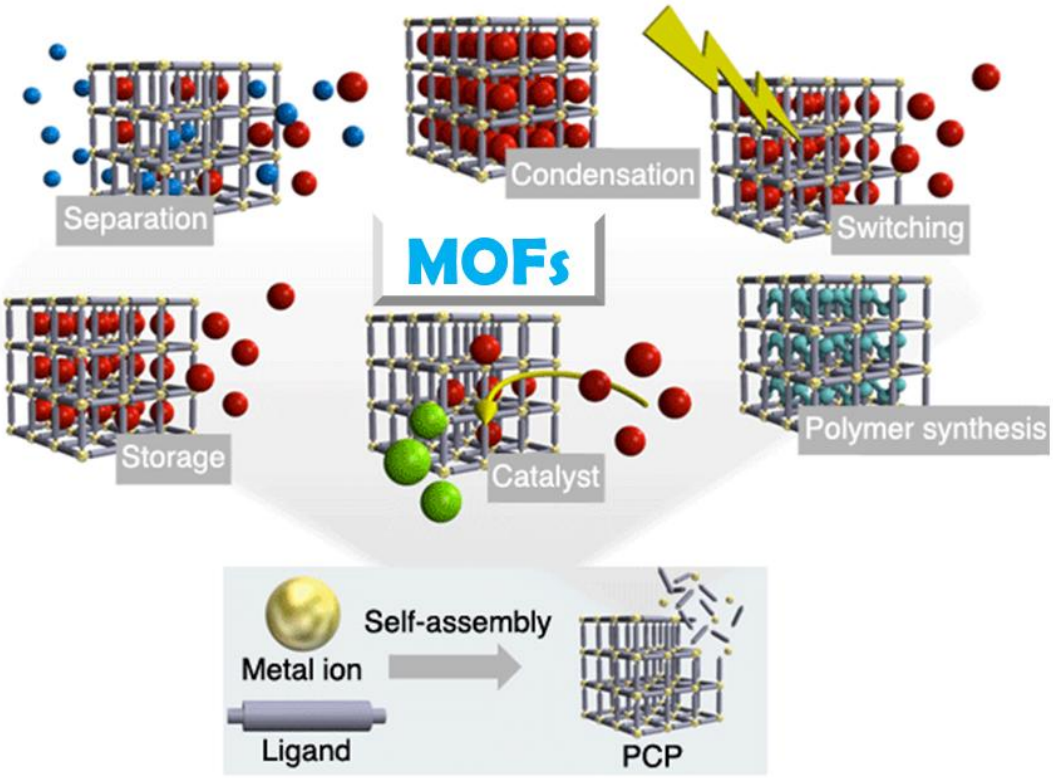

Fig. 2 MOFs and their applications.

The development of MOFs opened a world of new possibilities, which were beyond the scope of the two earlier classes of materials. MOFs have completely regular structures unique properties, e.g., BET surface areas up to 7000 $m^2.g^{-1}$, density as low as 0.4 $g.cc^{-1}$, tunable pore sizes up to 5 nm, channels connected in 1-, 2-, or 3-D. Also their internal surfaces can be functionalized.[1a, 7] MOFs hold enormous potential as a number of structural, magnetic, electrical, optical, and catalytic properties can be obtained through a wide selection of metal and infinite choice and design of ligands.[8] Unlike zeolites, MOF materials do not require the use of organic/inorganic templates, (e.g., amines, quaternary ammoniums, etc.), as the solvent itself acts as the main template. This is extremely advantageous as it makes most of the MOF materials neutral in nature. In case of zeolitic solid materials with a cationic framework, the framework often collapses during the extraction of the template owing to strong electrostatic host guest interactions. MOFs, however, have weaker interactions with solvents and therefore the structure evolves easily at low temperatures, keeping the framework intact in most of the cases thereby providing easily accessible porosity. Also, the existence of both inorganic and organic moieties in the framework allows the coexistence of both hydrophobic and hydrophilic parts within the pores, giving rise to interesting adsorption properties.[7a]

1.1.1 Synthesis

Transition metals are most commonly used as connectors to scaffold MOFs. Coordination numbers of these transition metals can range from 2 to 7, depending on the metal and its oxidation state. This gives rise to diverse geometries, which may be linear, T or Y-shaped, tetrahedral, square planar, square pyramidal, trigonal-bipyramidal, octahedral, trigonal-prismatic, pentagonal-bipyramidal, and their corresponding distorted forms (**Fig. 3**). The geometries formed also depend on reaction conditions, solvents, counter anions and organic ligands.

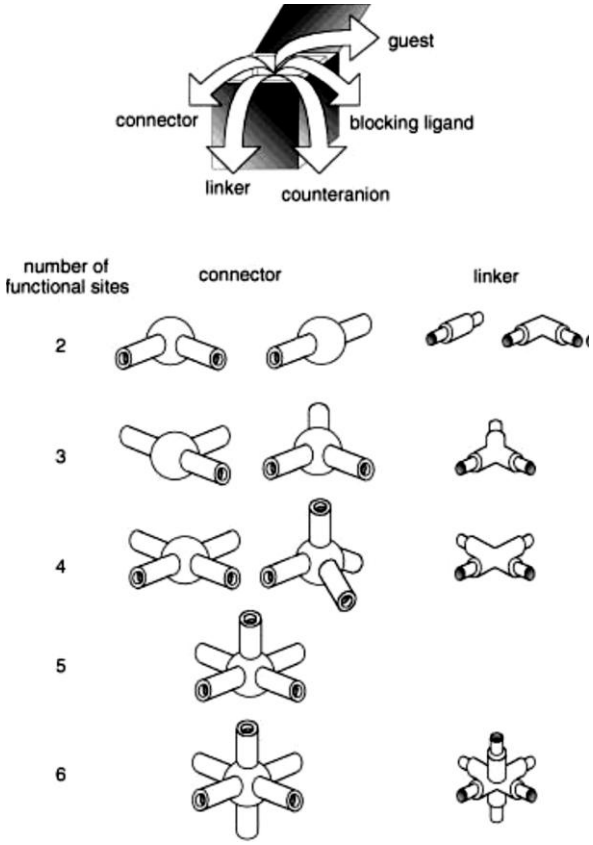

Fig. 3 Components of coordination polymers. Reprinted with permission from ref. no. 1a.

In these MOFs, coordinatively unsaturated metal sites can also be generated by the removal of the coordinated solvent molecules. The unsaturated metal sites thus formed can be used for chemical adsorption, heterogenous catalysis and sensing. In the frameworks, metal-complex connectors have greater advantage over naked metal ions as the bond angles can be controlled along with restriction of the number of coordination sites. The coordination sites that are not required can be obstructed by chelating or by macrocyclic ligands which link

directly to a metal connector, leaving specific sites free for linkers. This ligand regulated approach of a connector is extremely vital in MOF chemistry.[1a]

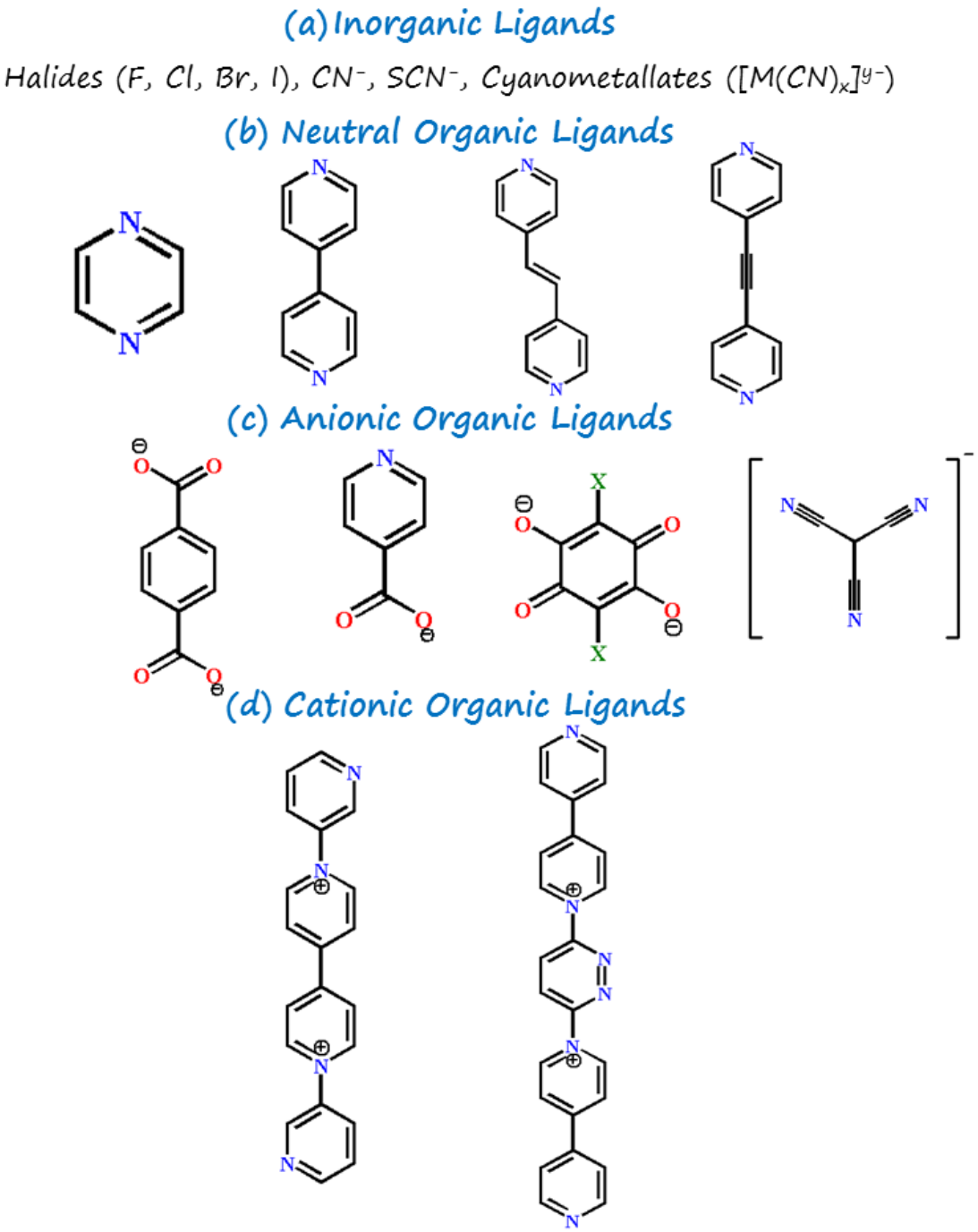

Fig. 4 Different types of ligands used for synthesizing MOFs

Diverse types of ligands further make the MOF structures dynamic and interesting. A few commonly used ligands have been listed in **Fig. 4**. The smallest and simplest inorganic linkers used in MOFs are halides, i.e., F, Br, Cl and I. CN^- and SCN^- also have similar coordinating abilities as the halides. Cyanometallate anions manifest several types of

geometries, for example, linear, as in $[M(CN)_2]$- (M=Au[9] and Ag[10]), trigonal, as in $[Cu(CN)_3]^{2-}$,[11] tetrahedral, as in $[Cd(CN)_4]^{2-}$,[12] square planar, as in $[M(CN)_4]^{2-}$, (M=Ni[13], Pd, and Pt[14]), octahedral, as in $[M(CN)_6]^{3-}$(M=Fe, Co[15], Cr[16], and Mn[17]), and pentagonal bipyramidal, as in $[Mo(CN)_7]$.[18] The octacyanometallates $[M(CN)_8]^{n-}$ (M=Mo and W) also show various coordination geometries like square-antiprism, dodecahedron, or bicapped trigonal-prism.[19] Apart from these, a wide and diverse range of organic ligands are used. These may be neutral, cationic or anionic. Di, tri or tetracarboxylate ligands are widely used among the organic linkers.[20] Pyrazine (pyz) and 4,4'-bpy are the most frequently used neutral organic linkers.[21]

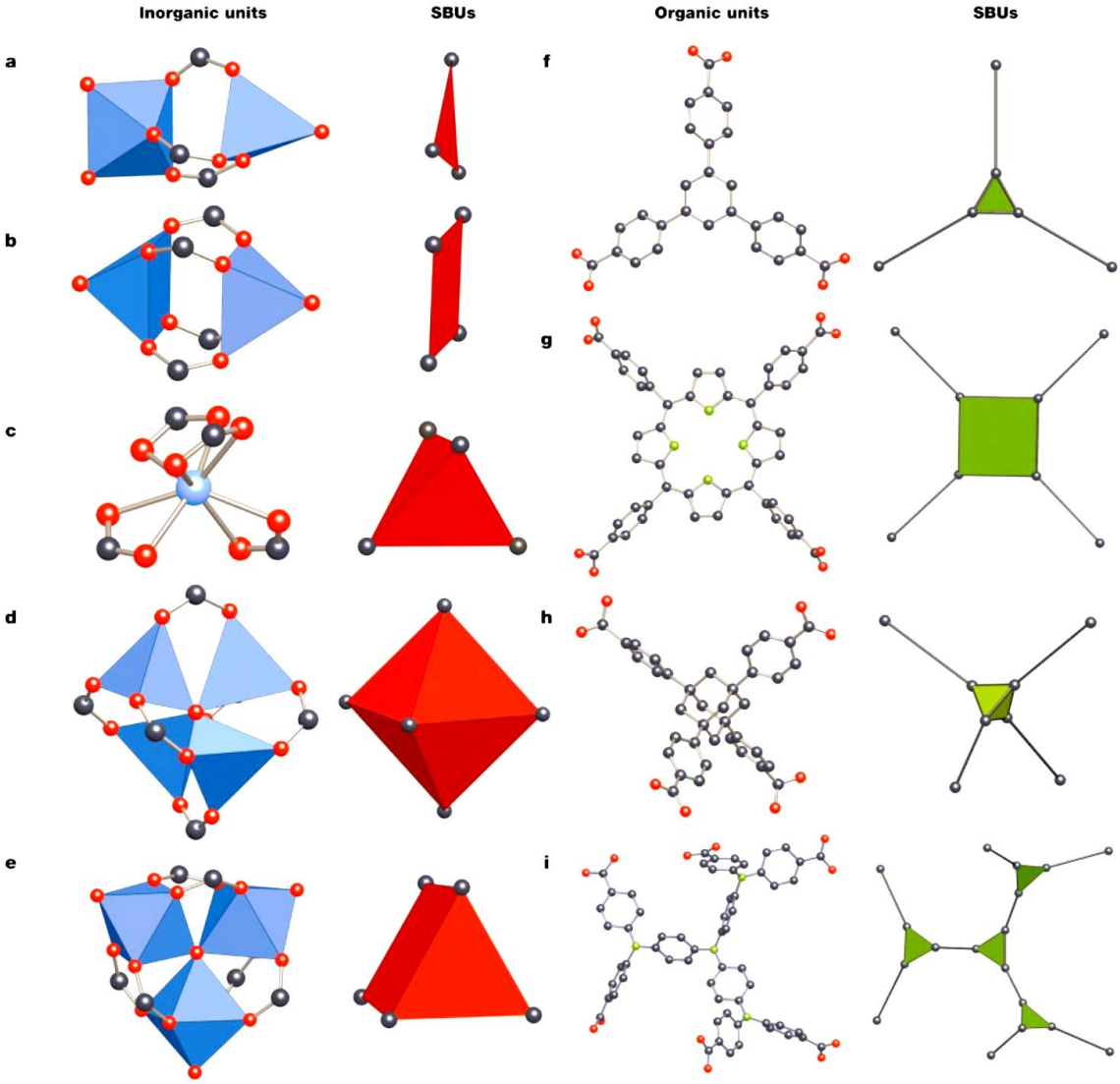

Fig. 5 Different types of SBUs. Reprinted with permission from ref. no. 7b.

Secondary Building Unit or SBU is an important term with respect to the structure of MOFs. SBU refers to the polynuclear clusters constructed by the assembly of two or more metal ions with multidentate carboxylate linkers[1a] (**Fig. 5**). Here carboxylate functionalities chelate metal ions and capture them in rigid and hence directional metal-oxygen-carbon clusters with points of extensions, defining specific geometrical shapes.[7b] Such SBUs are capable of having special coordination numbers and geometries. These polytopic units when assembled together with metal ions give rise to linked cluster entities in the assembled solid.[1a]

Fig. 6 summarizes the different synthetic methods used to synthesize MOFs. Apart from traditional solvothermal and room temperature syntheses, conventional electric heating, microwave heating, electrochemistry, mechanochemistry and ultrasonic methods have also been undertaken over the years. High-throughput methods are also employed in recent times for targeted synthesis of specific compounds. Many of the targeted syntheses are aimed towards achieving specific morphologies of the MOF products. There are numerous reports of thin films, membranes and specific crystal shape and size and all these require the application of different synthetic methods.[22]

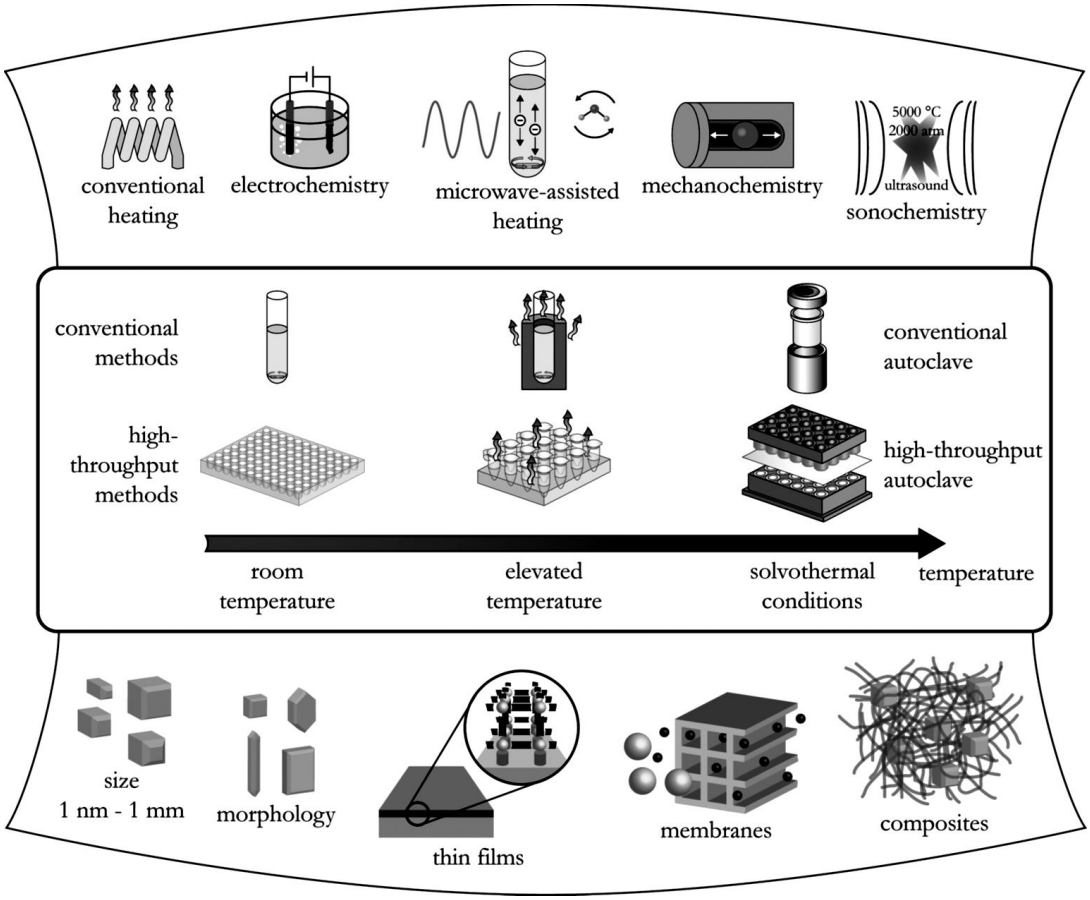

Fig. 6 Synthetic methods leading to MOFs. Reprinted with permission from ref. no. 22.

1.1.2 Classification of MOFs

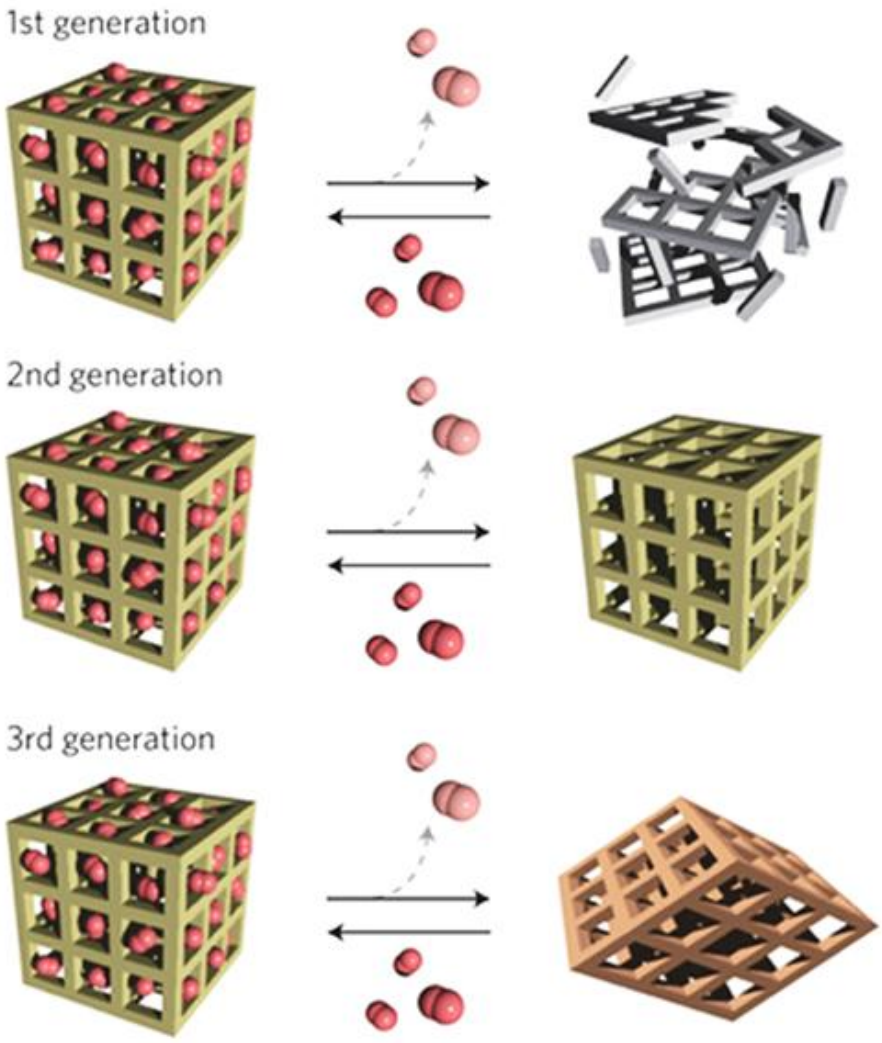

Fig. 7 Classification of MOFs. Reprinted with permission from ref. no. 23.

Back in 1998, porous compounds were classified as 1st, 2nd and 3rd generation on the basis of their robustness and ability to sustain. The 1st generation compounds possess microporous frameworks that exist only with the guest molecules and the framework collapses irreversibly on the removal of these guest molecules. The 2nd generation compounds show permanent porosity without any guest molecules in their pores and have stable and robust porous frameworks. The 3rd generation compounds have dynamic and flexible structures which respond to external stimuli, e.g., light, electric field, guest molecules and modify their channels or pores reversibly. Most inorganic porous compounds with covalent bonds are classified under the 2nd generation compounds. However, PCPs are not merely robust 2nd generation compound, they also yield the highly dynamic third generation frameworks.[1a, 23]

1.1.3 Applications of MOFs

The applications of MOFs are many and varied. It is extensively used for gas adsorption and storage because of its porous structure. Also its porous nature makes it attractive for heterogeneous catalysis and separation. However, it has also proved its efficiency in luminescence, drug delivery, molecular sensing, etc. A few of its applications are discussed in details below.

1.1.3.1 Gas adsorption and storage

Porous coordination polymers are endowed with a variety of coordination architectures with uniform and dynamic pore structures. They possess crystallographically well defined shapes, e.g., squares, rectangles and triangles. They have exhibited unprecedented adsorption profiles manifesting their uniform microporous nature.[1a] Hydrogen is the most promising candidate to replace the current fossil fuel based energy resources. However, the facile storage of H_2 gas is one of the biggest challenges in this regard. MOFs, with their porous structures, hold great promise to be successful H_2 storage materials.[24] The highest total H_2 storage capacity so far has been exhibited by MOF-210, which has a total capacity of 176mg.g^{-1} at 77K and 80 bar.[25]

CO_2 emission from industries is a major problem in the modern era which contributes to the global warming and poses a huge environmental threat. Hence the development of technologies for the effective CO_2 sequestration from the emission sources is vital. MOFs are particularly effective in CO_2 capture and the CO_2 adsorption properties of numerous MOFs have been studied extensively.[26] MOFs are particularly useful in the selective capture of CO_2 from a mixture of gases like flue gas. MOFs can also store natural gases like CH_4, C_2H_6, etc., and solvent vapours like methanol, ethanol, benzene, etc.

1.1.3.2 Luminescence

MOFs, being a hybrid of organic and inorganic materials, are promising multifunctional luminescent materials as both the inorganic and organic parts can contribute to the luminescent property. Furthermore, guest molecules within the MOFs can induce or emit luminescence, while metal-ligand charge transfer related luminescence can also be observed within MOFs. In some luminescent MOFs, the permanent porosity has allowed the reversible storage and release of guest substrates and provided the differential recognition of these

substrates by acting as sensing species.[27] Broadly, the origin of luminescence in MOFs can occur in four different ways as discussed below.

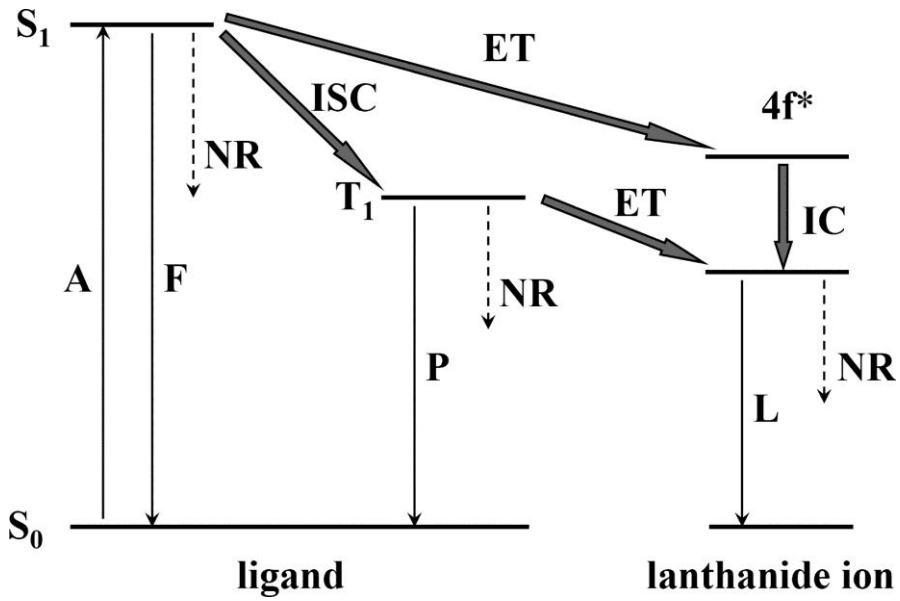

Fig. 8 Schematic representation of energy absorption, migration, emission, and processes in MOFs. Abbreviations: A = absorption; F = fluorescence; P = phosphorescence; L = lanthanide-centered luminescence; ISC = intersystem crossing; ET = energy transfer; IC = internal conversion; S = singlet; T = triplet. Plain arrows indicate radiative transitions; dotted arrows indicate nonradiative transitions. Reprinted with permission from ref. no. 27.

(a) Linker based luminescence

An organic molecule on absorbing a photon of energy starts a series of photophysical events, including internal conversion or vibrational relaxation, fluorescence, intersystem crossing and phosphorescence (**Fig. 8**). These luminescent properties can be characterized by the emission spectra, quantum yield and lifetime measurement of the emissive species. In many cases, the fluorescence properties, e.g., maximum emission wavelength and lifetime of organic linkers are different in solid MOFs than those of the free molecules. The ligand 2,4,6-pyridinetricarboxylate (pta) exhibits a weak luminescence at 415 nm whereas the MOF $Zn_3(\mu_5\text{-pta})_2(\mu_2\text{-}H_2O)_2$ constructed from the same ligand shows a very strong luminescence at 467nm when excited at 338nm at room temperature. This fluorescent enhancement and red shift of emission can be attributed to the formation of framework which induces rigidity in the aromatic backbones, thereby maximizing the intramolecular/intermolecular interactions among the organic linkers for energy transfer and decreasing the HOMO-LUMO energy gap.[28]

(b) Luminescence based on charge transfer

Charge transfer luminescence is general generated by the allowed transition from a charge transfer-excited state to the ground state. Ligand-to-metal charge transfer (LMCT) and Metal-to-ligand charge transfer (MLCT) are commonly prevalent in MOFs. LMCT corresponds to the electronic transition from an organic linker-localized orbital to a metal-centered orbital, whereas MLCT involves the electronic transition from a metal-centered orbital to an organic linker localized orbital. Charge transfer luminescence is often observed in d^{10} metal based MOFs.[27] An example of luminescence originating from LMCT in MOFs can be seen in the MOFs $[Zn(2,3\text{-pydc})(bpp)]_3 \cdot 2.5H_2O$ and $[Cd(2,3\text{-pydc})(bpp)(H2O)]_3 \cdot 3H_2O$ ($2,3\text{-pydcH}_2$ = pyridine-2,3-dicarboxylic acid), which show intense fluorescent emissions at 436 and 438nm upon excitation at 372 and 370nm respectively, although the organic linker $2,3\text{-pydcH}_2$ shows a very weak emission upon excitation at 370nm.[29]

(c) Guest induced luminescence

MOFs can act as rigid or flexible hosts for the encapsulation of the guest luminescence species such as lanthanide ions or fluorescent dyes. The MOF scaffold can sensitize the encapsulated Ln^{III} ions using the antenna effect and also protects them from the outside chemical environment.[27] Using this principle, Luo et al. prepared the Eu^{III} and Tb^{III} doped MOFs which exhibit tunable luminescent properties and can sense metal ions.[30]

(d) Luminescent MOFs base on lanthanide ions

Lanthanide ions with electronic configurations $[Xe]4f_n$ (n=0-14) configurations generate a wide variety of electronic energy levels thus producing intricate optical properties. Ln^{III} ions are less sensitive to the surrounding chemical environment since the 4f orbitals are well shielded by the filled $5s^25p^6$ subshells. Hence the electronic energy levels are well defined and and each Ln^{III} ion exhibits sharp characteristic 4f-4f transitions. The Eu^{III}, Tb^{III}, Sm^{III}, and Tm^{III} emit red, green, orange, and blue light, respectively, while the Yb^{III}, Nd^{III}, and Er^{III} exhibit near-infrared luminescence. The lanthanide ions are weakly absorbing in nature since f-f transition is forbidden[27] (**Fig. 9**). Hence direct excitation of the metal to produce emission is rather futile. However, when a MOF is formed, the organic ligand can itself absorb the energy and transfer it to the Ln^{III} excited state, thereby acting as an antenna.[31] This forms the basis of the much celebrated "luminescence sensitization" or "antenna effect".[32]

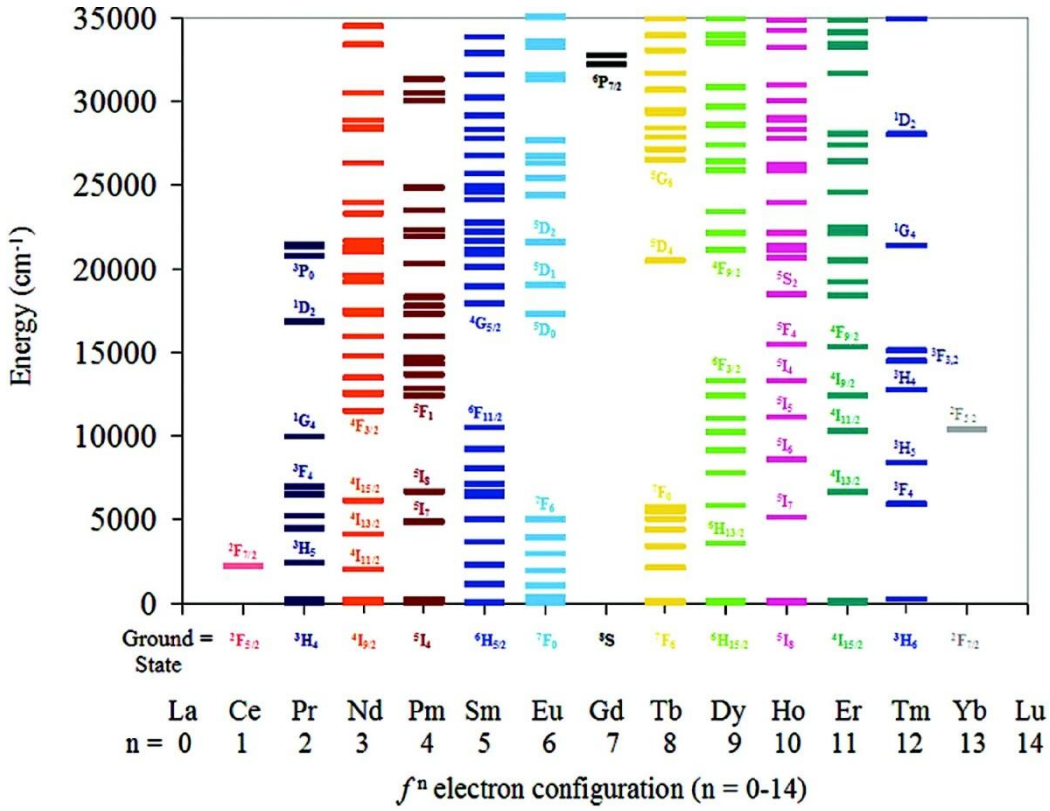

Fig. 9 Summary of electronic excited state energy levels of Ln^{III} ions. Reprinted with permission from ref. no. 32.

1.1.3.3 Sensors

The exceptional tunable structure and properties of MOFs give them an edge over other chemo-sensory materials. There is a pressing demand for materials that can selectively and sensitively sense gas and vapour phase analytes for a range of applications including industrial process management, medical diagnostics, environmental monitoring, chemical threat and explosive detection. The prevalent commercialized sensors primarily depend upon organic-polymeric or inorganic semiconductor materials which can adsorb or react with the analyte molecule. The sensing process is usually detected by changes in electrical, photophysical or mechanical properties of these materials[33].

MOFs show sensing properties via the following ways:

(a) Solvatochromism/ vapourchromism[34]

(b) Luminescence based sensing[35]

(c) Interferometry[36]

(d) Localized surface plasmon resonance[37]

(e) Colloidal crystals[38]

(f) Impedance spectroscopy[39]

(g) Electromechanical sensors[33]

Among these, luminescence based sensing is the most widely used and easily detectable form of sensing. The advantage of using luminescent MOFs for sensing is the production of a signal that is visible to the eye. Moreover, it can be easily detected through fluorescence spectroscopy up to the single molecule level, without having to fabricate films, directly with the powdered sample. An interesting example of luminescence based sensing can be seen in the flexible 3D supramolecular framework {[Zn(ndc)(*o*-phen)]·DMF}*n* (*o*-phen=1,10-phenanthroline, ndc=2,6-napthalenedicarboxylate). This MOF can accommodate different electron donating aromatic amine guests within the confined nanospaces of its structure. These aromatic amines can be detected with selective turn-on emission signalling and the system serves as a molecular recognition platform through an emission readout process. This tunable emission signalling with different amines can be attribute to its charge transfer complexation with o-phen linkers[40].

1.2 Flexible MOFs

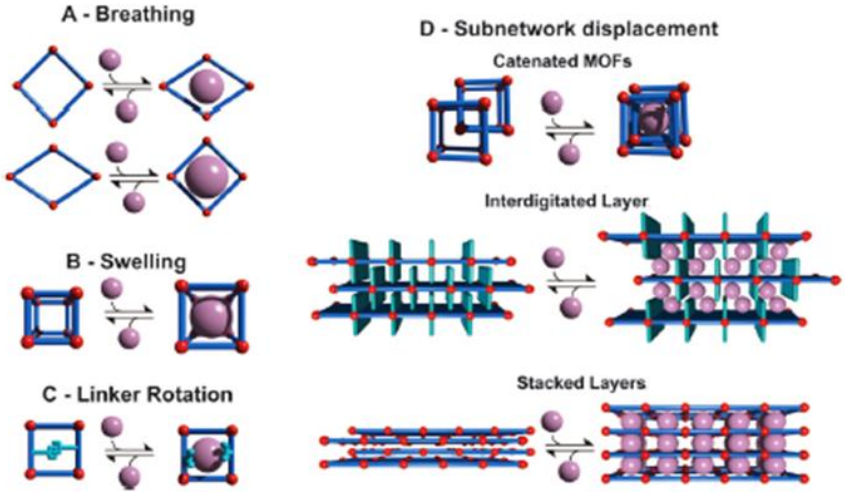

Fig. 10 Different modes of framework flexibility. Reprinted with permission from ref. no.41.

Flexible MOFs, or the so-called breathing MOFs are characterized by a drastic change in the unit cell volume upon the application of external stimuli, e.g. guest molecule adsorption/ desorption and are prominent examples of soft porous crystals (SPCs).[41] Soft porous crystals have been described by Horike, et al. as porous solids having both a highly ordered network

and structural transformability. These are bistable or multistable crystalline materials with long range structural ordering which show a reversible transformability between states and permanent porosity.[23] MOFs can show framework flexibility in the absence of guests or without the involvement of adsorption and desorption as well. Flexibility may also be triggered by external stimulus, e.g., mechanical stress, temperature, interactions with light, electrical or magnetic interactions. There are different classes of flexibility which have been discussed below.

1.2.1 Breathing, swelling, linker rotation and subnetwork displacement

Breathing (**Fig. 10**) refers to the transition of MOFs where displacement of atoms in the framework is accompanied by a change in the unit cell volume. The characteristic angles and bond distances of the unit cell may change and the space groups of the two distinct phases may be different.[41] This kind of flexibility is observed in the MIL-53 family ($[M(bdc)(OH)]_n$,where bdc = 1,4-benzenedicarboxylate and M= Al[42], Fe[43], Cr[44], Sc[45], Ga[46], In[47]).

The *swelling* mode can be characterized by a gradual enlargement of the MOF unit cell volume, without any change in the unit cell shape and the space group.[41]

A continuous transition where the spatial alignment of a linker is changed by turning around a rotational axis is defined as *Linker rotation.*[41] A typical example of this flexibility mode is ZIF-8 (Zeolitic IMidazolate Framework, $[Zn(mIm)_2]_n$, mIm= 2-methylimidazole).[48]

The phenomenon of *subnetwork displacement* is restricted primarily to systems with individual frameworks which are not connected by strong chemical bonds, but with weak interactions like van der Waals forces. So the subnets can drift, relocate or shift with respect to one another. This can occur in interpenetrated 3D frameworks as well as interdigitated and stacked 2D frameworks.[41]

1.2.2 Photoresponsivity

If MOFs are constructed with photoresponsive organic ligands which change their conformation or structure upon light irradiation, the pore size and shape of the MOF can be controlled by light irradiation (**Fig. 11**). Photoactive groups are attached as a functional side group to the linker.[41] Azobenzene is the only photoactive group to have been incorporated in MOF so far. In most cases, pendent azobenzene photoswitch is present in the pore and changes its conformation from trans to cis upon irradiation at 365 nm.[49]

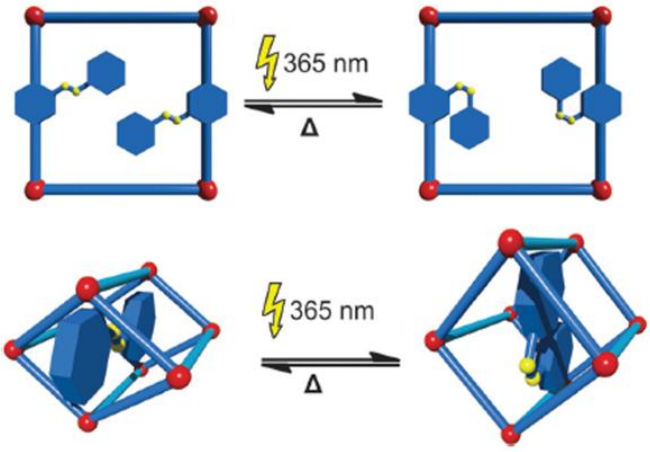

Fig. 11 Photoresponsivity of azobenzene linker in MOFs. Reprinted with permission from ref. no. 41.

1.2.3 Thermoresponsivity

MOFs that show a change in their lattice parameters upon the alteration of temperature without any change in the molecular composition are thermoresponsive. Thus materials containing solvent molecules are excluded from this class since in that case exposure to higher temperatures changes the compositions as well as a phase transition induced by guest desorption.[41]

1.2.4 Mechanical properties, elasticity

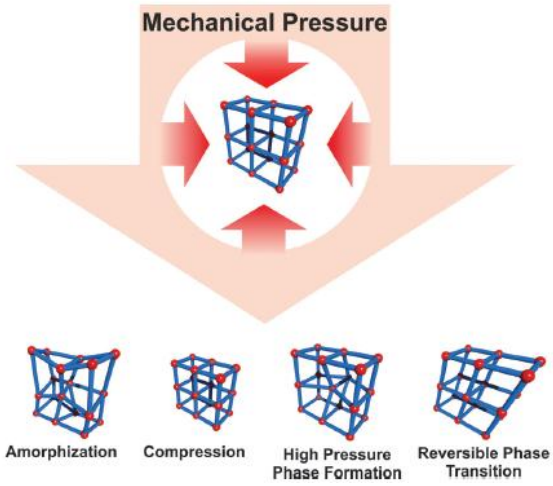

Fig. 12 Possible transformations MOFs can undergo on applying mechanical pressure. Reprinted with permission from ref. no. 41.

The mechanical softness of MOFs is associated with highly anisotropic elastic behaviour (**Fig. 12**). These structural transformations are not necessarily reversible, although compressions are usually reversible, after the pressure is changed back to initial conditions[41]. Interpenetrated grid frameworks are extremely relevant in this case, as they can form open and closed forms by interdigitation using simply a glide motion without any bond cleavage or distortion[23].

1.3 Postsynthetic Modification in MOFs

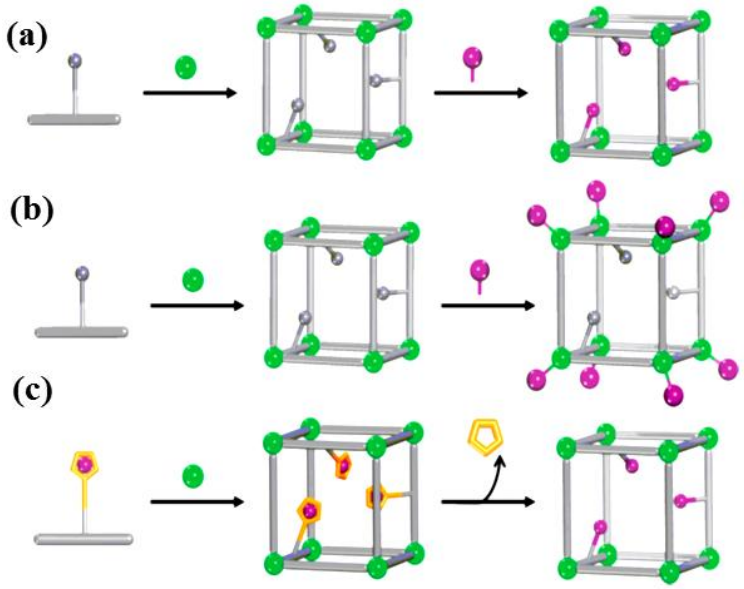

Fig. 13 A few different types of post synthetic modifications in MOFs. Reprinted with permission from ref. no. 50.

The solvothermal synthetic methods generally used to prepare MOFs limits the synthesis of highly functionalized MOFs. Ligands generally lose their thermally labile groups during the solvothermal processes. Also the groups that have problematic solubility or can coordinate metal ions are lost.[50] Also, targeted synthesis of a MOF for specific application becomes difficult in such cases. Thus, post synthetic modifications (PSM) have been used to induce specific functionalities in an already synthesized MOF through chemical modifications. PSM is particularly effective for MOFs since MOFs contain organic ligands which can undergo a vast range of organic transformations. Moreover, since MOFs are highly porous, during PSM, the reagents can act on both the interior and exterior of the material.

There are quite a few different ways in which a MOF can be modified physically and chemically.[50] A few of the common methods are listed below (**Fig. 13**).

(a) covalent PSM[51]

(b) dative PSM[52]

(c) post synthetic deprotection[52b]

(d) guest molecule exchange including cation/anion exchange[53]

PSM through cation and anion exchange has been observed in several robust MOFs including ZIFs and MILs. Ligand exchange in the solid state under mild conditions was observed in the topologically distinct MOFs MIL-53 (Al) and MIL-68 (In). Metal ion exchange is also observed between intact MOF microcrystalline particles of MIL-53 (Al) and MIL-53 (Fe)[54] (**Fig. 14**).

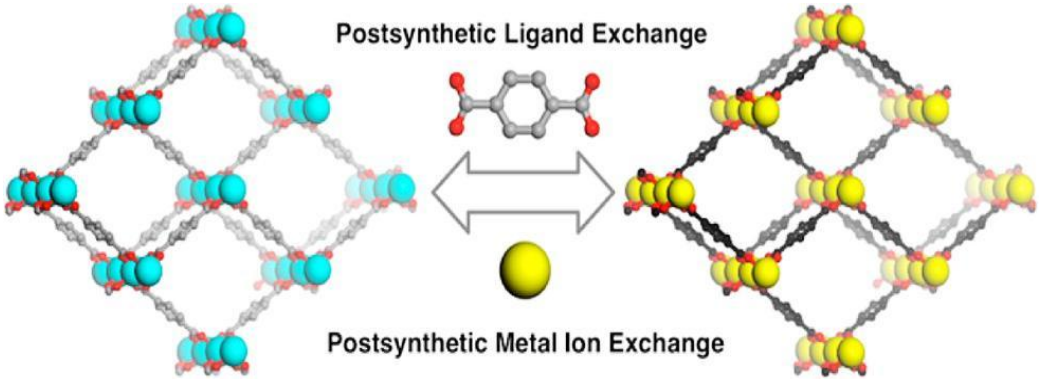

Fig. 14 Post synthetic metal and ligand exchange in MOFs. Reprinted with permission from ref. no. 45.

1.4 Anionic MOFs

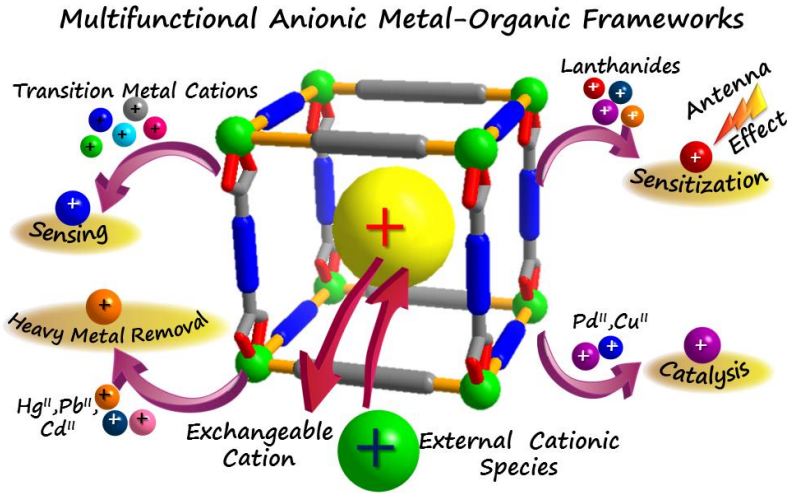

Fig. 15 Various applications achieved by cation exchange in an AMOF.

Metal-organic frameworks are usually neutral in nature. But in some cases, the framework itself is charged and the overall framework neutrality is maintained by guest counter ions residing within the pores of the MOFs. In case of anionic MOFs (AMOFs), the framework itself is anionic nature, and the structural neutrality is maintained by guest cations present in the pore channels. Many such AMOFs have been reported in recent times and have shown diverse applications by the exchange of the guest cation with other cationic species.[53] The nature of the cation species imbibed in the framework determines the application that can be achieved from the AMOF (**Fig. 15**).

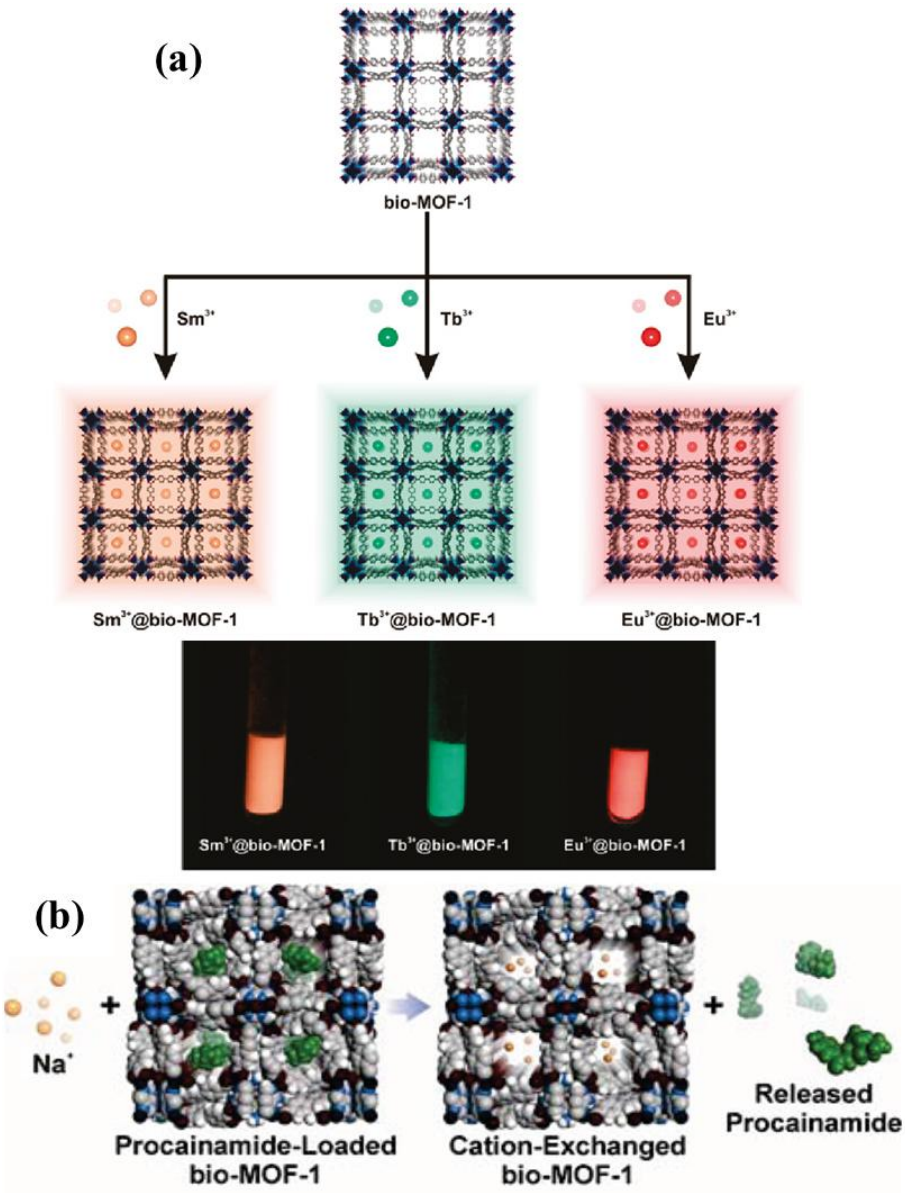

Fig. 16(a) Luminescence through cation exchange in bioMOF-1 **(b)** Cation exchange mediated drug release in bioMOF-1. Reprinted with permission from ref.no. 53a and 53c.

An interesting instance of AMOF is bioMOF-1 formulated as $Zn_8(ad)_4(BPDC)_6O•2Me_2NH_2$. $8DMF.11H_2O$, (ad=adeninate; BPDC =biphenyldicarboxylate) reported by Rosi, et al. Here, dimethyl amine (NH_2Me_2) (DMA) cations are present within the pores of the framework in order to maintain neutrality. Owing to the stability of bioMOF-1 in PBS buffer, its non-toxic and anionic nature, it appears to be an ideal material for the capture and controlled release of drug. For this purpose the antiarrhythmia drug procainamide HCl was chosen and bioMOF-1 proved to be an excellent material for its storage and controlled release[53a] (**Fig. 16(b)**). The same framework was further used to encapsulate and sensitize several visible and near infrared emitting lanthanide cations in aqueous media to produce luminescence[53c] (**Fig. 16(a)**). Furthermore, tunable emission was also achieved using the same framework and in this case, cation exchange is performed by introducing tetramethylammonium (TMA), tetraethylammonium (TEA), and tetrabutylammonium (TBA) into the pores to systematically decrease the pore volume and surface area of the material.[53b] AMOFs can also be used in catalytic processes, e.g., DMA cation containing ZJU-28 was made to undergo cation exchange with several Rh, Pd, Ir, Fe and Ru complexes. The MOF supported $[Rh(dppe)(COD)]BF_4$ was found to catalyse the hydrogenation of 1-octene to n-octane with better yield and recyclability than the homogenous catalyst.[53d] Another interesting application of AMOFs can be seen in second harmonic generation in nonlinear optics. $[(H_2NMe_2)_2Cd_3(C_2O_4)_4]·MeOH·2H_2O$ is an octupolar open 3D framework, which shows high cation exchange rates with NH_4^+, Na^+ and K^+ and shows an unprecedented guest-cation-dependant non-linear optical activity.[53e] Thus AMOFs are turning out to be an interesting class of MOFs where different specific applications can be generated by PSM of the framework via facile exchange with a definite cationic species.

1.5 Cationic MOFs

In the vast MOF library, although several anionic MOFs are reported, there are only a few permanently porous MOFs with positive frameworks[55] although there is a rising demand for the development of new materials with positive frameworks for selective anion exchange and separation or storage and delivery.[56] MOFs provide a hope in this direction, where tuning the stoichiometric ratio appropriately can lead to the formation of cationic MOFs, where the framework itself is cationic and the net charge on the framework is balanced by the presence

of extra-framework counter ions.[57] Anion exchange in cationic MOFs has been already used for certain specific applications, e.g., water pollutant removal,[57-58] drug delivery,[59] tunable emission,[60] selective dye encapsulation[55c, 56] and structural dynamism.[60]

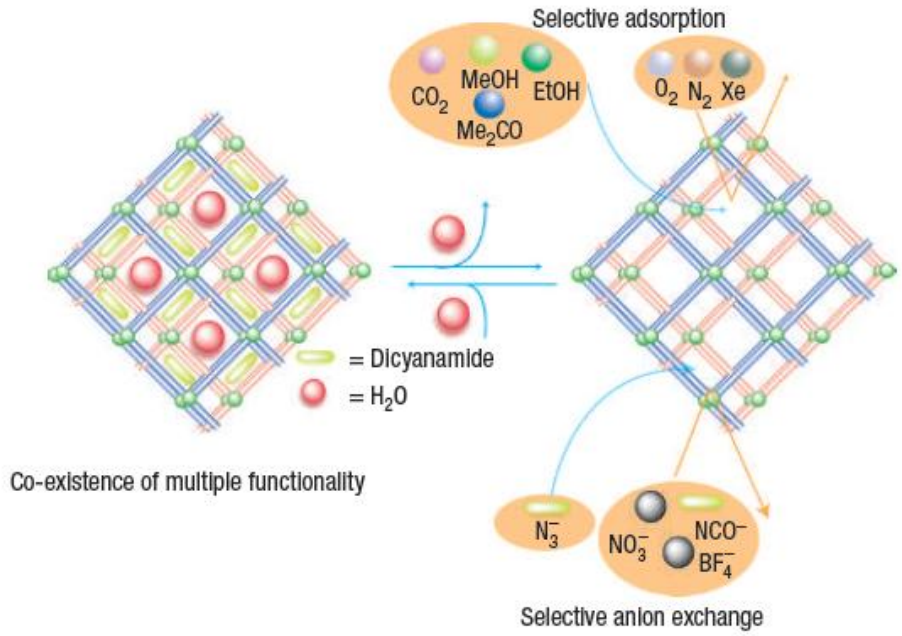

Fig. 10 Sub-network shifting in a 3D Ni framework induced by anion exchange. Reprinted with permission from ref. no. 61.

Using the advantages of flexibility and softness along with the concepts of interdigitation, catenation and anion exchange in a cationic MOF, sorption selectivity can be induced by guest selective induced subnetwork movements. An excellent example of this principle can be observed in the pillared layer framework comprising 2D $[Ni(bpe)_2]_n$ (bpe = 1,2-bis(4-pyridyl)ethane) sheets, stacked together by dicyanamide ($N(CN)_2^-$) pillars.[61] The assynthesized framework has the molecular formula $[(Ni(bpe)_2(N(CN_2)))(N(CN_2))(H_2O)5]_n$ and contains both guest H_2O molecules as well as $N(CN)_2^-$ groups. On activation at elevated temperature to remove the guest water, $[Ni(bpe)_2(N(CN_2))][(N(CN_2))]_n$ is obtained, where the pore structure is retained with minute changes. This permanently porous framework can undergo a subnetwork shifting transition simply by exchanging $N(CN)_2^-$ with N_3^- group which alters the adsorption properties accordingly (**Fig. 17**).

1.6 MOF Derived Carbonaceous Materials

The post synthetic modification of MOFs allows the conversion of other porous functional materials for specific applications. The growing interest regarding functional materials associated with molecules, ions and clusters in the nanometer ranges demands the controlled synthesis of nanomaterials with molecular, nanoscopic and mesoscopic structures. The exclusive interactions of such nanomaterials within confined nanospaces produce unique nanoporous materials with a diverse range of specific applications starting from adsorption[62] and catalysis[63] to electronics[64] and drug delivery[65]. Nanoporous carbon is the most significant in this regard for their great thermal and chemical stability. Quite a few MOFs have been employed in order to synthesize nanoporous carbons with ordered structure, narrow pore size distribution and higher surface areas.[62a, 66] A few very well-known MOFs, e.g., IRMOF-3,[67] MOF-5,[68] Al-PCP[69] and ZIF-8[70] have efficiently played the role of a promising precursor material, resulting in highly nanoporous carbons showing exceptional adsorption,[71] electrochemical capacitance,[72] drug delivery[65] and catalytic properties.[71]

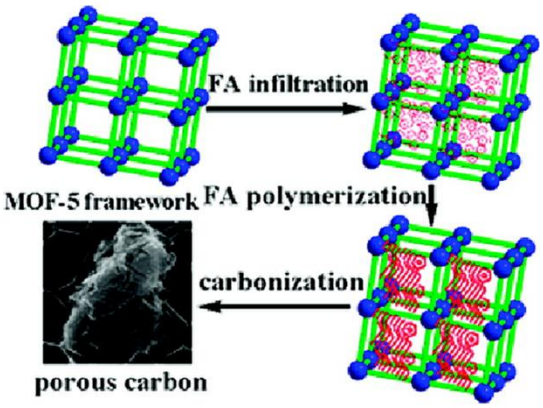

Fig. 18 Synthesis of porous carbon using MOF-5 as a sacrificial template. Reprinted with permission from ref. no. 72.

The first instance of using a MOF as a sacrificial template for the preparation of porous carbon was reported by Xu, et al. in 2008. Furfuryl alcohol was impregnated into MOF-5 for this purpose followed by carbonization at 1000°C (**Fig. 18**). The porous carbon material thus synthesized showed a high specific Brunauer-Emmett-Teller (BET) surface area of 2872 $m^2.g^{-1}$. This nanoporous carbon showed a good hydrogen storage capacity as well as exceptional electrochemical activity as an electrode material for electrochemical double layer capacitor.[72] Apart from furfuryl alcohol, glycerol[73], carbon tetrachloride, ethylenediamine and phenolic

resin[66b] have been used as carbon sources with MOF-5. Extremely high surface area nanoporous carbons have also been achieved by the carbonization of sucrose impregnated IRMOF-3[74] and the direct carbonization of pristine Al-PCP.[75]

Introduction of heteroatoms like boron, sulphur and nitrogen in the carbon framework imparts interesting physical properties in the material.[76] The use of nitrogen doped carbon networks as metal-free base catalysts, hydrogen storage material, CO_2 adsorbent and supercapacitor electrodes are already well-known[77]. Porous graphitic carbon nitride has been synthesized using a few MOF frameworks as template using pre-bonded C-N moiety as a precursor.[78] Yamauchi et al. have synthesized graphitic carbon nitride using Al-PCP as a template with dicyandiamide precursor[78b] while Kurungot, et al. have used MOF-5 template with melamine precursor.[78c] However, reports of direct carbonization of nitrogen containing frameworks (e.g., ZIFs) to achieve graphitic carbon nitride are rare, since during carbonization C-N bonds are broken, resulting in low nitrogen content of the resultant material.[66a, 71]

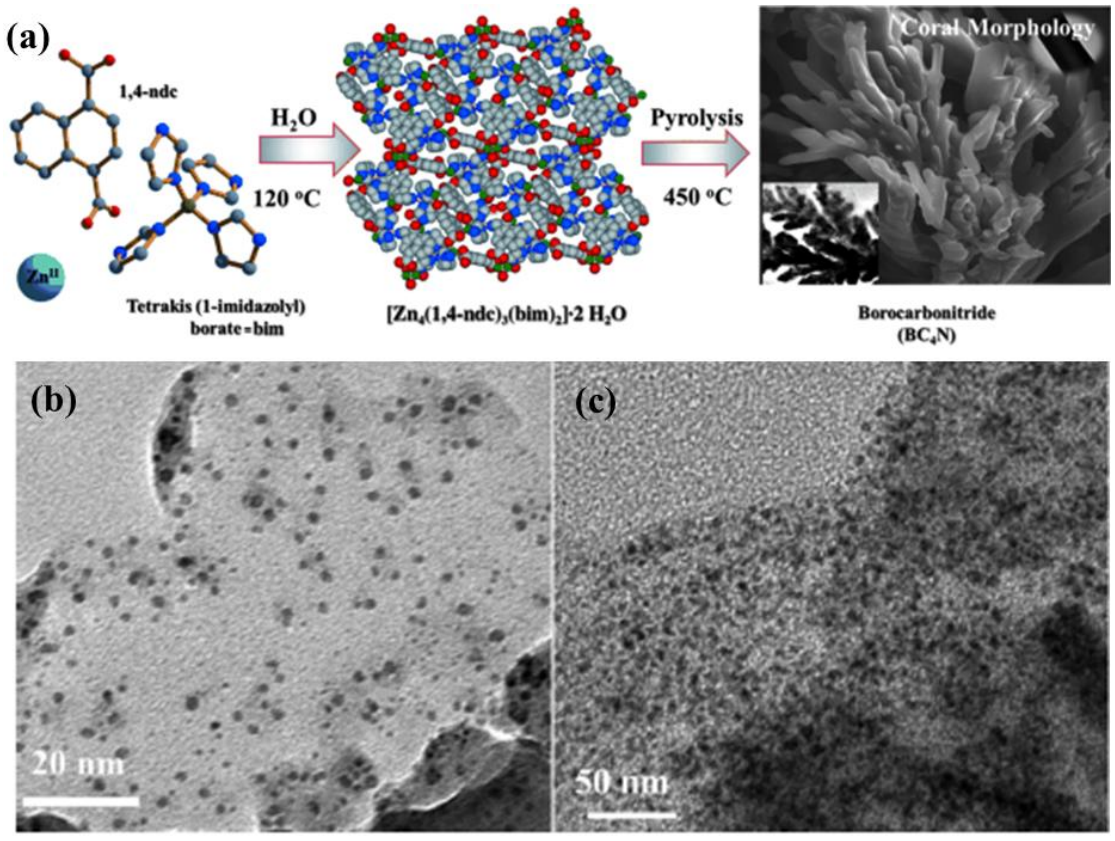

Fig. 19(a) Synthesis of BC_4N from a boron imidazolate based Zn-MOF **(b)** Au nanoparticles stabilized on BC_4N **(c)** Pd nanoparticles stabilized on BC_4N. Reprinted with permission from ref. no. 63.

An extremely interesting study is the synthesis of borocarbonitride by the direct carbonization of a boron imidazolate based framework $[Zn_4(1,4\text{-ndc})_3(bim)_2]\cdot 2H_2O$ [bim = (tetrakis(1-imidazolyl)borate) and 1,4-ndc = naphthalenedicarboxylate] reported by Maji, et al. The borocabonitride thus synthesized exhibits a coral like morphology with a surface area of 988 $m^2.g^{-1}$ (**Fig. 19**). Apart from showing a good hydrogen and CO_2 storage capacity, this material also acts as a novel material for the stabilization Au and Pd nanoparticles.[79]

Outlook

Over the years, MOFs or PCPs have emerged as a new generation porous material for varied applications like gas storage and separation, heterogeneous catalysis, luminescence, drug delivery and sensing. Although extensive research has been carried out on the properties and applications of various neutral frameworks, the properties of ionic frameworks are much less studied. These ionic MOFs can be tailored to suit diverse specific applications like drug delivery, sensing, catalysis, tunable adsorption, simply by the exchange of the guest counter ion with exogenous ionic species. Despite the emergence of recent studies on AMOFs, there is no report of any MOF showing the bimodal functionalities of selective sensing and specific sensitization. Also there have been no attempts to exploit the guest cations present in these AMOFs as precursors for other MOF derived materials. Hence, we have aimed at the targeted synthesis of such an AMOF which can act as both a selective Cu^{II} sensor and specific Eu^{III} sensitizer. Also this AMOF has been used for the dual synthesis of nanoporous carbon with exceptionally high surface area as well as graphitic carbon nitride using the guest cation as a precursor. Two different tetracarboxylate ligand based Cu^{II} MOFs with very different structural properties have also been studied in this thesis. We have also investigated the adsorption properties and structural aspects of cage like 2D MOF and interpenetrated 3D framework. The selective adsorption of gases and solvent vapours based on structural aspects and functionalities are particularly interesting.

1.5 References

1. (a) S. Kitagawa, R. Kitaura and S.-i. Noro, *Angew. Chem. Int. Ed.*, 2004, **43**, 2334-2375; (b) M. L. Foo, R. Matsuda and S. Kitagawa, *Chem. Mater.*, 2014, **26**, 310-322.
2. (a) P. Vanelderen, J. Vancauwenbergh, B. F. Sels and R. A. Schoonheydt, *Coord. Chem. Rev.*, 2013, **257**, 483-494; (b) J. Jiang, J. Yu and A. Corma, *Angew. Chem. Int. Ed.*, 2010, **49**, 3120-3145.
3. A. K. Cheetham, G. Férey and T. Loiseau, *Angew. Chem. Int. Ed.*, 1999, **38**, 3268-3292.
4. J. V. Smith, *Chem. Rev.*, 1988, **88**, 149-182.
5. B. M. Weckhuysen, R. R. Rao, J. A. Martens and R. A. Schoonheydt, *Eur. J. Inorg. Chem.*, 1999, **1999**, 565-577.
6. (a) L. Li, P. A. Quinlivan and D. R. U. Knappe, *Carbon*, 2002, **40**, 2085-2100; (b) T. Kyotani, *Carbon*, 2000, **38**, 269-286.
7. (a) G. Ferey, *Chem. Soc. Rev.*, 2008, **37**, 191-214; (b) O. M. Yaghi, M. O'Keeffe, N. W. Ockwig, H. K. Chae, M. Eddaoudi and J. Kim, *Nature*, 2003, **423**, 705-714.
8. S. L. James, *Chem. Soc. Rev.*, 2003, **32**, 276-288.
9. D. B. Leznoff, B.-Y. Xue, R. J. Batchelor, F. W. B. Einstein and B. O. Patrick, *Inorg. Chem.*, 2001, **40**, 6026-6034.
10. V. Niel, M. C. Muñoz, A. B. Gaspar, A. Galet, G. Levchenko and J. A. Real, *Chem. Eur. J.*, 2002, **8**, 2446-2453.
11. S.-I. Nishikiori, *J. Coord. Chem.*, 1996, **37**, 23-38.
12. S.-S. Yun, Y.-P. Kim and C.-H. Kim, *Acta Crystallogr. C*, 1999, **55**, 2026-2028.
13. H. Yuge, Y. Noda and T. Iwamoto, *Inorg. Chem.*, 1996, **35**, 1842-1848.
14. D. W. Knoeppel, J. Liu, E. A. Meyers and S. G. Shore, *Inorg. Chem.*, 1998, **37**, 4828-4837.
15. J. O. Eriksen, A. Hazell, A. Jensen, J. Jepsen and R. D. Poulsen, *Acta Crystallogr.C*, 2000, **56**, 551-553.
16. A. Marvilliers, S. Parsons, E. Rivière, J.-P. Audière, M. Kurmoo and T. Mallah, *Eur. J. Inorg. Chem.*, 2001, **2001**, 1287-1293.
17. M. W. B. Ziegler, M. Schwarten, D. Babel, *Z. Naturforsch. B*, 1999, **54**, 6.
18. J. Larionova, O. Kahn, S. Golhen, L. Ouahab and R. Clérac, *Inorg. Chem.*, 1999, **38**, 3621-3627.

19. A. K. Sra, G. Rombaut, F. Lahitete, S. Golhen, L. Ouahab, C. Mathoniere, J. V. Yakhmi and O. Kahn, *New J. Chem.*, 2000, **24**, 871-876.
20. (a) Y. Ling, Z.-X. Chen, F.-P. Zhai, Y.-M. Zhou, L.-H. Weng and D.-Y. Zhao, *Chem. Commun.*, 2011, **47**, 7197-7199; (b) X. Lin, J. Jia, X. Zhao, K. M. Thomas, A. J. Blake, G. S. Walker, N. R. Champness, P. Hubberstey and M. Schröder, *Angew. Chem. Int. Ed.*, 2006, **45**, 7358-7364; (c) L. H. Wee, C. Wiktor, S. Turner, W. Vanderlinden, N. Janssens, S. R. Bajpe, K. Houthoofd, G. Van Tendeloo, S. De Feyter, C. E. A. Kirschhock and J. A. Martens, *J. Am. Chem. Soc.*, 2012, **134**, 10911-10919; (d) Z. Pan, H. Zheng, T. Wang, Y. Song, Y. Li, Z. Guo and S. R. Batten, *Inorg. Chem.*, 2008, **47**, 9528-9536.
21. P. J. Hagrman, D. Hagrman and J. Zubieta, *Angew. Chem. Int. Ed.*, 1999, **38**, 2638-2684.
22. N. Stock and S. Biswas, *Chem. Rev.*, 2012, **112**, 933-969.
23. S. Horike, S. Shimomura and S. Kitagawa, *Nat. Chem.*, 2009, **1**, 695-704.
24. M. P. Suh, H. J. Park, T. K. Prasad and D.-W. Lim, *Chem. Rev.*, 2012, **112**, 782-835.
25. H. Furukawa, N. Ko, Y. B. Go, N. Aratani, S. B. Choi, E. Choi, A. Ö. Yazaydin, R. Q. Snurr, M. O'Keeffe, J. Kim and O. M. Yaghi, *Science*, 2010, **329**, 424-428.
26. K. Sumida, D. L. Rogow, J. A. Mason, T. M. McDonald, E. D. Bloch, Z. R. Herm, T.-H. Bae and J. R. Long, *Chem. Rev.*, 2012, **112**, 724-781.
27. Y. Cui, Y. Yue, G. Qian and B. Chen, *Chem. Rev.*, 2012, **112**, 1126-1162.
28. X. Li, X.-W. Wang and Y.-H. Zhang, *Inorg. Chem. Commun.*, 2008, **11**, 832-834.
29. G.-H. Wang, Z.-G. Li, H.-Q. Jia, N.-H. Hu and J.-W. Xu, *CrystEngComm*, 2009, **11**, 292-297.
30. (a) F. Luo and S. R. Batten, *Dalton Trans.*, 2010, **39**, 4485-4488; (b) K. Binnemans, *Chem. Rev.*, 2009, **109**, 4283-4374.
31. S. Roy, A. Chakraborty and T. K. Maji, *Coord. Chem. Rev.*, 2014, **273–274**, 139-164.
32. E. G. Moore, A. P. S. Samuel and K. N. Raymond, *Acc. Chem. Res.*, 2009, **42**, 542-552.
33. L. E. Kreno, K. Leong, O. K. Farha, M. Allendorf, R. P. Van Duyne and J. T. Hupp, *Chem. Rev.*, 2012, **112**, 1105-1125.
34. (a) Z.-Z. Lu, R. Zhang, Y.-Z. Li, Z.-J. Guo and H.-G. Zheng, *J. Am. Chem. Soc.*, 2011, **133**, 4172-4174; (b) L. G. Beauvais, M. P. Shores and J. R. Long, *J. Am. Chem. Soc.*, 2000, **122**, 2763-2772.

35. (a) Y. Qiu, H. Deng, J. Mou, S. Yang, M. Zeller, S. R. Batten, H. Wu and J. Li, *Chem. Commun.*, 2009, 5415-5417; (b) L.-G. Qiu, Z.-Q. Li, Y. Wu, W. Wang, T. Xu and X. Jiang, *Chem. Commun.*, 2008, 3642-3644.
36. G. Lu and J. T. Hupp, *J. Am. Chem. Soc.*, 2010, **132**, 7832-7833.
37. L. E. Kreno, J. T. Hupp and R. P. Van Duyne, *Anal. Chem.*, 2010, **82**, 8042-8046.
38. G. Lu, O. K. Farha, L. E. Kreno, P. M. Schoenecker, K. S. Walton, R. P. Van Duyne and J. T. Hupp, *Adv. Mater.*, 2011, **23**, 4449-4452.
39. S. Achmann, G. Hagen, J. Kita, I. Malkowsky, C. Kiener and R. Moos, *Sensors*, 2009, **9**, 1574-1589.
40. R. Haldar, R. Matsuda, S. Kitagawa, S. J. George and T. K. Maji, *Angew. Chem.*, 2014, **126**, 11966-11971.
41. A. Schneemann, V. Bon, I. Schwedler, I. Senkovska, S. Kaskel and R. A. Fischer, *Chem. Soc. Rev.*, 2014, **43**, 6062-6096.
42. T. Loiseau, C. Serre, C. Huguenard, G. Fink, F. Taulelle, M. Henry, T. Bataille and G. Férey, *Chem. Eur. J.*, 2004, **10**, 1373-1382.
43. F. Millange, N. Guillou, R. I. Walton, J.-M. Greneche, I. Margiolaki and G. Ferey, *Chem. Commun.*, 2008, 4732-4734.
44. F. Millange, C. Serre and G. Ferey, *Chem. Commun.*, 2002, 822-823.
45. J. P. S. Mowat, V. R. Seymour, J. M. Griffin, S. P. Thompson, A. M. Z. Slawin, D. Fairen-Jimenez, T. Duren, S. E. Ashbrook and P. A. Wright, *Dalton Trans.*, 2012, **41**, 3937-3941.
46. C. Volkringer, T. Loiseau, N. Guillou, G. Ferey, E. Elkaim and A. Vimont, *Dalton Trans.*, 2009, 2241-2249.
47. E. V. Anokhina, M. Vougo-Zanda, X. Wang and A. J. Jacobson, *J. Am. Chem. Soc.*, 2005, **127**, 15000-15001.
48. D. Fairen-Jimenez, S. A. Moggach, M. T. Wharmby, P. A. Wright, S. Parsons and T. Düren, *J. Am. Chem. Soc.*, 2011, **133**, 8900-8902.
49. (a) A. Modrow, D. Zargarani, R. Herges and N. Stock, *Dalton Trans.*, 2011, **40**, 4217-4222; (b) J. W. Brown, B. L. Henderson, M. D. Kiesz, A. C. Whalley, W. Morris, S. Grunder, H. Deng, H. Furukawa, J. I. Zink, J. F. Stoddart and O. M. Yaghi, *Chem. Sci.*, 2013, **4**, 2858-2864.
50. S. M. Cohen, *Chem. Rev.*, 2012, **112**, 970-1000.
51. (a) Z. Wang and S. M. Cohen, *J. Am. Chem. Soc.*, 2007, **129**, 12368-12369; (b) K. K. Tanabe, Z. Wang and S. M. Cohen, *J. Am. Chem. Soc.*, 2008, **130**, 8508-8517.

52. (a) S. S.-Y. Chui, S. M.-F. Lo, J. P. H. Charmant, A. G. Orpen and I. D. Williams, *Science*, 1999, **283**, 1148-1150; (b) T. Yamada and H. Kitagawa, *J. Am. Chem. Soc.*, 2009, **131**, 6312-6313.

53. (a) J. An, S. J. Geib and N. L. Rosi, *J. Am. Chem. Soc.*, 2009, **131**, 8376-8377; (b) J. An and N. L. Rosi, *J. Am. Chem. Soc.*, 2010, **132**, 5578-5579; (c) J. An, C. M. Shade, D. A. Chengelis-Czegan, S. Petoud and N. L. Rosi, *J. Am. Chem. Soc.*, 2011, **133**, 1220-1223; (d) D. T. Genna, A. G. Wong-Foy, A. J. Matzger and M. S. Sanford, *J. Am. Chem. Soc.*, 2013, **135**, 10586-10589; (e) Y. Liu, G. Li, X. Li and Y. Cui, *Angew. Chem.*, 2007, **119**, 6417-6420.

54. M. Kim, J. F. Cahill, H. Fei, K. A. Prather and S. M. Cohen, *J. Am. Chem. Soc.*, 2012, **134**, 18082-18088.

55. (a) S. R. J. Oliver, *Chem. Soc. Rev.*, 2009, **38**, 1868-1881; (b) A. Schoedel, L. Wojtas, S. P. Kelley, R. D. Rogers, M. Eddaoudi and M. J. Zaworotko, *Angew. Chem. Int. Ed.*, 2011, **50**, 11421-11424; (c) G. Nickerl, A. Notzon, M. Heitbaum, I. Senkovska, F. Glorius and S. Kaskel, *Crystal Growth & Design*, 2013, **13**, 198-203.

56. X. Zhao, X. Bu, T. Wu, S.-T. Zheng, L. Wang and P. Feng, *Nat. Commun.*, 2013, **4**.

57. H. Fei, D. L. Rogow and S. R. J. Oliver, *J. Am. Chem. Soc.*, 2010, **132**, 7202-7209.

58. A. Nalaparaju and J. Jiang, *J. Phys. Chem. C*, 2012, **116**, 6925-6931.

59. Q. Hu, J. Yu, M. Liu, A. Liu, Z. Dou and Y. Yang, *J. Med. Chem.*, 2014, **57**, 5679-5685.

60. B. Manna, A. K. Chaudhari, B. Joarder, A. Karmakar and S. K. Ghosh, *Angew. Chem.*, 2013, **125**, 1032-1036.

61. T. K. Maji, R. Matsuda and S. Kitagawa, *Nat. Mater.*, 2007, **6**, 142-148.

62. (a) W. Wang and D. Yuan, *Sci. Rep.*, 2014, **4**; (b) I. Cabasso, S. Li, X. Wang and Y. Yuan, *RSC Adv.*, 2012, **2**, 4079-4091.

63. M. G. Stevens, K. M. Sellers, H. C. Foley and S. Subramoney, *Chem. Commun.*, 1998, 2679-2680.

64. C. Merlet, B. Rotenberg, P. A. Madden, P.-L. Taberna, P. Simon, Y. Gogotsi and M. Salanne, *Nat. Mater.*, 2012, **11**, 306-310.

65. Y. L. Nagy L. Torad, Shinsuke Ishihara, Katsuhiko Ariga, Yuichiro Kamachi, Hong-Yuan Lian, Hicham Hamoudi, Yoshio Sakka, Watcharop Chaikittisilp, Kevin C.-W. Wu and Yusuke Yamauchi, *Chem. Lett.*, 2014, **43**, 2.

66. (a) W. Chaikittisilp, K. Ariga and Y. Yamauchi, *J. Mater. Chem. A*, 2013, **1**, 14-19; (b) J. Hu, H. Wang, Q. Gao and H. Guo, *Carbon*, 2010, **48**, 3599-3606.

67. J. L. C. Rowsell and O. M. Yaghi, *J. Am. Chem. Soc.*, 2006, **128**, 1304-1315.
68. H. Li, M. Eddaoudi, M. O'Keeffe and O. M. Yaghi, *Nature*, 1999, **402**, 276-279.
69. A. Comotti, S. Bracco, P. Sozzani, S. Horike, R. Matsuda, J. Chen, M. Takata, Y. Kubota and S. Kitagawa, *J. Am. Chem. Soc.*, 2008, **130**, 13664-13672.
70. K. S. Park, Z. Ni, A. P. Côté, J. Y. Choi, R. Huang, F. J. Uribe-Romo, H. K. Chae, M. O'Keeffe and O. M. Yaghi, *Proceedings of the National Academy of Sciences*, 2006, **103**, 10186-10191.
71. A. Aijaz, N. Fujiwara and Q. Xu, *J. Am. Chem. Soc.*, 2014, **136**, 6790-6793.
72. B. Liu, H. Shioyama, T. Akita and Q. Xu, *J. Am. Chem. Soc.*, 2008, **130**, 5390-5391.
73. D. Yuan, J. Chen, S. Tan, N. Xia and Y. Liu, *Electrochem. Commun.*, 2009, **11**, 1191-1194.
74. K. Jayaramulu, K. K. R. Datta, K. Shiva, A. J. Bhattacharyya, M. Eswaramoorthy and T. K. Maji, *Microporous Mesoporous Mater.*, 2015, **206**, 127-135.
75. M. Hu, J. Reboul, S. Furukawa, N. L. Torad, Q. Ji, P. Srinivasu, K. Ariga, S. Kitagawa and Y. Yamauchi, *J. Am. Chem. Soc.*, 2012, **134**, 2864-2867.
76. A.-M. Alexander and J. S. J. Hargreaves, *Chem. Soc. Rev.*, 2010, **39**, 4388-4401.
77. (a) A. Thomas, A. Fischer, F. Goettmann, M. Antonietti, J.-O. Muller, R. Schlogl and J. M. Carlsson, *J. Mater. Chem.*, 2008, **18**, 4893-4908; (b) J. Zhu, P. Xiao, H. Li and S. A. C. Carabineiro, *ACS Applied Materials & Interfaces*, 2014, **6**, 16449-16465; (c) Y. Zhang, Q. Pan, G. Chai, M. Liang, G. Dong, Q. Zhang and J. Qiu, *Sci. Rep.*, 2013, **3**.
78. (a) M. Hu, J. Reboul, S. Furukawa, L. Radhakrishnan, Y. Zhang, P. Srinivasu, H. Iwai, H. Wang, Y. Nemoto, N. Suzuki, S. Kitagawa and Y. Yamauchi, *Chem. Commun.*, 2011, **47**, 8124-8126; (b) L. Radhakrishnan, J. Reboul, S. Furukawa, P. Srinivasu, S. Kitagawa and Y. Yamauchi, *Chem. Mater.*, 2011, **23**, 1225-1231; (c) S. Pandiaraj, H. B. Aiyappa, R. Banerjee and S. Kurungot, *Chem. Commun.*, 2014, **50**, 3363-3366.
79. K. Jayaramulu, N. Kumar, A. Hazra, T. K. Maji and C. N. R. Rao, *Chem. Eur. J.*, 2013, **19**, 6966-6970.

Chapter 2

A Bimodal Anionic MOF: Turn-off Sensing for Cu^{II} and Specific Sensitization of Eu^{III}

A manuscript based on this work has been published in *Chem. Commun.*, 2014, 50, 13567.

Abstract

This chapter describes the synthesis of a novel porous anionic metal-organic framework (AMOF) {[$Mg_3(ndc)_{2.5}(HCO_2)_2(H_2O)$][$NH_2Me_2$]·$2H_2O$·DMF}(**1**) and its metal ion sequestration and sensing properties. In this AMOF, the stoichiometric ratio is such that the framework itself is anionic, however the overall charge neutrality of the framework is maintained by exchangeable dimethyl amine (DMA) cations residing in the 1D channels. These DMA cations can undergo facile exchange with other exogenous cationic species in order to suit specific applications. When **1** is made to undergo cation exchange with Cu^{II}, the characteristic blue emission of **1** is quenched in the Cu^{II} exchanged compound (**Cu^{II}@1'**). Moreover, the colour of **1** changes from white to bright green in **Cu^{II}@1'**. Hence **1** can provide a fast fluorescence read-out for sensing Cu^{II}. Also, the framework is capable of encapsulating several lanthanide cations, e.g., Eu^{III}, Tb^{III}, Sm^{III} and Dy^{III}. However, it can selectively sensitize Eu^{III} resulting in a bright red luminescent framework. Through cation exchange, **1** manifests bimodal functionality, being a turn-off sensor of Cu^{II} on one hand, and a selective sensitizer of Eu^{III} emitting intense pure red emission on the other.

2.1 Introduction

Zeolites, the much studied microporous aluminosilicates, are established ion exchangers owing to the presence of extra framework cations.[1] However, zeolites do not allow the functionalization of pore surfaces and thus selective sequestration and read-out signalling of a specific metal cation is not possible. This drawback has been overcome in metal-organic frameworks (MOFs), which are tunable porous materials with modifiable pore surfaces and functionalities.[2] The efficiency of MOFs in gas storage and separation,[3] catalysis, drug delivery and optoelectronic devices are well documented[2b]. However, unlike zeolites, ion exchange is infrequent in MOFs,[4] which are generally neutral in nature. Applying proper synthetic strategies, it is possible to get anionic MOFs (AMOFs),[5] where the cationic guest molecules can undergo facile exchange with other exogenous cationic species. Such post-synthetically modified AMOFs have already shown potential in second harmonic generation,[5a, 5c] drug delivery,[5d] tunable adsorption,[5g] and catalysis.[5b, 5e] However the chemical affinity of the coordination spaces determines the selective capture of a specific metal ion, therefore proper functionalization of pore surface is crucial.[6] Furthermore flexible cation exchangeable nano-spaces constructed from chromophoric linkers would provide a fast fluorescence read-out of the recognition process through change in emission intensity for a particular metal ion leading to sensory MOFs. Hence, it should have correct pore window dimensions and proper stabilization environment, preferably the presence of Lewis basic sites for better interaction with the specific metal cation. Selective uptake of Cu^{II} ion by such AMOFs would be particularly interesting as this strategy would ensue a novel route for Cu^{II} sensing,[7] which is of paramount importance for biological applications. The study of prognosis of copper imbalance related diseases, e.g., Menkes, Wilson and Alzheimer's diseases, prion disorders, and amyotrophic lateral sclerosis demand effective sensing and removal of copper[8] in biological systems. Also, by exploiting the cation exchange in AMOFs, new luminescent materials can be designed by inclusion of lanthanide (Ln) ions. The role of the AMOF as a light harvesting antenna for sensitizing Ln^{III} cations to furnish novel Ln-doped luminescent materials and new Ln sensors has been studied previously.[9] However, selective Eu^{III} sensitization by an AMOF is very unusual and finds its application in low-energy driven pure red emitters in optoelectronic devices and also for biological labelling.[10]

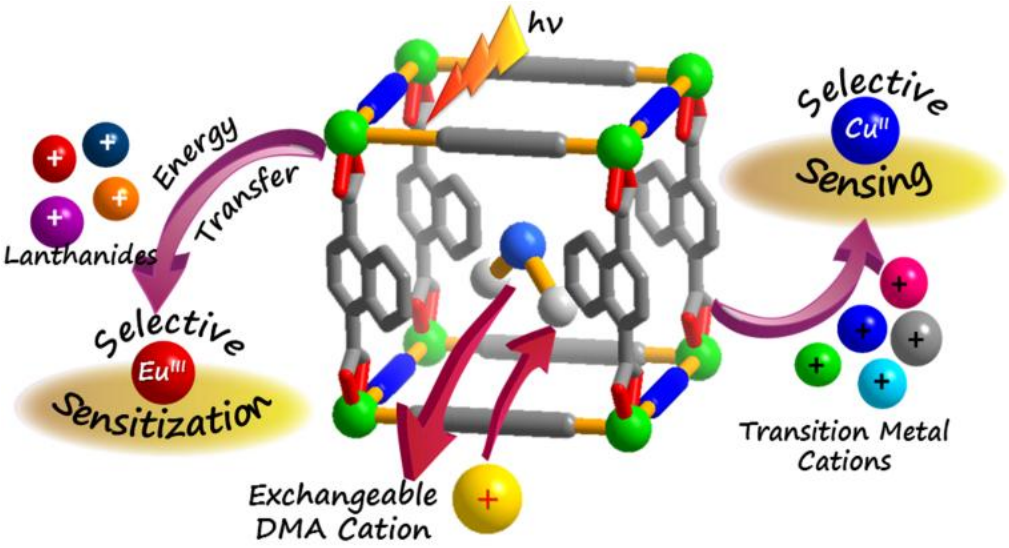

Scheme 1: Schematic representation of the bimodal functionalities in **1** through cation exchange.

This chapter describes the synthesis and structural characterization of a 3D anionic MOF, $\{[Mg_3(ndc)_{2.5}(HCO_2)_2(H_2O)][NH_2Me_2]\cdot 2H_2O\cdot DMF\}$ (**1**) [ndc: 1,4-naphthalenedicarboxylate] and its metal ion sequestration and sensing properties. The framework contains 1D channels occupied by the cationic guest $\mathbf{NH_2Me_2^+}$ [dimethyl ammonium (**DMA**)] which can be selectively replaced by Cu^{II} ions among other transition metal cations. Moreover the framework can encapsulate several lanthanide metal ions but selectively sensitize Eu^{III} resulting in a bright red luminescent framework (Scheme 1). Such bimodal functionalities of specific sensing[11] and removal of a transition metal (Cu^{II}) and selective sensitization of a lanthanide metal (Eu^{III}) based on luminescence quenching and enhancing respectively using a single framework system is really unique.

2.2 Experimental Section

2.2.1 Materials

All the reagents and solvent were used as obtained from commercial supplies without any further purification. 1,4-Naphthalene dicarboxylic acid(ndc) and the metal salts used were procured from Alfa Aesar and Aldrich Chemical Co. Ltd. respectively.

2.2.2 Synthesis of $[Mg_3(ndc)_{2.5}(HCO_2)_2(H_2O)(NH_2Me_2)]\cdot 2H_2O\cdot DMF$ (1)

$Mg(NO_3)_2\cdot 6H_2O$(1mmol, 256mg) and 1,4-ndc(1mmol, 216mg) were mixed well in 20 mL DMF. Then a few drops of water were added and the mixture was sonicated for 10 mins. The resulting mixture was transferred into a Teflon sealed autoclave and the system was kept at 120ºC for two days. On cooling colourless single crystals of **1** were obtained.Yield:76% relative to Mg^{II}. Anal. Calculated for $C_{37}H_{37}Mg_3O_{18}N_2$: H:4.28 C:51.04 N: 3.22% Found: H: 4.12 C: 51.63 N:3.27%

2.2.3 Preparation of M^{II}@1' and Ln^{III}@1'

For preparing the different metal ion exchanged compounds, **1** is activated at 110°C under high vacuum overnight before immersing it in the respective metal ion solutions. 50 mg of activated **1**(**1'**) is immersed in 30 mL 0.01 (M) M^{II} (where M is any transition metal) solutions in ethanol for 7 days and the solution is changed daily within these 7 days. For Stern-Volmer plots, **1'** is dipped in standard solutions for 7 days as mentioned in the main text. Then it is washed repeatedly with ethanol. For **Ln^{III}@1'**, 0.01 (M) solutions of $Eu^{III,}$ $Dy^{III,}$ Tb^{III} and Sm^{III} are used in the same way.

2.2.4 Physical Measurements

The elemental analysis was carried out using a Thermo Fischer Flash 2000 Elemental Analyzer. Thermogravimetric analysis (TGA) was carried out (Mettler Toledo) in nitrogen atmosphere (flow rate = 50 mL min^{-1}) in the temperature range 30 – 550 °C (heating rate = 3°C min-1). Powder XRD pattern was recorded by using Cu-Kα radiation (Bruker D8 Discover; 40 kV, 30 MA). Electronic absorption spectra were recorded on a Perkin Elmer Lambda 750 UV-VIS-NIR Spectrometer and emission spectra were recorded on Perkin Elmer Ls 55 Luminescence Spectrometer. Solid state UV spectrum was recorded in reflectance mode. IR spectra of the compounds were recorded on a Bruker IFS 66v/S spectrophotometer using the KBr pellets in the region 4000−400 cm^{-1}. Inductively Coupled Plasma-Optical Emission Spectroscopy (ICP-OES) measurements were recorded on Perkin Elmer Optima 7000dv ICP-OES.

2.2.5 Crystallography

A suitable single crystal of compound 1 was mounted on a thin glass fibre with commercially available super glue. X-ray single crystal structural data were collected on a Bruker Smart-CCD diffractometer equipped with a normal focus, 2.4 kW sealed tube X-ray source with graphite monochromated Mo-Kα radiation (λ = 0.71073 Å) operating at 50 kV and 30 mA. The program SAINT[12] was used for the integration of diffraction profiles and absorption correction was made with SADABS[13] program. All the structures were solved by SIR 92[14] and refined by full matrix least square method using SHELXL.[15] All the hydrogen atoms were fixed by HFIX and placed in ideal positions. Potential solvent accessible area or void space was calculated using the PLATON[16] multipurpose crystallographic software. All crystallographic and structure refinement data of **1** is summarized in Table 1. All calculations were carried out using SHELXL 97,[15] PLATON,[16] SHELXS 97 [15] and WinGX system, Ver 1.80.05.[17]

2.2.6 Preparation of Sample for Adsorption

Adsorption isotherms of CO_2 at 195 K and N_2 at 77 K were recorded with the dehydrated sample using QUANTACHROME QUADRASORB-SI analyzer. To prepare the dehydrated sample of **1** (**1'**) approximately 100 mg of sample was taken in a sample holder and degassed at 110ºC under 10^{-1} pa vacuum for about 12hours prior to the measurements. Dead volume of the sample cell was measured using helium gas of 99.999% purity. The amount of gas adsorbed was calculated from the pressure difference ($P_{cal} - P_e$), where P_{cal} is the calculated pressure with no gas adsorption and P_e is the observed equilibrium pressure. All the operations were computer-controlled and automatic.

2.2.7 Characterization

The phase purity was checked by comparing the PXRD pattern (**Fig. 1**) of the bulk powder sample with the simulated data from single-crystal data. The phase purity of the compound is confirmed by the similarity between simulated and as-synthesized patterns. The IR spectrum was also recorded (**Fig. 2(a)**).

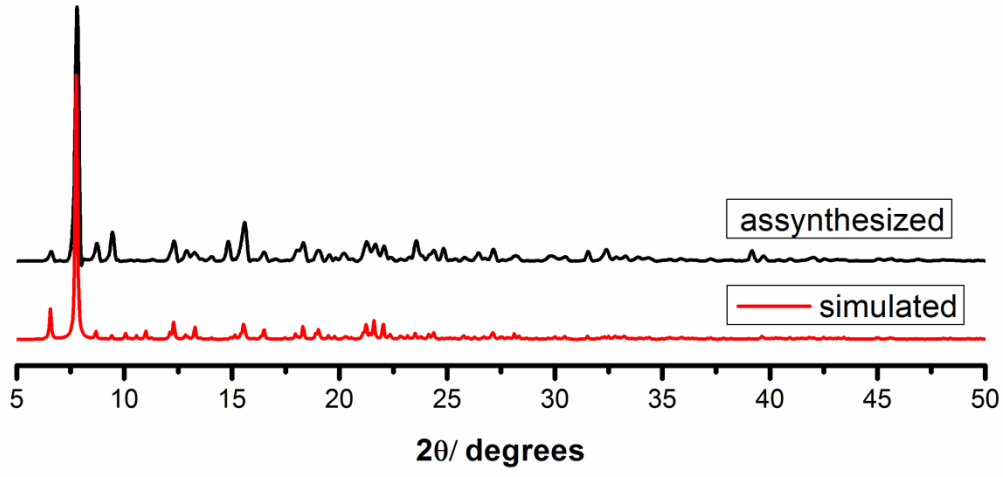

Fig. 1 The simulated and as-synthesized PXRD pattern of **1**.

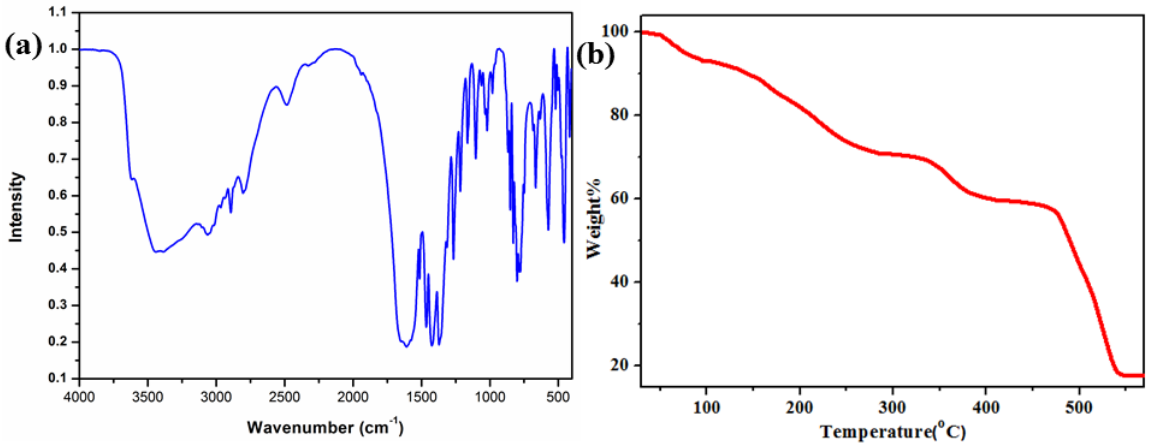

Fig. 2(a) FT-IR spectrum of **1 (b)** TGA analysis for **1**.

Table 1: Principal Peaks in IR (**Fig. 2(a)**)

Peak Position	Nature	Vibration
1640 cm^{-1}	strong	C=O stretch
795 cm^{-1}	strong	Aromatic C-H stretch
1269, 1374 cm^{-1}	strong	C-N stretch
2809, 3063 cm^{-1}	strong, broad	N-H stretch

The thermogravimetric analysis (TGA) of **1** shows an initial ~6% weight loss corresponding to 1 coordinated water and 2 guest water molecules till 100°C. Next ~ 8% weight loss till 170°C corresponds to one DMF molecule. Beyond this the framework starts decomposing continuously (**Fig. 2(b)**).

2.3 Results and Discussion

2.3.1 Crystal Structure Description

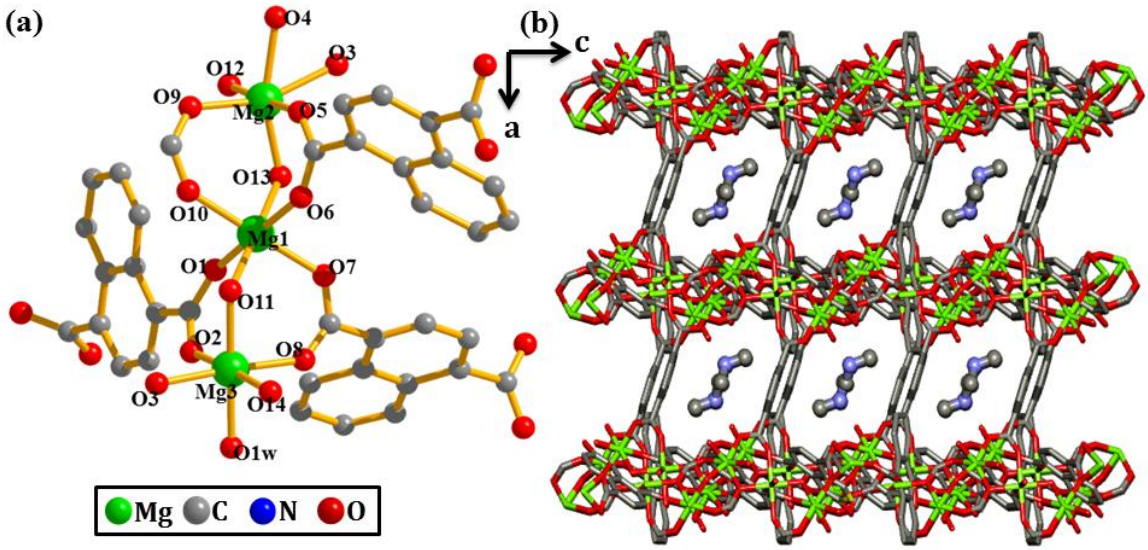

Fig. 3 (a) Coordination environment of Mg^{II} centers in **1 (b)** View of 3D framework of **1** along *b* axis showing DMA cations in the pore

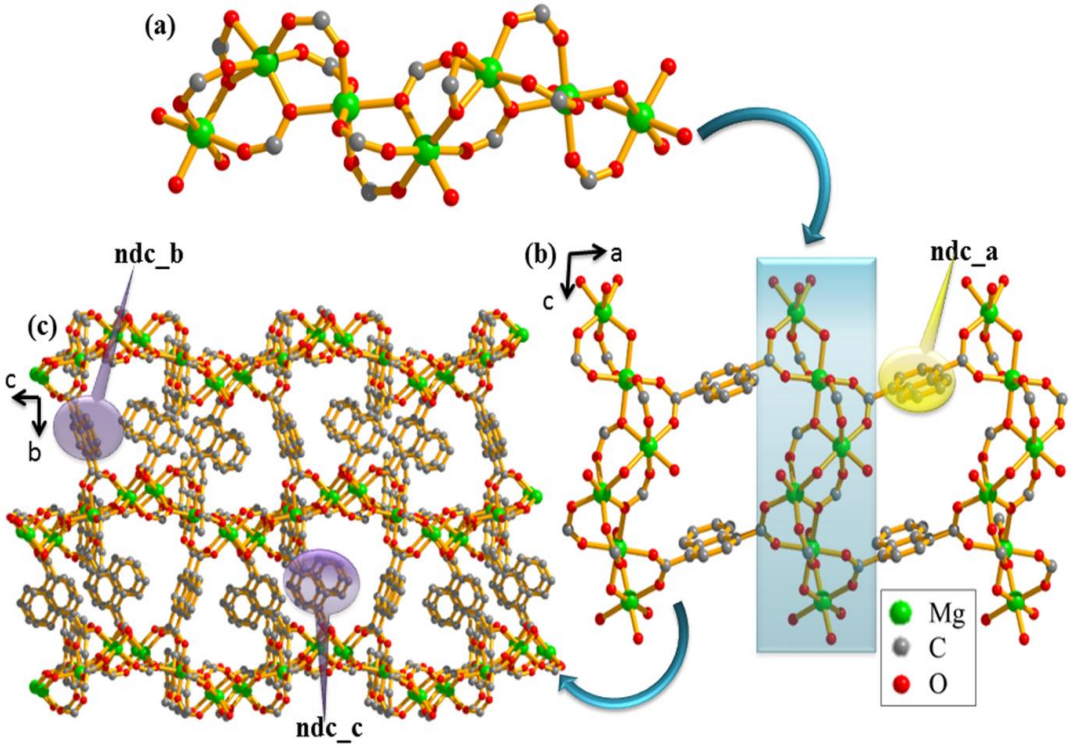

Fig. 4 (a) 1D chain of **1** along crystallographic *c* direction **(b)** 2D sheet of **1** along the crystallographic *ac* plane **(c)** View of 3D network of **1** along crystallographic *a* axis

Single crystal X-ray diffraction analysis reveals that compound **1** crystallizes in $P2_1/c$ space group. Each asymmetric unit contains three crystallographically independent hexa-coordinated Mg^{II} centers, all of which are distorted from perfectly octahedral geometry (**Fig. 3(a)**). The hexa-coordination of Mg1 is fulfilled by oxygen atoms (O1, O6, O7 and O10) from three different ndc ligands and two oxygen atoms (O11 and O13) from two different formate ligands. Mg2 adopts a similar coordination environment with O3, O4, O5 and O9 atoms from ndc and O12 and O13 from formate ligands. In case of Mg3, three oxygens from three different ndc moieties (O2, O3, and O8), two oxygen atoms (O11 and O14) from formate and one coordinated water molecule (O1w) ligate to fulfill the hexa-coordination (**Fig. 3(a)**). Mg1 and Mg3 centers are bridged to each other through two ndc and one formate ligands. Mg1 and Mg2 centers are also connected similarly. Thus three Mg^{II} centers are arranged to form a 1D chain along *c* direction (**Fig. 4(a)**). These 1D chains are further connected with each other through ndc_a molecules to generate a 2D network in the crystallographic *ac* plane (**Fig. 4(b)**). These 2D sheets are further cross-linked by ndc_b and ndc_c and repeat themselves along *b* direction to generate the 3D framework (**Fig. 4(c)**) with 1D channels occupied by the guest H_2O, DMF and extra framework DMA cations (**Fig. 3(b)**). The formate and DMA cations are formed *in situ* from DMF under solvothermal conditions[5d, 5e]. The solvent accessible void space of the desolvated framework (**1'**) is 28% including the cation.

Table 2. Crystal Data and Structure Refinement for $[Mg_3(ndc)_{2.5}(HCO_2)_2(H_2O)(NH_2Me_2)]\cdot 2H_2O\cdot DMF$ (CCDC number: 1017348)

Parameter	**1**
Empirical formula	$C_{37}H_{37}Mg_3O_{18}N_2$
Formula weight	870.61
Crystal system	*Monoclinic*
Space group	*P21/c* (No.14)
a, Å	11.3593(4)
b, Å	22.5823(8)
c, Å	16.5923(5)
β, deg	92.129(2)
V, Å^3	4253.3(2)
Z	4
T, K	120
μ,mm^{-1}	0.147
D_{calcd},g/cm^3	1.353
F (000)	1796
reflections [$I>2\sigma(I)$]	3619
unique reflections	7457
measured reflections	57145
R_{int}	0.185
GOF on F^2	1.01
$R_1[I>2\sigma(I)]$[a]	0.0992
$R_w[I>2\sigma(I)]$[b]	0.2988

($R = \sum||F_o|-|F_c||/\sum|F_o|$,$R_w = [\sum\{w(F_o^2-F_c^2)^2\}/\sum\{w(F_o^2)^2\}]^{1/2}$)

Table 3. Selected bond distances (Å) for **1**.

Mg1-O1	2.011(5)	Mg2-O13	2.047(5)
Mg1-O6	2.036(5)	Mg2-O9	2.023(5)
Mg1-O11	2.114(5)	Mg2-O3	2.125(5)
Mg1-O13	2.134(5)	Mg2-O4	2.183(5)
Mg1-O7	2.063(5)	Mg2-O12	2.041(5)

Table 4. Selected bond angles (°) of Compound **1**.

O1-Mg1-O6	176.4(2)	O3-Mg2-O12	90.7(2)
O1-Mg1-O7	90.7(2)	O4-Mg2-O12	91.9(2)
O1w-Mg3-O2	88.8(2)	O3-Mg2-O5	88.1(2)
O1-Mg1-O11	91.3(2)	O6-Mg1-O11	91.3(2)
O2-Mg3-O8	90.9(2)	O4-Mg2-O5	85.0(2)
O1w-Mg3-O11	177.0(2)	O1-Mg1-O10	91.3(2)

2.3.2 Adsorption Properties

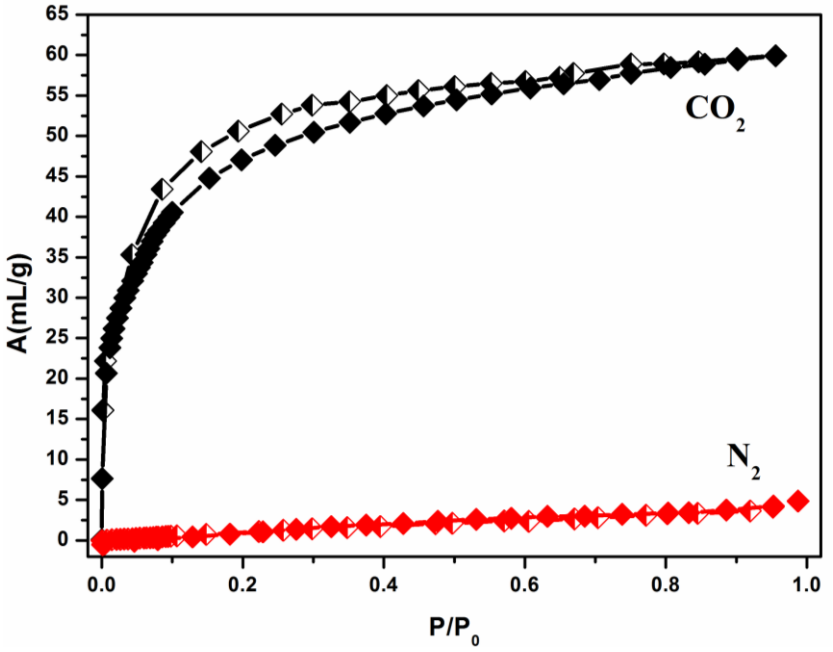

Fig. 5 N_2 (red) and CO_2 (black) adsorption isotherms of **1'**

To check the adsorption properties, **1** is activated at 110°C under high vacuum overnight to prepare **1'**. **1'** shows type-1 CO_2 adsorption isotherm at 195 K, while N_2

adsorption reveals only surface adsorption (**Fig. 5**). The typical type I adsorption profile clearly indicates that **1** is microporous in nature. The preferential interaction of CO_2 with **1'** could be attributed to the presence of polar carboxylate groups and unsaturated Mg^{II} sites in **1'**, which can interact well with the quadruple moment of CO_2.[18]

2.3.3 Cation Exchange

The presence of guest DMA cations and several carboxylate oxygen atoms on the pore surface prompted us to study the exchange properties of **1** with different transition metal cations by immersing **1'** in 0.01M solutions of different metal chlorides. Inductively Coupled Plasma Optical Emission Spectroscopy (ICP-OES) analysis of the exchanging solution showed the absence of Mg^{II} ions, implying that only the guest DMA cations are exchanged. Also ICP analysis of resulting samples showed that 88% of the DMA guests are exchanged with Cu^{II} ions, while the extent of exchange for Mn^{II}, Co^{II}, Ni^{II} and Zn^{II} are 0, 4, 12 and 0% respectively (**Fig. 6(a), Table 5**). This high percentage of exchange for Cu^{II} is evident as a green solution of Cu^{II} in ethanol becomes colourless on immersing **1'** in it, while the white solid **1'** yields bright green **Cu^{II}@1'** (**Fig. 6(b)**).

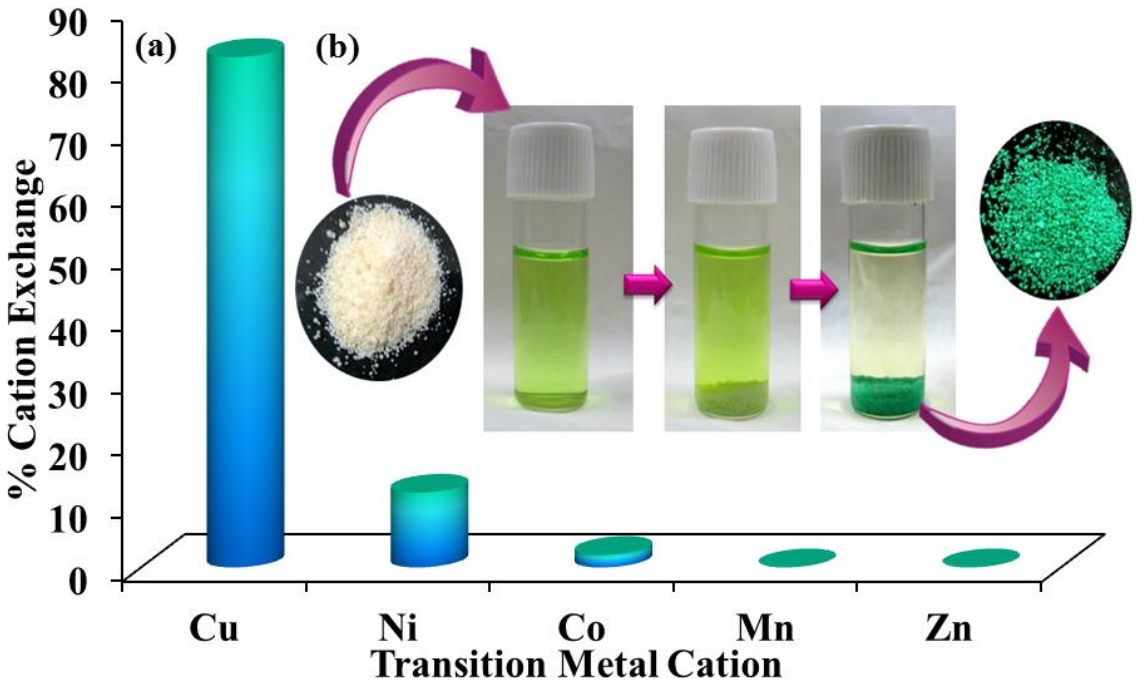

Fig. 6(a) Uptake of different cations by **1'** from an equimolar mixture of all the cations **(b)** Cu^{II} exchange in **1'** in ethanol medium

Table 5: ICP-MS data for cation exchange in individual cation solutions (0.01M of each metal cation)

Sl. No.	Cation	Number of Cations per Formula Unit	Maximum Number of Cations Possible per Formula Unit	% Exchange of Cation with DMA
1	Mn^{II}	0	0.5	0.0
2	Co^{II}	0.02	0.5	4
3	Ni^{II}	0.06	0.5	12
4	Cu^{II}	0.44	0.5	88
5	Zn^{II}	0	0.5	0.0

2.3.3.1 Selective Cu^{II} Sensing

As evident from the ICP-OES data, Cu^{II} uptake is more than other transition metal cations. The Cu^{II} uptake amount can also be quantified from the UV spectrum of the Cu^{II} solution used for the exchange prcess. The decrease in the absorbance intensity of the UV spectra of the supernatant solution indicates that 84.5% DMA are exchanged with Cu^{II} (**Fig. 7**)

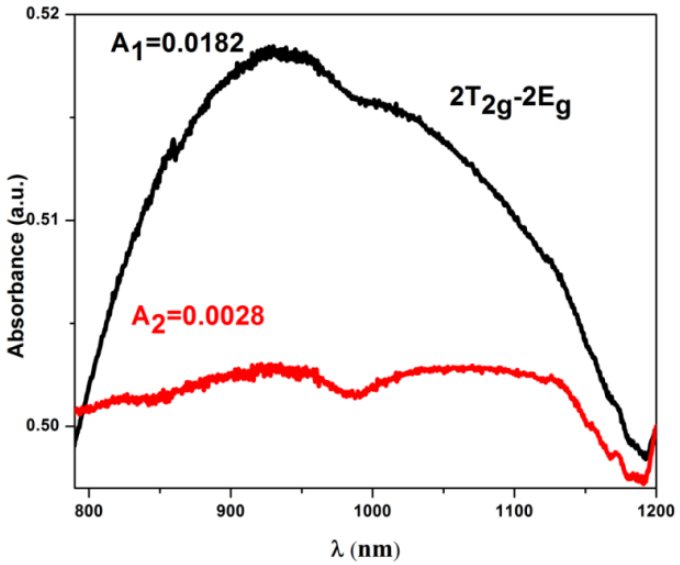

Fig. 7 UV-VIS spectra: (Black) Cu^{II} solution of $6.25x10^{-4}$ (M) and (Red) Cu^{II} solution obtained after immersing **1'** for 7 days

Due to d-d transition, a new band appears in the UV spectra of **Cu^{II}@1'** at ~720 nm in addition to the band at ~317 nm as observed in **1** (**Fig. 11**). This further supports the coordination of Cu^{II} with the carboxylate oxygens of **1**. Due to structural reorganization after encapsulation of Cu^{II}, there are some changes in the PXRD pattern of Cu^{II}@1' as well as the appearance of a few new peaks (**Fig. 8**).

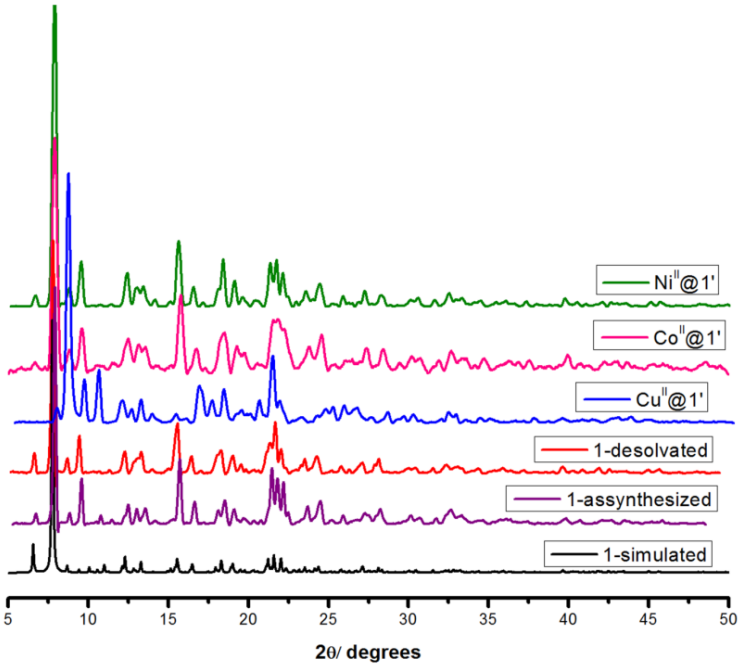

Fig. 8 PXRD patterns of **1** and **M^{II}@1'**, (where M^{II} is a transition metal cation)

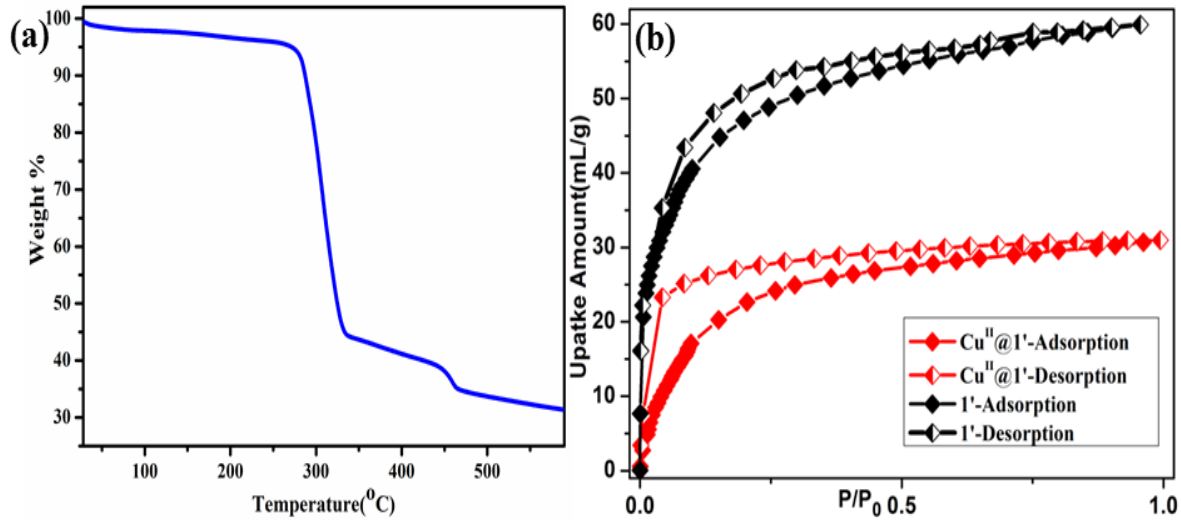

Fig. 9 (a) TGA for **Cu^{II}@1'**. **(b)** Comparison of the adsorption profile of **Cu^{II}@1'** with **1'**

The thermal stability of **Cu^{II}@1'** was also analysed and it was found that the framework is stable till 250°C after an initial loss of 2% (**Fig. 9(a)**).

The inclusion of Cu^{II} into the pore of **1** was further confirmed from the CO_2 adsorption isotherm (**Fig. 9(b)**) of **Cu^{II}@1'** at 195 K, which shows a 48% decrease in CO_2 uptake compared to that of **1**. This decrease in uptake may be attributed to the fact that Cu^{II} ions occupy the pores of **1** randomly, thus inhibiting the diffusion of CO_2. Furthermore, the Cu^{II} selectivity of **1** was studied by immersing **1'** in an equimolar solution of a mixture of Mn^{II} , Cu^{II}, Co^{II}, Ni^{II} and Zn^{II} ions. ICP-OES analysis confirmed the exchange of 85% of the DMA cations with Cu^{II}, which is much higher compared to the other metal ions (**Table 6**). This selective capture of Cu^{II} may be explained based on the flexible geometry of Cu^{II} owing to which it can be accommodated in a variety of coordination environments, unlike other transition metal ions.

Table 6: ICP-MS data for cation exchange in a mixture (0.01 (M) of each metal cation).

Sl. No.	Cation	Number of Cations per Formula Unit	Maximum Number of Cations Possible per Formula Unit	% Exchange of Cation with DMA
1	Mn^{II}	0	0.5	0.0
2	Co^{II}	0.016	0.5	3.2
3	Ni^{II}	0.090	0.5	17.9
4	Cu^{II}	0.423	0.5	84.5
5	Zn^{II}	0	0.5	0.0

Furthermore, **1** shows ndc linker based emission maximum at ~410 nm when excited at 317 nm in solid state (**Fig. 12(a)**). We anticipated that the emission intensities would be affected by the incorporation of Cu^{II} and this was validated by the significant quenching of emission in **Cu^{II}@1'**. The quenching of emission can be attributed to the ligand field splitting of d-orbitals of Cu^{II} resulting in reabsorption of emission energy by the framework. The XPS analysis clearly shows the different peaks for Cu $2p_{3/2}$ and $2p_{1/2}$, implying ligand field splitting of the d-orbitals of Cu in **Cu^{II}@1'** (**Fig. 10(a)**).

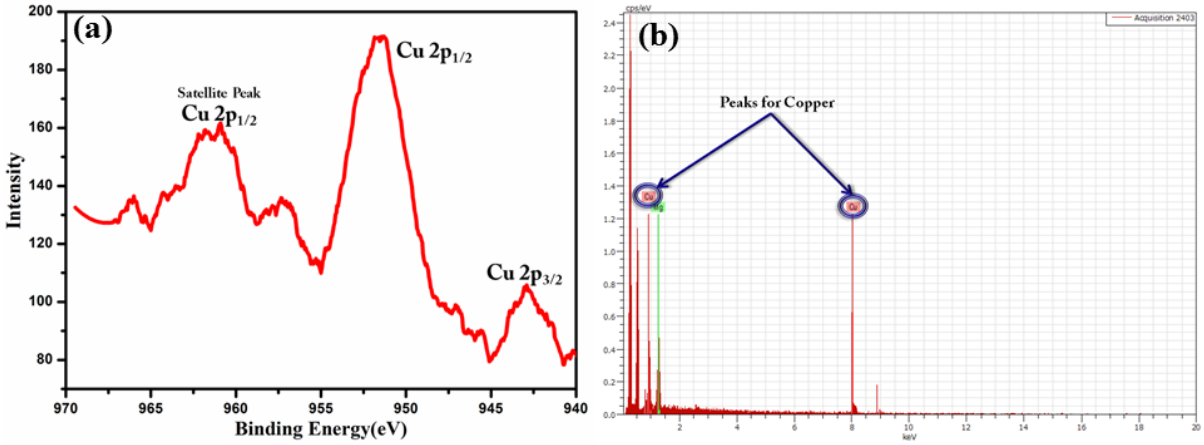

Fig 10(a) XPS data for Cu 2p in **Cu^{II}@1'. (b)** EDS analysis of **Cu^{II}@1'**. Peaks for Cu in the EDS analysis plot has been marked.

In order to check the sensing efficiency, **1'** was immersed in 10^{-3}, 10^{-4}, 10^{-5}, 10^{-6} and 10^{-9} M solutions of Cu^{II} and emission is quenched gradually as the concentration of the Cu^{II} solution increases (**Fig. 12(b)**). To determine the efficiency of **1** as a Cu^{II} sensor, the Stern-Volmer plot at room temperature(~30°C) was constructed and the quenching constant was found to be 1.986×10^3 M^{-1} (**Fig. 12(d)**), which decreased to 3.621×10^2 M^{-1} on repeating the experiment at 80°C (**Fig. 12(c) and (d)**). This suggests that the quenching follows a static mechanism, presumably by the complexation of Cu^{II} with **1'**. Increase in temperature decreases this complexation promoting the decrease in the quenching constant. The new band in the UV spectra at ~720 nm is also an evidence of the static quenching (**Fig. 11**).

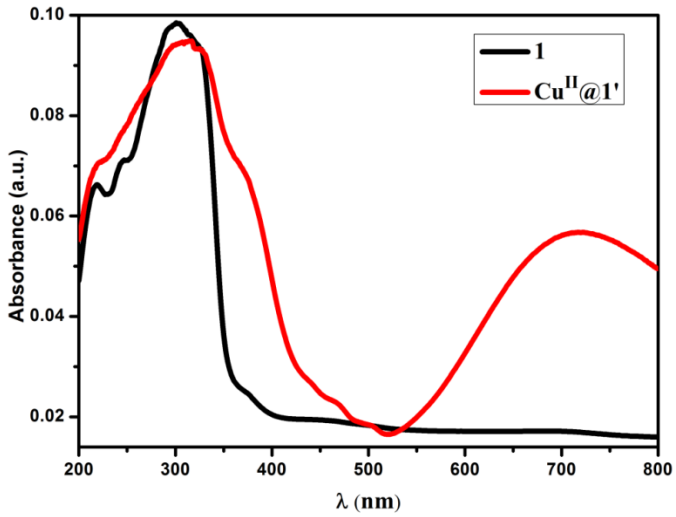

Fig. 11 UV-vis spectra of solid **1** and **Cu^{II}@1'**.

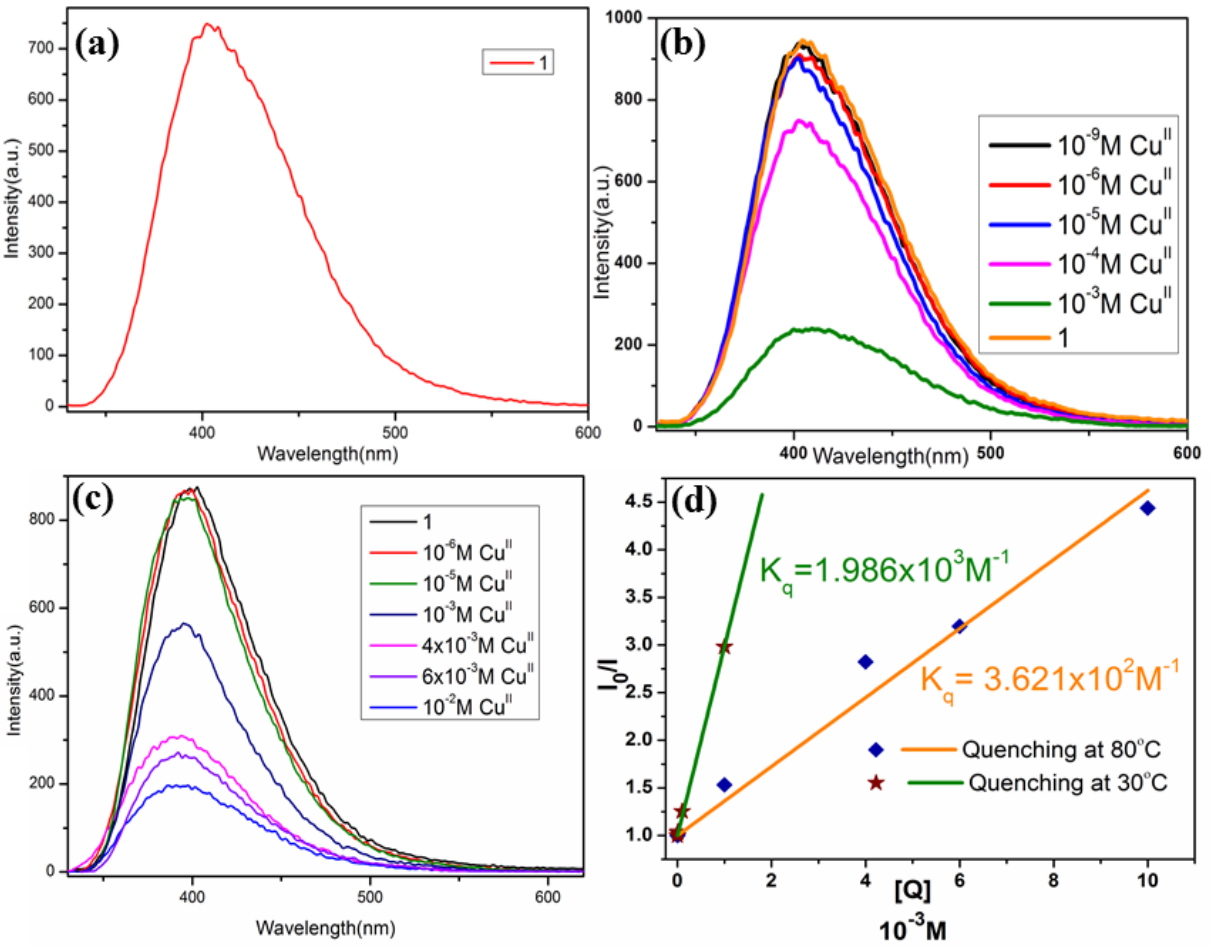

Fig. 12 (a) Characteristic emission spectrum of **1**. (b) Characteristic emission of **1** quenched by different concentration of Cu^{II} solutions at 30°C. (c) Characteristic emission of **1** quenched by different concentration of Cu^{II} solutions at 80°C. (d) Stern Volmer plot for quenching by Cu^{II} at 30°C and 80°C.

2.3.3.2 Selective Eu^{III} Sensitization

As the pore surface of **1** is studded with hard oxygen donors, we anticipated the framework to be a potential candidate for encapsulating different hard acid Ln^{III} cations. The Ln^{III} ions are capable of expanding the coordination spheres based on their flexible geometry. **Ln^{III}@1'** samples were prepared by immersing **1** in 0.01M solutions of nitrate salts of Eu^{III}, Tb^{III}, Sm^{III} and Dy^{III}. ICP-OES data suggests that the exchange is about 62% with Sm^{III}, 68 % with Eu^{III}, 75% with Tb^{III} and 77% with Dy^{III} in the respective exchanged compounds. After the exchange, structural integrity of **1** is maintained, as evident from the PXRD pattern (**Fig. 13**).

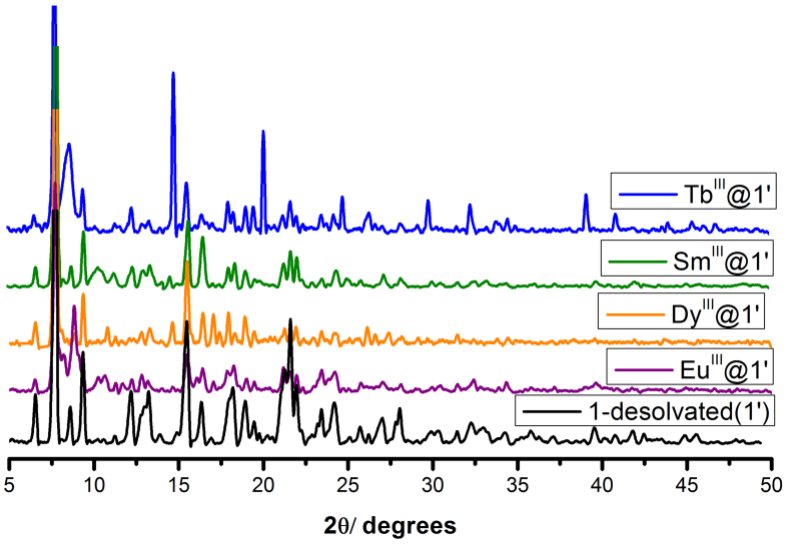

Fig. 134 PXRD patterns of **1** and **Ln^{III}@1'**,(where Ln^{III} is a lanthanide cation)

The emission properties of **Ln^{III}@1'** were studied since typically non emissive Ln^{III} ions were expected to furnish new luminescent materials through the antenna effect[19] when captured in the pores of **1'.** However, to our surprise, **1** fails to sensitize Dy^{III}, Sm^{III} or Tb^{III} which is evident from the absence of the characteristic peaks of Dy^{III}, Sm^{III} or Tb^{III} from emission spectra of the respective exchanged compounds when excited at 317 nm (**Fig. 14(a)**). Rather **Ln^{III}@1'** [Ln=Dy, Sm, Tb] samples show a blue emission similar to as-synthesized **1** which is observed under UV lamp (**Fig. 14(b)**). The emission spectrum of **Eu^{III}@1'** is rather remarkable, showing the appearance of characteristic emission bands of the Eu^{III} ion centred at 591, 615, 659, 693nm which can be attributed to the $^5D_0 \rightarrow {}^7F_{1\text{-}4}$ transitions. This is accompanied with concomitant decrease in the emission intensity of the AMOF at ~410 nm (**Fig. 14(a)**). The spectrum is dominated by the $^5D_0 \rightarrow {}^7F_2$ intense band and it is responsible for the brilliant red emission of the **Eu^{III}@1'** hybrid. This confirms that **1** acts as an antenna and selectively sensitizes Eu^{III}, although it takes up other Ln^{III} cations. Probably this unprecedented selective sensitization of Eu^{III} is realized due to the facile energy transfer to the excited $^5D_0$ state of Eu^{III} from the singlet excited states of **1**, which is not favourable in case of the other lanthanides.

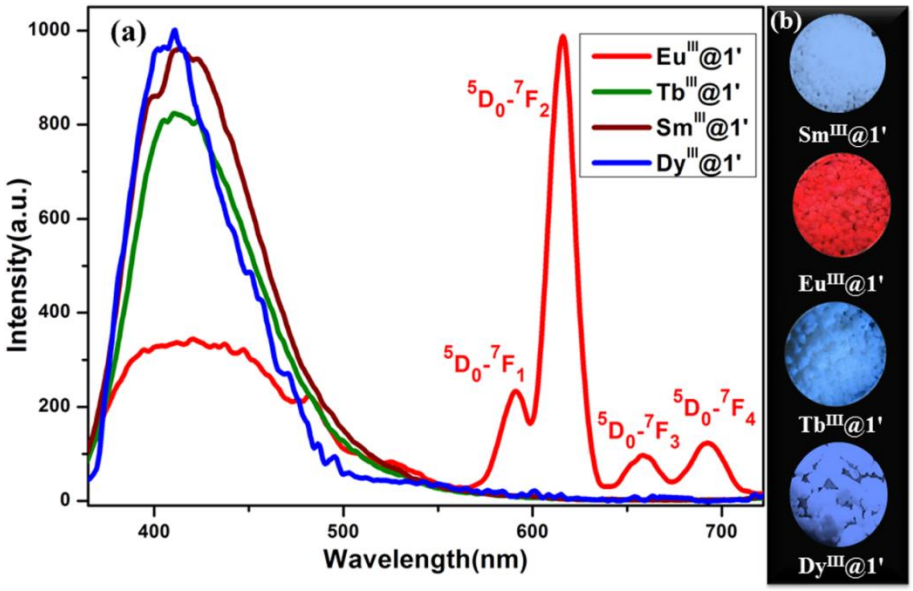

Fig. 14(a) Emission spectra of **Eu^{III}@1'**, **Tb^{III}@1'**, **Sm^{III}@1'** and **Dy^{III}@1'**.**(b)** Photographs of the respective samples under UV lamp

2.4 Conclusion

In conclusion, a new Mg based AMOF (**1**) with 1D cation exchangeable channels has been synthesized that has been exploited for selective sequestration for Cu^{II} ions. This can be realized through fluorescence read out by the turn-off of emission. The AMOF can also encapsulate several hard lanthanide metal ions through preferential binding with the hard oxygen centers. The Ln^{III} exchanged framework exhibits unprecedented specific sensitization for Eu^{III} resulting in a red luminescent material through Post Synthetic Modification. Such bimodal functionalities are accomplished through proper size and functionalities of the cation exchangeable channels in **1**. Inclusion of specific cationic groups in such AMOFs would also facilitate targeted fabrication of smart materials with versatile properties like catalytic activity, adsorption, magnetism, nonlinear optical response etc., which is currently being explored in our laboratory.

2.5 References

1. (a) P. Vanelderen, J. Vancauwenbergh, B. F. Sels and R. A. Schoonheydt, *Coord. Chem. Rev.*, 2013, **257**, 483-494; (b) J. Jiang, J. Yu and A. Corma, *Angew. Chem. Int. Ed.*, 2010, **49**, 3120-3145.
2. (a) R. Haldar and T. K. Maji, *CrystEngComm*, 2013, **15**, 9276-9295; (b) *Themed Issue: Metal-organic Frameworks Chem. Rev.*, 2012, **112**, 673-1268.
3. Z. Zhang, Z.-Z. Yao, S. Xiang and B. Chen, *Energy Environ. Sci.*, 2014, **7**, 2868-2899.
4. S. Y. Vyasamudri and T. K. Maji, *Chem. Phys. Lett.*, 2009, **473**, 312-316.
5. (a) Y. Liu, G. Li, X. Li and Y. Cui, *Angew. Chem.*, 2007, **119**, 6417-6420; (b) E. Quartapelle Procopio, F. Linares, C. Montoro, V. Colombo, A. Maspero, E. Barea and J. A. R. Navarro, *Angew. Chem. Int. Ed.*, 2010, **49**, 7308-7311; (c) J. Yu, Y. Cui, C. Wu, Y. Yang, Z. Wang, M. O'Keeffe, B. Chen and G. Qian, *Angew. Chem. Int. Ed.*, 2012, **51**, 10542-10545; (d) J. An, S. J. Geib and N. L. Rosi, *Journal of the American Chemical Society*, 2009, **131**, 8376-8377; (e) D. T. Genna, A. G. Wong-Foy, A. J. Matzger and M. S. Sanford, *J. Am. Chem. Soc.*, 2013, **135**, 10586-10589; (f) J. Tian, L. V. Saraf, B. Schwenzer, S. M. Taylor, E. K. Brechin, J. Liu, S. J. Dalgarno and P. K. Thallapally, *J. Am. Chem. Soc.*, 2012, **134**, 9581-9584; (g) S. Yang, X. Lin, A. J. Blake, G. S. Walker, P. Hubberstey, N. R. Champness and M. Schröder, *Nat Chem*, 2009, **1**, 487-493.
6. S. Yang, G. S. B. Martin, J. J. Titman, A. J. Blake, D. R. Allan, N. R. Champness and M. Schröder, *Inorg. Chem.*, 2011, **50**, 9374-9384.
7. K. Jayaramulu, R. P. Narayanan, S. J. George and T. K. Maji, *Inorg. Chem.*, 2012, **51**, 10089-10091.
8. T. Hirayama, G. C. Van de Bittner, L. W. Gray, S. Lutsenko and C. J. Chang, *Proceedings of the National Academy of Sciences*, 2012, **109**, 2228-2233.
9. (a) J.-S. Qin, S.-J. Bao, P. Li, W. Xie, D.-Y. Du, L. Zhao, Y.-Q. Lan and Z.-M. Su, *Chemistry – An Asian Journal*, 2014, **9**, 749-753; (b) J.-S. Qin, S.-R. Zhang, D.-Y. Du, P. Shen, S.-J. Bao, Y.-Q. Lan and Z.-M. Su, *Chem. Eur. J.*, 2014, **20**, 5625-5630.
10. C. Yang, L.-M. Fu, Y. Wang, J.-P. Zhang, W.-T. Wong, X.-C. Ai, Y.-F. Qiao, B.-S. Zou and L.-L. Gui, *Angew. Chem. Int. Ed.*, 2004, **43**, 5010-5013.

11. (a) Y.-Q. Chen, G.-R. Li, Z. Chang, Y.-K. Qu, Y.-H. Zhang and X.-H. Bu, *Chem. Sci.*, 2013, **4**, 3678-3682; (b) S. Liu, J. Li and F. Luo, *Inorg. Chem. Commun.*, 2010, **13**, 870-872; (c) Y.-W. Li, J.-R. Li, L.-F. Wang, B.-Y. Zhou, Q. Chen and X.-H. Bu, *J. Mater. Chem. A*, 2013, **1**, 495-499.
12. S. V. a. SMART (V 5.628), XPREP, SHELXTL; Bruker AXS Inc. Madison, Wisconsin, USA, 2004.
13. G. M. Sheldrick, *SADABS, Empirical Absorption Correction Program, University of Göttingen, Göttingen*, 1997.
14. A. Altomare, G. Cascarano, C. Giacovazzo and A. Guagliardi, *J. Appl. Crystallogr.*, 1993, **26**, 343-350.
15. G. M. Sheldrick, *SHELXL 97, Program for the Solution of Crystal Structure, University of Göttingen, Germany*, 1997.
16. A. Spek, *J. Appl. Crystallogr.*, 2003, **36**, 7-13.
17. L. Farrugia, *J. Appl. Crystallogr.*, 1999, **32**, 837-838.
18. J.-R. Li, R. J. Kuppler and H.-C. Zhou, *Chem. Soc. Rev.*, 2009, **38**, 1477-1504.
19. (a) Y. Cui, Y. Yue, G. Qian and B. Chen, *Chem. Rev.*, 2011, **112**, 1126-1162; (b) S. Roy, A. Chakraborty and T. K. Maji, *Coordination Chemistry Reviews*, 2014, **273–274**, 139-164; (c) S. Mohapatra, S. Adhikari, H. Riju and T. K. Maji, *Inorg. Chem.*, 2012, **51**, 4891-4893; (d) B. Chen, L. Wang, Y. Xiao, F. R. Fronczek, M. Xue, Y. Cui and G. Qian, *Angew. Chem. Int. Ed.*, 2009, **48**, 500-503.

Chapter 3

Two from One: Synthesis of Nanoporous Carbon and Carbon Nitride Nano Dots from an Anionic MOF

Abstract

In this chapter, a novel templated synthesis of both graphitic carbon nitride and nanoporous carbon from an AMOF $[Mg_3(ndc)_{2.5}(HCO_2)_2(H_2O)]\cdot[NH_2Me_2]\cdot 2H_2O\cdot DMF$ (**1**) has been described. Nanoporous carbon can be synthesized from **1** by simply carbonizing at a high temperature, using it as a sacrificial template. This porous carbon has an exceptionally high BET surface area along with high CO_2 uptake. Graphitic carbon nitride is typically synthesized by the condensation of precursors containing pre-bonded C-N moieties. Here **1** contains dimethyl amine ($NH_2Me_2^+$) (DMA) cations which act as a source of the pre-bonded C-N moiety. As a result of this, porous carbon nitride can be synthesized easily from **1** simply by heating at an ambient temperature, without the use of any external agent. The graphitic carbon nitride thus synthesized has spherical morphology, with diameters in the lower nanoranges. This spherical morphology combined with the semiconductor properties of graphitic carbon nitride are one of the rare instances of carbon nitride nano dots. This synthetic method is unique and novel since graphitic carbon nitride and nanoporous carbon can both be synthesized from the same MOF **1** without the use of any external agent, by condensation at the respective temperatures.

3.1 Introduction

Porous carbon materials have emerged as an important class of materials over the years due to their high chemical and thermal stability which can be employed in diverse practical applications[1] e.g., adsorption,[2] separation,[3] catalysis,[4] electronics[5] and drug delivery.[6] Among these, nanoporous carbons have received the maximum attention compared to the other porous materials because of its low density, high thermal stability and chemical inertness.[1] Such carbon materials are traditionally prepared simply by the pyrolysis followed by physical or chemical activation of organic precursors. However, the materials thus derived possess disordered structures with broad pore size distributions, making them unsuitable for molecular selection related applications. Therefore, the synthesis of high surface area nanoporous carbon material with optimized structure and tunable properties remains a challenge. The attempts to construct nanoporous carbon materials with high surface area, ordered porous structures and narrow pore size distributions have given rise to templating approaches. The conventional templating approaches involve the carbonization or chemical vapour deposition of carbon sources over ordered hard carbon templates or carbonization of ordered polymeric carbon gels, which are soft templates. Among these, the former is capable of producing nano, meso or macroporous compound depending on the type of hard template used. Metal-organic frameworks(MOFs)[7] have received spotlight in recent times owing to their flexible porous structure and tunable properties. Their high surface area, large pore volume and diverse structures imply that they are potential alternative precursors to synthesize nanoporous carbons[1]. MOFs therefore are capable of enriching the collection of porous carbon materials by imparting novel structures and properties to them. Moreover, using MOFs as a template ensure high surface area of the resultant material and also the percentage of the heteroatom doping can be tuned easily. Highly nanoporous carbons have been derived using several MOFs, e.g. MOF-5[8], Al-PCP[9] and ZIF-8[10] manifesting excellent gas storage,[11] catalytic,[11] drug delivery[6] and electrochemical capacitance[12] properties. In many cases, precursors like furfuryl alcohol,[12] carbon tetrachloride, glycerol, phenolic resin,[13] etc. have been impregnated in MOF-5 as a source of carbon to generate nanoporous carbon materials. Also, sucrose has been incorporated in IRMOF-3[14] to get nanoporous carbon with extremely high surface area.[15] The highest surface area so far has been reported by the nanoporous carbon prepared by the direct carbonization of Al-PCP, which has a surface area greater than 5000 $m^2.g^{-1}$.[16] However, the reports of the

synthesis of nanoporous carbon using MOF as a template without the use of any template are less in number.

High surface area carbon materials with hetero atom doping, e.g., nitrogen and boron have attracted chemists as they play an important role in energy research, with immense applications in fuel cells, lithium ion batteries, dye sensitized solar cells, super capacitors, etc.[17] The most exciting among these hetero atom doped materials is graphitic carbon nitride.[18] The unique electron rich properties of graphitic carbon nitride coupled with its high thermal and chemical stability makes it a lucrative metal-free photocatalytic material.[18b, 19] Conventionally, graphitic carbon nitride is prepared by the condensation of pre-bonded C-N moiteies, e.g., dicyandiamide[18a] or urea.[20] However, due to the graphitic stacking, the materials prepared in this way have low surface area, which is detrimental to its adsorption and heterogeneous catalytic properties.[18b] To overcome this problem, several templating approaches have been used, where diverse porous materials like porous silica[21] and MOFs have been employed. Recently well-known MOF structures, e.g., Al-PCP[22] and MOF-5,[23] have been used as templates for the preparation of carbon nitride with enhanced surface area and properties. However, in each case, organic precursors like melamine or dicyandiamide were used to provide the pre-bonded C-N moiety for the construction of carbon nitride. However, if the MOF itself contains a C-N bonded moiety in its molecule, it is possible to synthesize carbon nitride in situ by simply carbonizing the MOF material at an optimum temperature, without the use of any external reagent. The resultant graphitic carbon nitride is expected to have higher surface area than bulk graphitic carbon nitride owing to the porous MOF structure.

Anionic MOFs (AMOF)[24] can be extremely useful in this regard. AMOFs have anionic frameworks, where the overall structural neutrality is maintained by a guest cation present within the pores. By exchanging this extra-framework guest cation with different cationic species, various applications, e.g., sensing,[24h] luminescence,[24h] drug delivery,[24d] catalysis,[24b, 24e] etc., has been realized in AMOFs. If the guest cation of an AMOF has a C-N moiety, it can act as a precursor for carbon nitride material, while the framework itself acts as a template. Thus the AMOF can be used for the templated synthesis of graphitic carbon nitride without the use of any external precursor. This same AMOF can also be used for the preparation of nanoporous carbon simply by altering the carbonizing temperature. Hence the same material can be used for the dual synthesis of graphitic carbon nitride as well as nanoporous carbon without the use of any external agent, by only changing the carbonizing temperature.

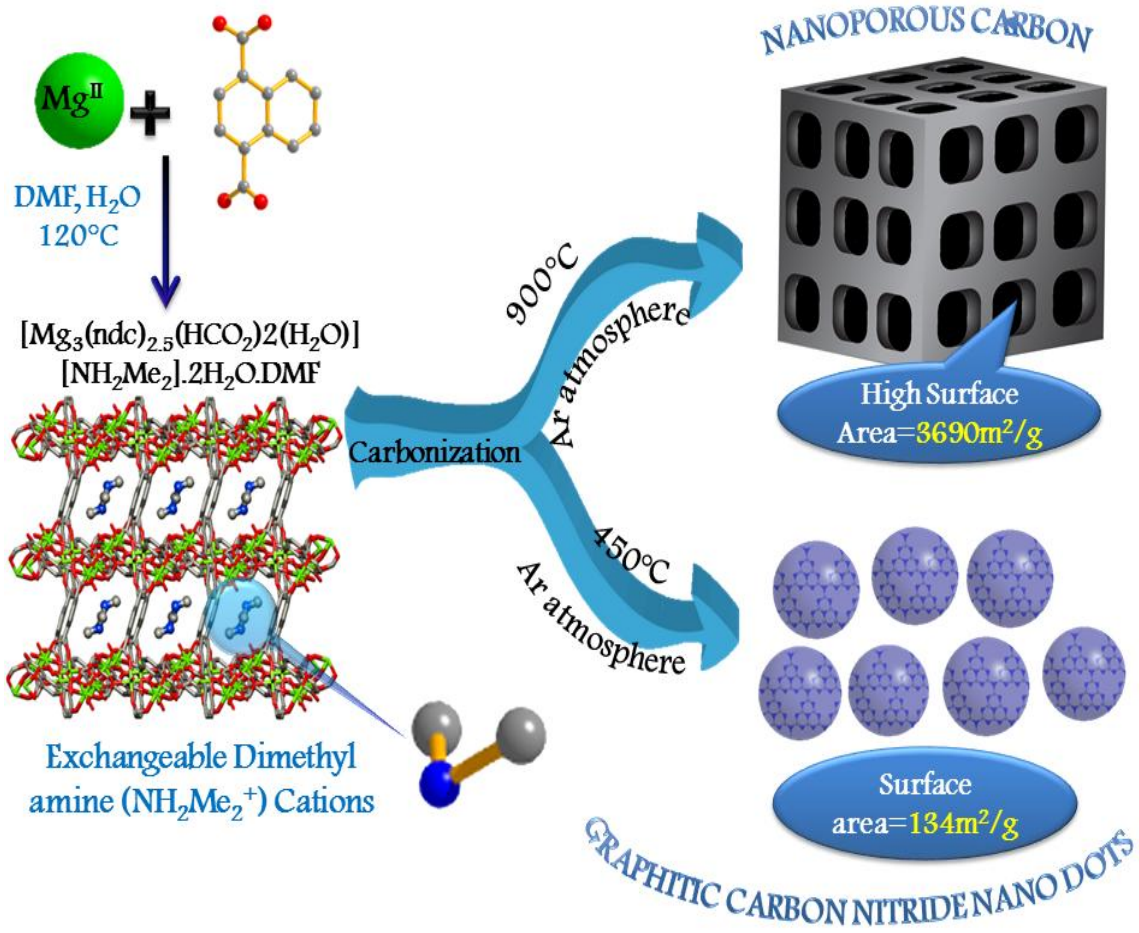

Scheme 1: The preparation of graphitic carbon nitride and nanoporous carbon from **1**.

In this chapter, the synthesis of both graphitic carbon nitride as well as nanoporous carbon from an AMOF without the use of any external precursor has been documented. $[Mg_3(ndc)_{2\cdot5}(HCO_2)_2(H_2O)]\cdot[NH_2Me_2]\cdot2H_2O\cdot DMF$ (**1**) is an AMOF where the charge neutrality is maintained by dimethyl amine (NH_2Me_2) (DMA) cations residing in its pores.[24h] When heated at 450°C, these DMA cations act as precursors to produce graphitic carbon nitride with spherical morphology in the nanometer range. These can be referred to as carbon nitride nano dots, owing to their morphological similarities to carbon nano dots. Also on being heated to 900°C, **1** is capable of producing nanoporous carbon with extremely high surface area of 3690 $m^2.g^{-1}$. Such templated synthesis of graphitic carbon nitride and nanoporous carbon from the same MOF simply by changing the carbonization temperature without the use of any external precursor is unprecedented.

3.2 Experimental Section

3.2.1 Materials

All the reagents and solvent were used as obtained from commercial supplies without any further purification. 1,4-Naphthalene dicarboxylic acid(ndc) and $MgNO_3 \cdot 6H_2O$ used were procured from Alfa Aesar and Aldrich Co. Ltd. respectively.

3.2.2 Synthesis of $[Mg_3(ndc)_{2.5}(HCO_2)_2(H_2O)]\cdot[NH_2Me_2]\cdot 2H_2O\cdot DMF$ (1)

$[Mg_3(ndc)_{2.5}(HCO_2)_2(H_2O)]\cdot[NH_2Me_2]\cdot 2H_2O\cdot DMF$ (**1**) was synthesized and characterized as described in Chapter 2.

3.2.3 Carbonization of 1

1 was carbonized at two different temperatures in a programmable furnace by Elite Thermal Heating Systems.

3.2.4 Synthesis of PC_1

Crystals of **1** are powdered finely. Then it is heated at 900°C for 6hrs. The heating rate is 5 °C. min^{-1}. The crude product obtained is washed with a solution of 50 % concentrated HCl and 50 % conc. HNO_3 to remove any metal traces. Thereafter it is repeatedly washed with water and dried to get **PC_1**.

3.2.5 Synthesis of CN _1

The crystals of **1** are powdered finely and carbonized at 450°C under Ar atmosphere for 6 hours to prepare **CN_1**. The crude product obtained is washed with a solution of 50% conc. HCl and 50% conc. HNO_3 to remove any metal traces. Thereafter it is repeatedly washed with water and dried.

3.2.6 Physical Measurements

The elemental analysis was carried out using a Thermo Fischer Flash 2000 Elemental Analyzer. Thermogravimetric analysis (TGA) was carried out (Mettler Toledo) in nitrogen atmosphere (flow rate = 50 ml min^{-1}) in the temperature range 30 – 550 °C (heating rate = 3 °C. min^{-1}). Powder XRD pattern was recorded by using Cu-Kα radiation (Bruker D8 Discover; 40 kV, 30 MA). Electronic absorption spectra were recorded on a

Perkin Elmer Lambda 750 UV-VIS-NIR Spectrometer and emission spectra were recorded on Perkin Elmer Ls 55 Luminescence Spectrometer. Solid state UV spectrum was recorded in reflectance mode. IR spectra of the compounds were recorded on a Bruker IFS 66v/S spectrophotometer using the KBr pellets in the region 4000−400 cm^{-1}. The Raman spectra were recorded in backscattering arrangement, using 532 nm laser excitation using 6 mW laser power.

3.2.7 Preparation of Sample for Adsorption

Adsorption isotherms of CO_2 at 195 K and N_2 at 77 K were recorded with the dehydrated sample using QUANTACHROME QUADRASORB-SI analyzer. To prepare the dehydrated sample of **PC_1** and **CN_1** approximately 100 mg of sample was taken in a sample holder and degassed at 110ºC under 10^{-1} pa vacuum for about 12 hours prior to the measurements. Dead volume of the sample cell was measured using helium gas of 99.999% purity. The amount of gas adsorbed was calculated from the pressure difference ($P_{cal} - P_e$), where P_{cal} is the calculated pressure with no gas adsorption and P_e is the observed equilibrium pressure. All the operations were computer-controlled and automatic.

3.3 Results and Discussion

3.3.1 Morphology

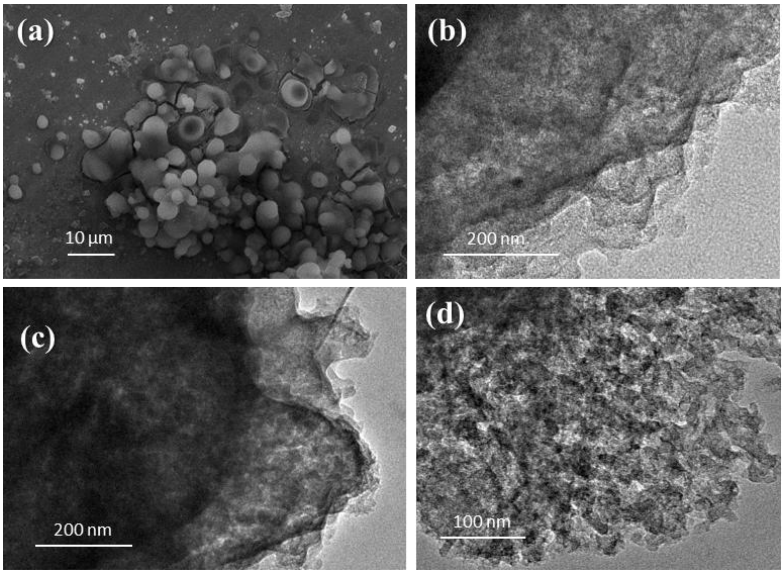

Fig. 1(a) SEM image of **PC_1 (b), (c), (d)** TEM images of **PC_1**

Carbon materials generally manifest diverse morphologies and structure, which affect their properties. Hence, after characterizing the respective samples, it is necessary to study their morphology. Under TEM, **PC_1** shows layered structure (**Fig. 1**) which indicates towards its porous nature. This porous nature is further reflected in its adsorption properties.

On performing Field Emission Scanning Electron Microscopy (FESEM) of **CN_1**, small spherical particles were observed (**Fig. 2(a)**). This was further supported by the Transmission Electron Microscopy (TEM) of **CN_1**. Under TEM, the sample was observed to have uniform spherical morphology throughout its bulk (**Fig. 2 (b)** and **(c)**). When an individual sphere was focussed under the microscope, its diameter was found to be in the lower nanoranges – around 10nm (**Fig. 2(d)**). These spheres may be regarded as carbon nitride nano dots (CN-dots) owing to their morphological similarity to carbon nano dots (C-dots). C-dots are a new class of carbon materials with spherical morphology and sizes below 10nm, which due to their chemical inertness, abundance and tunable fluorescence, have found wide applications in energy and catalysis[25].

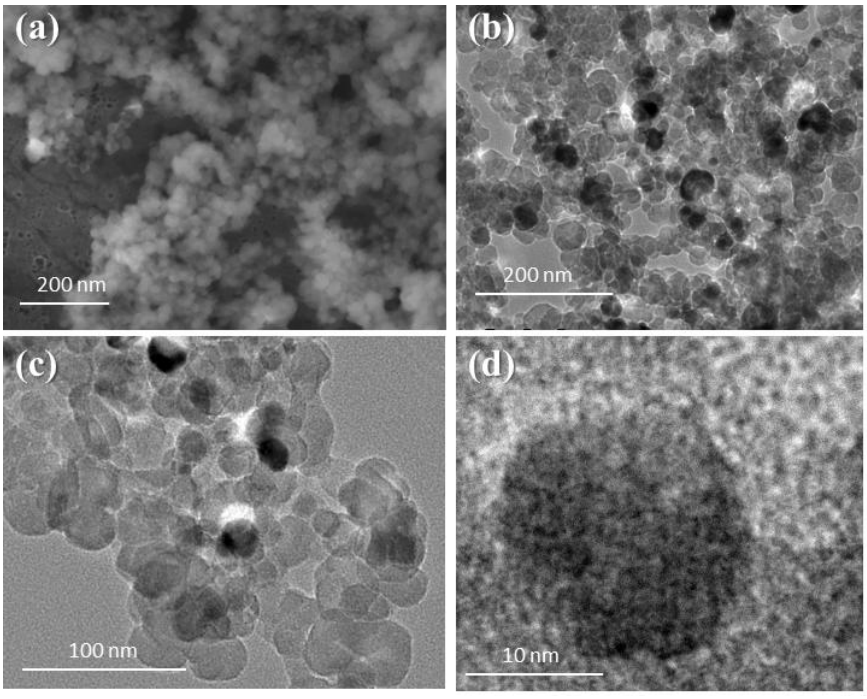

Fig. 2(a) FESEM image of **CN_1 (b), (c)** TEM images of **CN_1 (d)** TEM image of an isolated dot

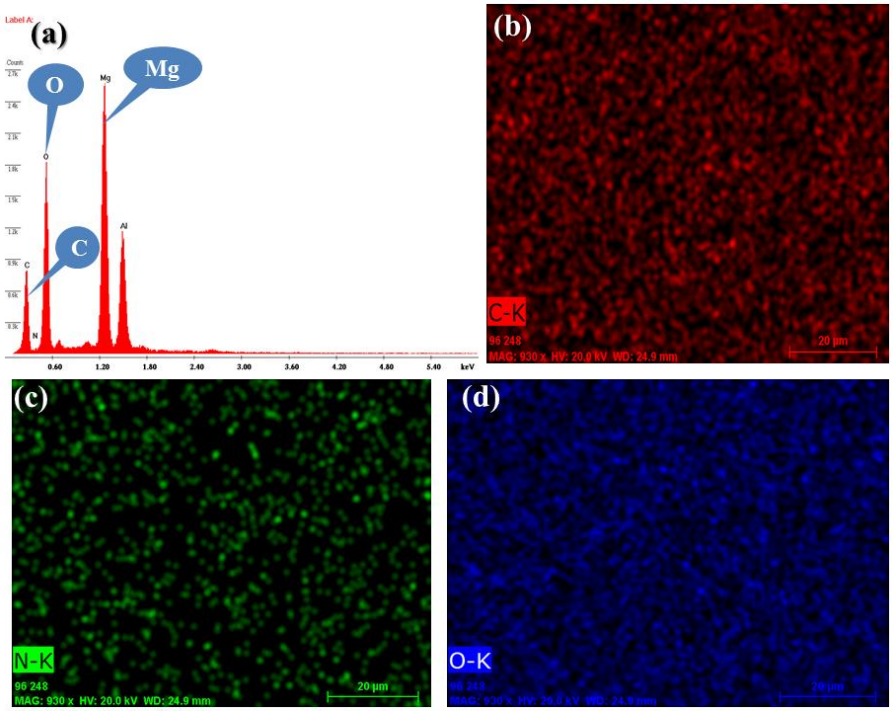

Fig. 3(a) EDS analysis of crude **CN_1 (b), (c)** and **(d)** Elemental mapping of **CN_1**

The Electron Dispersion Spectroscopic Analysis of the crude sample before washing showed the presence of C, N and O along with Mg, which is probably present in the oxide form. The elemental mapping of the sample after acid wash showed a uniform distribution of C, N and O all over the sample. This indicates that the sample prepared is not only carbon nitride, but also contains some oxygen impurity along with C and N (**Fig. 3**).

3.3.2 PXRD analysis

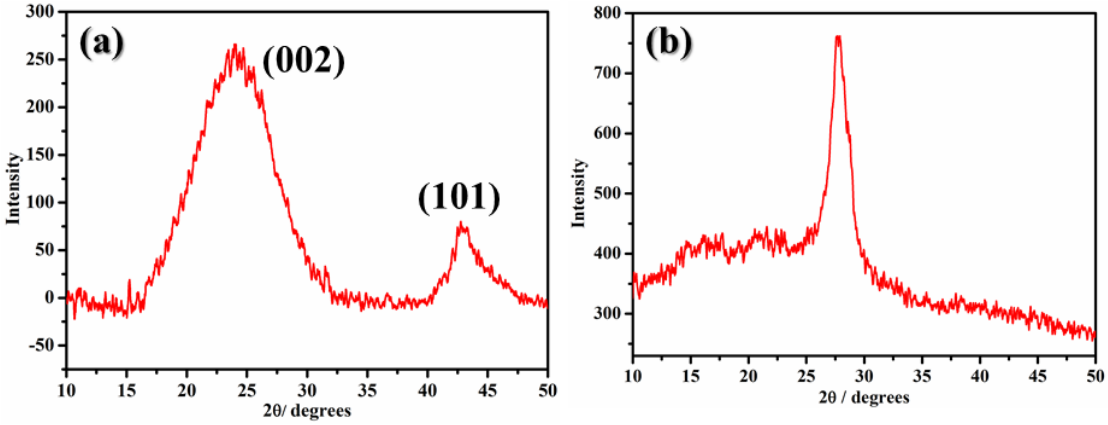

Fig. 4(a) PXRD pattern of **PC_1 (b)** PXRD pattern of **CN_1**

The PXRD pattern of **PC_1** contains a peak around 2θ = 24° and another at 2θ = 42.8° corresponding to (002) and (101) planes respectively. These two peaks are the signature peaks for nanoporous carbons (**Fig. 4(a)**).

The PXRD pattern of **CN_1** shows a strong peak at 2θ = 27·7°, indicating graphitic stacking (**Fig. 4(b)**), with inter-stacking distance of 3·22Å.

3.3.3 XPS and Elemental analysis

In order to ascertain the type of bonding present in both the samples, X-ray Photoelectron Spectroscopy (XPS) was performed. In case of **PC_1**, from the XPS analysis of C 1s, two major peaks are obtained. The band at 291eV corresponds to the C-C bonding. However, another band of almost similar intensity is also present at 288eV and this corresponds to C-O species (**Fig. 5(a)**). So from here it can be concluded that **PC_1** contains O in addition to C.

The XPS analysis of the N 1s spectra of **CN_1** shows the presence of a major broad peak at ~400eV, which implies the presence of C-N-C and N-$(C)_3$ species. However, there is another peak, much lower in intensity, which can be correlated to the presence of N-H species in a very small proportion due to incomplete condensation[18b] (**Fig. 5(b)**). From this, the molecular formula of **CN_1** is determined to be C_2N_4O. Hence **CN_1** can be denoted as g-C_2N_4O.

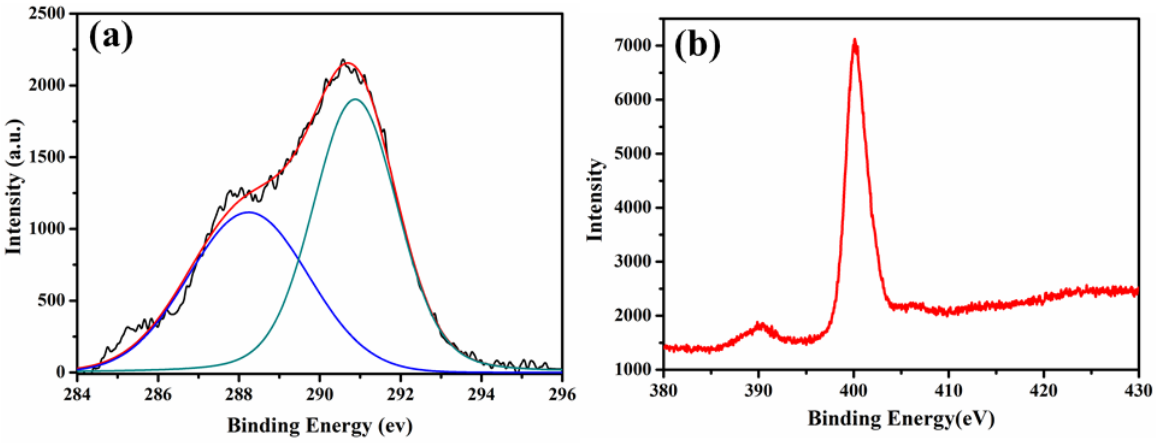

Fig. 5(a) XPS analysis of **PC_1 (b)** XPS analysis of **CN_1**

3.3.4 IR and Raman Spectroscopy

In order to ascertain the functionalities present in the samples and further study their morphology and structure, IR and Raman spectroscopy was performed on them.

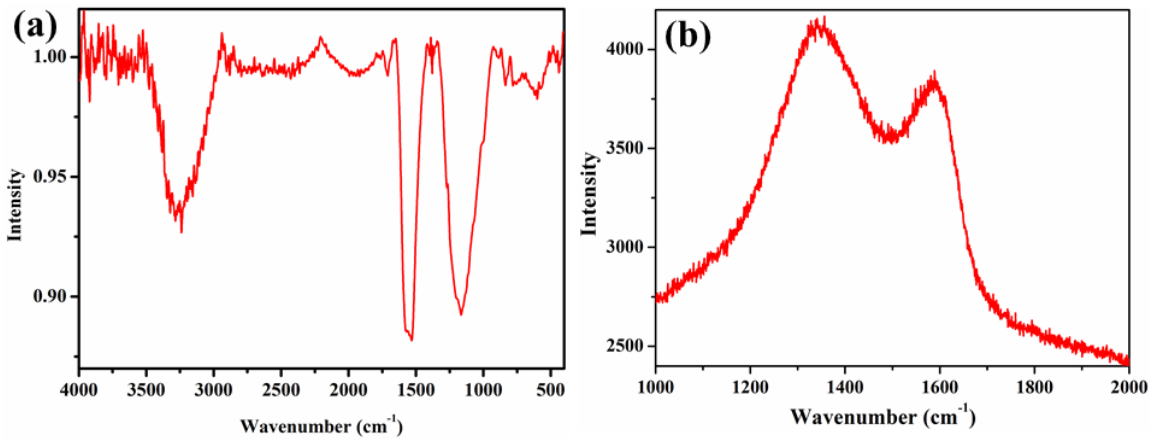

Fig. 6(a) IR spectrum of **PC_1 (b)** Raman spectrum of **PC_1**

Table 1: Principal peaks in the IR spectrum of **PC_1** (**Fig. 6(a)**)

Peak position	Nature	Vibration
1566 cm^{-1}	Very strong, broad	Aromatic C-C stretching
1160 cm^{-1}	Very strong, broad	C-H wag

The Raman spectrum of **PC_1** has two distinct bands at 1340 and 1590 cm^{-1} which can be related to D and G bands respectively. Here the ratio of the intensity of the D band to that of the G band is $\mathbf{I_D / I_G}$ **~1·1** (**Fig. 6(b)**).

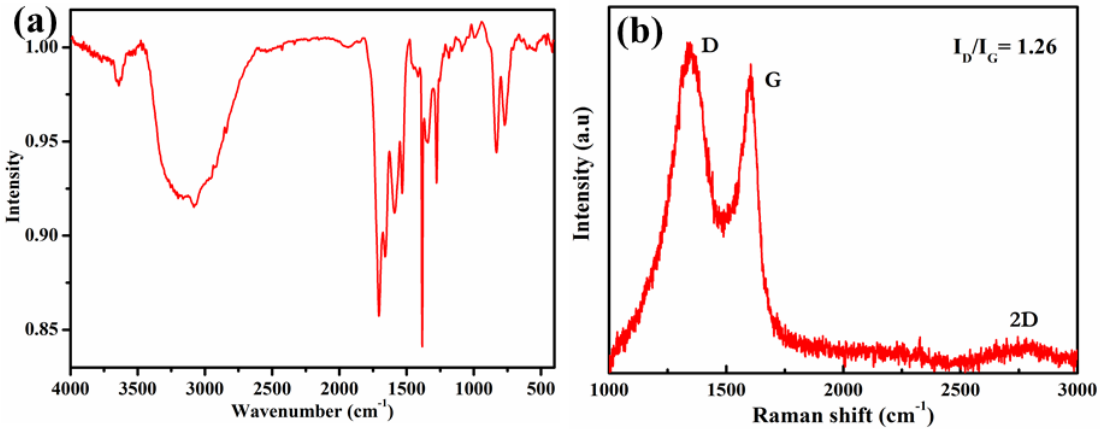

Fig. 7(a) IR spectrum of **CN_1 (b)** Raman spectrum of **CN_1**

Table 2: Principal peaks in the IR spectrum of **CN_1** (**Fig. 7(a)**)

Peak Position	Nature	Vibration
834 cm^{-1}	medium	N-H wag
1270 cm^{-1}	strong	C-N stretch
1370 cm^{-1}	strong	Aromatic C-N stretch

1580 cm^{-1}	strong	1° N-H bending
3630 cm^{-1}	weak	1°, 2° N-H stretch

For **CN_1**, the normalized Raman spectrum is shown in **Fig. 7(b)**. Here, two distinct peaks are observed at 1350 and 1600 cm^{-1}, which can be related to D and G bands respectively. Moreover a weaker 2D band is also observed at 2770cm^{-1}. Here the ratio of the intensity of the D band to that of the G band, i.e., $\mathbf{I_D / I_G}$ **~1·26**. This ratio of intensities in both the samples indicates towards the degree of crystallization in the sample and also proves that in both cases, the local carbon structure has both graphitic carbon as well as disordered atoms

3.3.5 Surface Area and Storage Properties

In order to check the porous properties and surface area of **PC_1**, it was first activated at 200°C overnight. The porous properties of **PC_1** are very interesting. It shows a N_2 uptake of 3040 $mL.g^{-1}$ at 77K. The BET surface area, when calculated is found to be 3690$m^2.g^{-1}$(**Fig. 8(a)**). This is the second highest reported BET surface area of a nanoporous carbon material derived from MOF material after the porous carbon derived from Al-PCP.[16] The N_2 adsorption isotherm shows a hysteresis above P/P_0 = 0·4. This indicates the presence of both the meso and micropores in the system. This is further confirmed by the pore size distribution of **PC_1** (**Fig. 8(b)**). The system is mainly microporous, with pore dimensions of 1nm. However, two mesopores are also present with dimensions of 3.5 and 4.5 nm respectively. The high BET surface area of **PC_1** is also useful in CO_2 adsorption. At 195K, **PC_1** adsorbs nearly 250 $mL.g^{-1}$ of CO_2, thereby proving its competence as a CO_2 storing material (**Fig. 8(c)**).

The porous properties of **CN_1** were also investigated. **CN_1** adsorbs 550 $mL.g^{-1}$ of N_2 (**Fig. 9(a)**). The BET surface area of **CN_1** is calculated to be 362 $m^2.g^{-1}$. The relatively low surface area of **CN_1** can be attributed to the graphitic stacking present in the sample. Inspired by the surface area, the CO_2 adsorption capacity of **CN_1** was measured. It shows a CO_2 uptake of 46 $mL.g^{-1}$ at 273K and 77 $mL.g^{-1}$ at 195K (**Fig. 9(b)**).

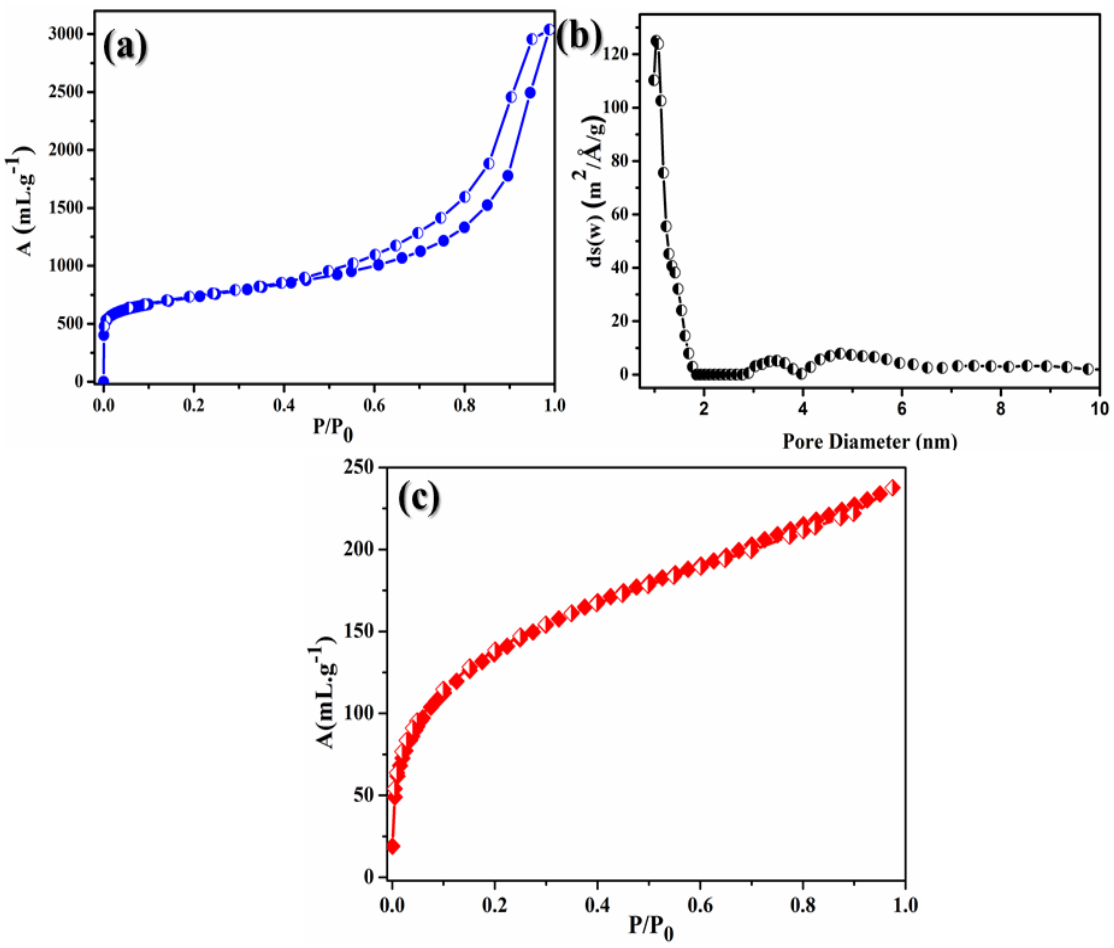

Fig. 8(a) N_2 adsorption isotherm of **PC_1** at 77K **(b)** The pore size distribution in **PC_1 (c)** CO_2 adsorption by **PC_1** at 195K

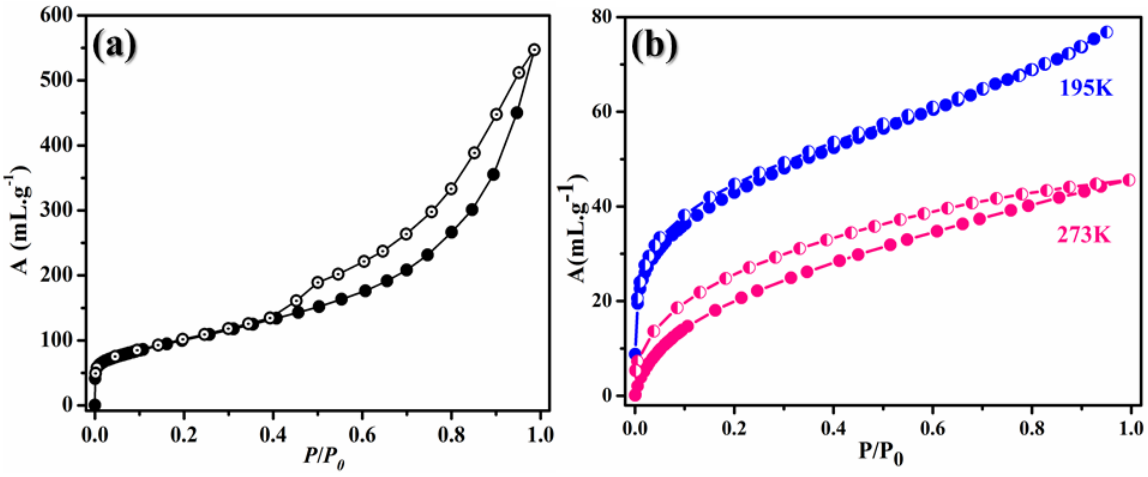

Fig. 9(a) N_2 adsorption isotherm of **CN_1** at 77K **(b)** CO_2 adsorption isotherm of **CN_1** at 195K and 273K

3.4 Conclusion

This chapter upholds a unique and novel synthetic strategy for porous carbon as well as carbon nitride materials. The synthetic strategy involves the use of an AMOF **1** as a template, where its extra-framework guest cation can be used as a precursor for preparing graphitic carbon nitride. The carbon nitride thus prepared (**CN_1**) has graphitic structure and spherical morphology with dimensions in the lower nanoranges. Thus **CN_1** having the dual benefit of a nanospherical morphology along with the intriguing semiconductor properties, is a prospective quantum dot material. Also the nanoporous carbon synthesized by using **1** as a template, without the intervention of any external reagent, has an extremely high surface area. Thus it holds the potential to be used in practical purposes for gas storage. Such a synthetic procedure to generate two different carbonaceous materials from the same template material without using any external precursor, simply by varying the reaction temperature, is truly unprecedented.

3.5 References

1. W. Chaikittisilp, K. Ariga and Y. Yamauchi, *J. Mater. Chem. A*, 2013, **1**, 14-19.
2. S. J. Yang, H. Jung, T. Kim and C. R. Park, *Prog. Nat. Sci. Mater. Int.*, 2012, **22**, 631-638.
3. S. M. Saufi and A. F. Ismail, *Carbon*, 2004, **42**, 241-259.
4. M. G. Stevens, K. M. Sellers, H. C. Foley and S. Subramoney, *Chem. Commun.*, 1998, 2679-2680.
5. C. Merlet, B. Rotenberg, P. A. Madden, P.-L. Taberna, P. Simon, Y. Gogotsi and M. Salanne, *Nat. Mater.*, 2012, **11**, 306-310.
6. Y. L. Nagy L. Torad, Shinsuke Ishihara, Katsuhiko Ariga, Yuichiro Kamachi, Hong-Yuan Lian, Hicham Hamoudi, Yoshio Sakka, Watcharop Chaikittisilp, Kevin C.-W. Wu and Yusuke Yamauchi, *Chem. Lett.*, 2014, **43**, 2.
7. S. Kitagawa, R. Kitaura and S.-i. Noro, *Angew. Chem. Int. Ed.*, 2004, **43**, 2334-2375.
8. H. Li, M. Eddaoudi, M. O'Keeffe and O. M. Yaghi, *Nature*, 1999, **402**, 276-279.
9. A. Comotti, S. Bracco, P. Sozzani, S. Horike, R. Matsuda, J. Chen, M. Takata, Y. Kubota and S. Kitagawa, *J. Am. Chem. Soc.*, 2008, **130**, 13664-13672.
10. K. S. Park, Z. Ni, A. P. Côté, J. Y. Choi, R. Huang, F. J. Uribe-Romo, H. K. Chae, M. O'Keeffe and O. M. Yaghi, *Proc. Natl. Acad. Sci.*, 2006, **103**, 10186-10191.
11. A. Aijaz, N. Fujiwara and Q. Xu, *J. Am. Chem. Soc.*, 2014, **136**, 6790-6793.
12. B. Liu, H. Shioyama, T. Akita and Q. Xu, *J. Am. Chem. Soc.*, 2008, **130**, 5390-5391.
13. (a) J. Hu, H. Wang, Q. Gao and H. Guo, *Carbon*, 2010, **48**, 3599-3606; (b) D. Yuan, J. Chen, S. Tan, N. Xia and Y. Liu, *Electrochem. Commun.*, 2009, **11**, 1191-1194.
14. J. L. C. Rowsell and O. M. Yaghi, *J. Am. Chem. Soc.*, 2006, **128**, 1304-1315.
15. K. Jayaramulu, K. K. R. Datta, K. Shiva, A. J. Bhattacharyya, M. Eswaramoorthy and T. K. Maji, *Micropor. Mesopor. Mater.*, 2015, **206**, 127-135.
16. M. Hu, J. Reboul, S. Furukawa, N. L. Torad, Q. Ji, P. Srinivasu, K. Ariga, S. Kitagawa and Y. Yamauchi, *J. Am. Chem. Soc.*, 2012, **134**, 2864-2867.
17. A.-M. Alexander and J. S. J. Hargreaves, *Chem. Soc. Rev.*, 2010, **39**, 4388-4401.

18. (a) A. Thomas, A. Fischer, F. Goettmann, M. Antonietti, J.-O. Muller, R. Schlogl and J. M. Carlsson, *J. Mater. Chem.*, 2008, **18**, 4893-4908; (b) J. Zhu, P. Xiao, H. Li and S. A. C. Carabineiro, *ACS Appl. Mater. Interfaces*, 2014, **6**, 16449-16465.
19. Y. Zhang, Q. Pan, G. Chai, M. Liang, G. Dong, Q. Zhang and J. Qiu, *Sci. Rep.*, 2013, **3**.
20. X.-X. Zou, G.-D. Li, Y.-N. Wang, J. Zhao, C. Yan, M.-Y. Guo, L. Li and J.-S. Chen, *Chem. Commun.*, 2011, **47**, 1066-1068.
21. X. Chen, J. Zhang, X. Fu, M. Antonietti and X. Wang, *J. Am. Chem. Soc.*, 2009, **131**, 11658-11659.
22. M. Hu, J. Reboul, S. Furukawa, L. Radhakrishnan, Y. Zhang, P. Srinivasu, H. Iwai, H. Wang, Y. Nemoto, N. Suzuki, S. Kitagawa and Y. Yamauchi, *Chem. Commun.*, 2011, **47**, 8124-8126.
23. S. Pandiaraj, H. B. Aiyappa, R. Banerjee and S. Kurungot, *Chem. Commun.*, 2014, **50**, 3363-3366.
24. (a) Y. Liu, G. Li, X. Li and Y. Cui, *Angew. Chem.*, 2007, **119**, 6417-6420; (b) E. Quartapelle Procopio, F. Linares, C. Montoro, V. Colombo, A. Maspero, E. Barea and J. A. R. Navarro, *Angew. Chem. Int. Ed.*, 2010, **49**, 7308-7311; (c) J. Yu, Y. Cui, C. Wu, Y. Yang, Z. Wang, M. O'Keeffe, B. Chen and G. Qian, *Angew. Chem. Int. Ed.*, 2012, **51**, 10542-10545; (d) J. An, S. J. Geib and N. L. Rosi, *J. Am. Chem. Soc.*, 2009, **131**, 8376-8377; (e) D. T. Genna, A. G. Wong-Foy, A. J. Matzger and M. S. Sanford, *J. Am. Chem. Soc.*, 2013, **135**, 10586-10589; (f) J. Tian, L. V. Saraf, B. Schwenzer, S. M. Taylor, E. K. Brechin, J. Liu, S. J. Dalgarno and P. K. Thallapally, *J. Am. Chem. Soc.*, 2012, **134**, 9581-9584; (g) S. Yang, X. Lin, A. J. Blake, G. S. Walker, P. Hubberstey, N. R. Champness and M. Schröder, *Nat Chem*, 2009, **1**, 487-493; (h) S. Bhattacharyya, A. Chakraborty, K. Jayaramulu, A. Hazra and T. K. Maji, *Chem. Commun.*, 2014, **50**, 13567-13570.
25. H. Li, Z. Kang, Y. Liu and S.-T. Lee, *J. Mater. Chem.*, 2012, **22**, 24230-24253.

Chapter 4

Tetracarboxylate Linker Based Flexible Cu^{II} Frameworks with Selective CO_2 Uptake and Solvent Adsorption Properties

Abstract

In this chapter, two different flexible tetracarboxylate linkers [5,5'-(1,4-(2-butene)bis(oxy)diisophthalic acid (L1) and 5,5'-(1,4-phenylenebis(methylene))bis(oxy)diisophthalic acid (L2)) of different lengths and flexibility have been used for the self-assembly with Cu^{II} to generate two different frameworks. These flexible linkers with metal ions and another coligand can indeed impart structural flexibility in the resulting framework structure. Self-assembly of L1 and 1,3-bis(4-pyridyl) propane (bpp) with Cu^{II} at room temperature results in a hydrophobic 2D MOF $\{[Cu_2(bpp)_3(L2)]\cdot(5H_2O)\cdot(bpp)\}$**(1)** with cage type structure, while L2 with Cu^{II} and 4,4'-bipyridine (bipy) forms a 3D MOF $\{[Cu_2(L1)(H_2O)_2(bipy)_2]\cdot(bipy)\cdot(5H_2O)\}$**(2)** with 2-fold interpenetration. The porosity and adsorption properties of compounds **1** and **2** vary in accordance with the flexibility and the length of the respective ligands. Compound **1** synthesized from **L1** has a 2D cage like structure and shows hydrophobic behaviour. Compound **2**, on the other hand, has a 3D structure with 2-fold interpenetration and shows high selective CO_2 uptake at 195K as well as room temperature. It also shows interesting solvent adsorption profiles. This can be attributed to its flexible structure, unsaturated metal sites and polar carboxylate groups.

4.1 Introduction

Metal-organic Frameworks (MOFs)[1] are a unique class of porous coordination polymers, which are well known for their diverse applications e.g., gas storage,[2] catalysis,[3] luminescence[4] and sensing properties.[5] Due to the use of different combinations of a wide range of metal ions and linker molecules, they may have high surface area, flexible structures and tunable properties.[6] This gives MOFs an edge over other porous materials like porous carbon and zeolites. Moreover, in recent times, MOFs with cage-like structure, particularly those with transition metal ions have been receiving the spotlight for their unique properties.[7] Besides interesting structural topologies, these cage-like MOFs have exceptional selective guest sequestration and gas storage properties.[8] These materials have also proved their efficiency as molecular sieves, nanoscale reaction vessels, catalysts and sensors.[9] Hence it is extremely important to adopt a proper targeted ligand design strategy in order to synthesize such MOFs and explore new possibilities.

Judicious synthesis of MOFs based on flexible ligands has attracted unmatched attention over the years.[10] These flexible ligands with versatile coordination modes, conformations and multi donor sites, are used broadly for constructing polynuclear MOFs. Such MOFs with flexible ligands manifest a wide range of structural diversity as the conformational mobility is coupled with coordination preferences of the metal ions. These MOFs may be flexible, dynamic and is capable of responding to external stimuli, *e.g.*, temperature, pressure, light, electric fields, chemical inclusion *etc.*[11] They can undergo stimuli responsive structural transformation and versatile framework functionalities including high adsorption uptake beyond the accessible porosity. Interesting features could be realized if the flexible framework has interpenetrated networks, as they can form open and closed phases by interdigitation using simple gliding motions without any bond cleavage or distortion.[12] The dynamic frameworks also manifest stepwise or gated adsorption at a certain pressure of an adsorbate molecule.[13] Such behaviour results in guest selectivity and gas separation. A balanced guest-framework interaction may also lead to selective sorption of gases.[14] Indeed, a large number of MOFs show CO_2 selectivity over other gases, owing to strong interaction of the framework with CO_2 molecule. Due to the growing environmental concerns over global warming, the effective sequestration of CO_2 has become extremely relevant. Flue gas from coal powered plants is a major source of CO_2 and hence materials designed for

CO_2 capture must have a high selectivity for CO_2 over N_2. Such selectivity in MOFs can be achieved by the careful selection of the organic linker and also by the implementation of unsaturated metal sites (UMS). For practical application in gas storage, catalysis, separation and fixation of atmospheric CO_2, such selectivity must be manifested at room temperature.

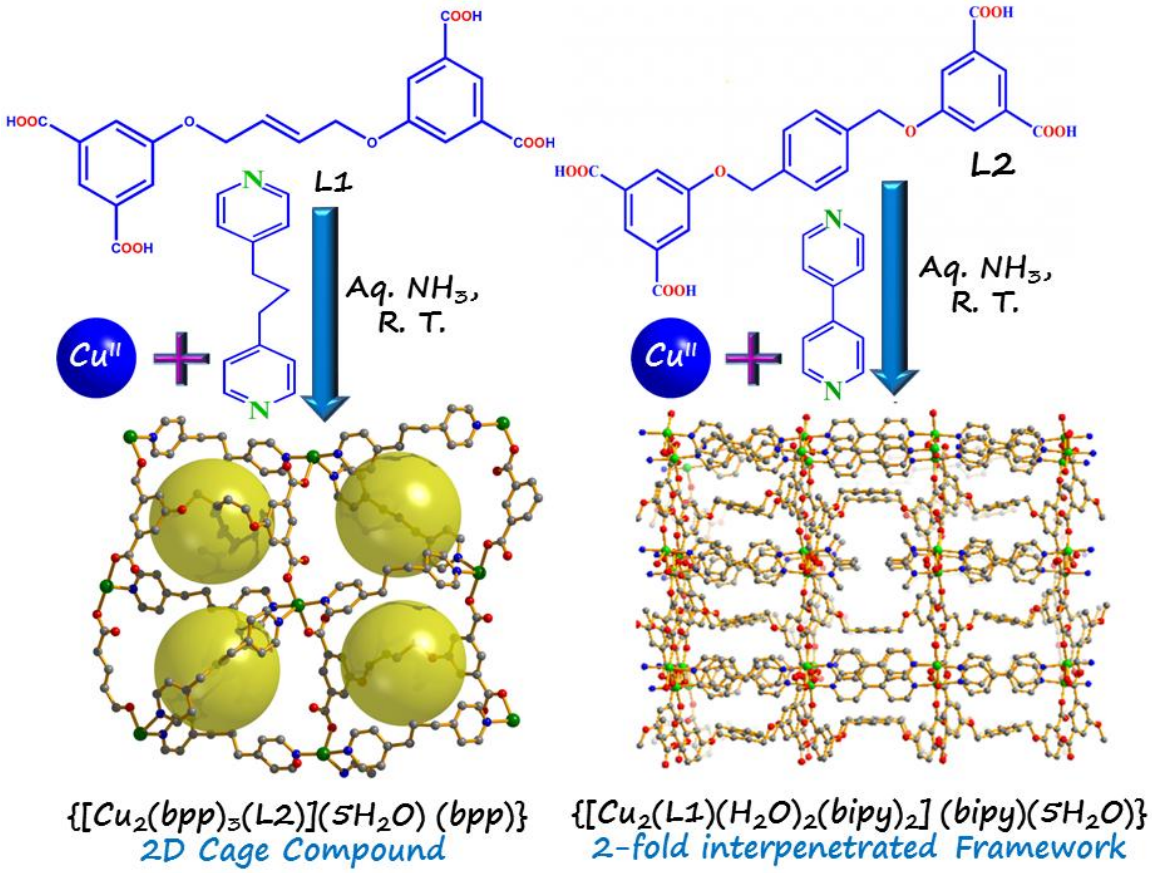

Scheme 1 pH dependant synthesis of compounds 1 and 2 by the self-assembly of Cu^{II} and the respective ligands at room temperature.

Carboxylates including di, tri and tetra carboxylates[15] are the most widely used ligand in MOF chemistry. Depending on the reaction conditions and stoichiometry, the metal ions can coordinate with the carboxylate ligands to form a wide range of multinuclear nodes with predictable geometries like binuclear paddle-wheel units, tri or tetranuclear units.[15b] In this regard, tetracarboxylate linkers are very efficient due to more number of coordinating sites.[15b, 15d] MOFs constructed from such tetracarboxylate ligands would have pore surface studded with large number of oxygen atoms, which would provide better interaction with gas molecules like CO_2. Furthermore, the flexibility of such ligands contributes in the tunable porosity of MOFs. In spite of such interesting properties, tetracarboxylate ligands have not been explored widely. In this work, we have

used two different flexible tetracarboxylate linkers [5,5'-(1,4-(2-butene)bis(oxy)diisophthalic acid (L1) and 5,5'-(1,4-phenylenebis(methylene))bis(oxy)diisophthalic acid (L2), Scheme 1) of different lengths and flexibility and envisioned that the self-assembly of these flexible linkers with metal ions and another coligand can indeed impart structural flexibility in the resulting framework structure. Self-assembly of L1 and bis-pyridyl propane (bpp) with Cu^{II} at room temperature results in a hydrophobic 2D MOF $\{[Cu_2(bpp)_3(L2)]\cdot(bpp)\cdot(5H_2O)\}$**(1)** with cage type structure. On the other hand, employing L2 in Cu^{II} and bipyridine (bipy) systems, we end up with a 3D MOF $\{[Cu_2(L1)(H_2O)_2(bipy)_2]\cdot(bipy)\cdot(5H_2O)\}$**(2)** with 2-fold interpenetration. The synthesis is pH dependant, done by stirring at room temperature in aqueous NH_3 after which the solution is left for slow evaporation. The crystals appear at an optimum pH by the evaporation of NH_3. Corresponding to the varying flexibility and the length of the ligand, the porosity and adsorption properties of compounds **1** and **2** vary. Compound **1** synthesized from **L1** has a 2D cage like structure which is hydrophobic in nature and the guest bpp molecules resides within the hydrophobic pockets. This hydrophobic nature of **1** is further reflected from various solvent adsorption measurements. The 2D framework of **1** is indeed flexible and shows structural transformation upon desolvation. Although there is no definite pore channel in **1**, the desolvated framework (**1'**) show CO2 selectivity, which may arise from the interaction of CO_2 with the electron rich aromatic rings that decorate the pore surface. On the other hand, compound **2** with a 2-fold interpenetrated 3D structure also undergoes structural change upon desolvation. At 195K, the desolvated framework (**2'**) exhibits high CO_2 adsorption uptake showing step at relatively high pressure and also shows significant uptake at room temperature. We attribute such behaviour to its flexible structure, presence of polar carboxylate groups and UMS in the pore surface. Furthermore, the flexibility of **2** was manifested in gate-opening H_2O adsorption isotherm.

4.2 Experimental Section

4.2.1 Materials

All the reagents and solvent were used as obtained from commercial supplies without any further purification. Dimethyl 5-hydroxy isophthalate, 1,4- Bis-bromomethyl-

benzene, Dibenzo-18-crown-6, 1,4-dibromobutene and K_2CO_3 were obtained from Aldrich Co. Ltd.

4.2.2 Synthesis of L1 & L2

4.2.2.1 Synthesis of L1-ester

A mixture of dimethyl 5-hydroxy isophthalate (2.10g, 10.0 mmol), 1,4-dibromobutene (5mmol) , dibenzo-18-crown-6 (0.10, 0.277 mmol) , and K_2CO_3 (2.21g, 16 mmol)were stirred in dry THF (40 ml) under dry atmosphere using a well fitted guard tube at 70°C for 24 hours. After this time 20ml 10 % aqueous Na_2CO_3 solution was added at 0°C under an ice bath. The resulting white solid was filtered and washed with water for several times and finally with diethyl ether and dried under vacuum.

4.2.2.2 Synthesis of 5,5'-(1,4-(2-butene)bis(oxy)diisophthalic acid (L1)

A mixture of L1 ester(2mmol), KOH (1.12g,20mmol), 40 ml MeOH and 40 ml distilled water were stirred at 80° C in oil bath for 48 hours. The reaction mixture was filtered to remove any unreacted starting materials. 30 ml 6(M) HCl was added dropwise to filtrate at 0°C under stirring. The white precipitate was filtered and washed with distilled water for several times and dried under vacuum.

4.2.2.3 Synthesis of 5,5'-(1,4-phenylenebis(methylene))bis(oxy)diisophthalic acid (L2)

The synthetic procedure of L2 is similar to that of L1, where 1,4- Bis-bromomethyl-benzene is used instead of 1,4-dibromobutene.

4.2.3 Synthesis of 1 $\{[Cu_2(bpp)_3(L2)]\cdot(bpp)\cdot(5H_2O)\}$

$CuCl_2.2H_2O$(0.2mmol, 34mg) and solid L2(0.1mmol, 47mg) were mixed with 10ml water and stirred for 10mins. Aqueous ammonia (20%) was added dropwise to this mixture till the solution becomes clear. To this 10ml methanol solution of 1,3-Bis(4-pyridyl) propane (0.5mmol, 99mg) was added and the resulting solution was stirred for 1 hour. The solution was allowed to settle at room temperature. After 3-4 days, dark blue needle shaped crystals appear. Yield: 60% relative to Cu^{II}. PXRD of the as-synthesized compound matches with the pattern simulated from the single crystal XRD data. Anal. calcd. for $C_{12}H_{17}Cu_2N_{17}$: C 61.051; H 5.123; N 7.910%. Found: C 60.99; H 5.43; N, 7.72%.

4.2.4 Synthesis of 2 {$[Cu_2(L1)(H_2O)_2(bipy)_2]\cdot(bipy)\cdot(5H_2O)$}

$CuCl_2.2H_2O$(0.2mmol, 34mg) and solid L1(0.1mmol, 47mg) were mixed with 20ml water and stirred for 10mins aqueous ammonia (20%) was added dropwise to this mixture till the solution becomes clear. To this 10ml methanol solution of 4,4'-bipyridine(0.5mmol, 78mg) was added and the solution was stirred overnight. The solution was kept in room temperature. A mixture of light blue crystals and powder appears after 3-4 days. Yield: 70% relative to Cu^{II}. Anal. calcd. for $C_{54}H_{46}Cu_2N_6O$: C 55.054; H 3.935; N 7.133%. Found: C, 55.26; H 3.45; N 7.27%.

4.2.5 Physical measurements

The elemental analyses were carried out using a Thermo Fischer Flash 2000 Elemental Analyzer. IR spectra were recorded with a Bruker IFS 66v/S spectrophotometer using KBr pellets in the region 4000–400 cm^{-1} with 10 scans for each measurement. Thermogravimetric analysis (TGA) were carried out (Metler Toledo) in a nitrogen atmosphere (flow rate = 50 ml min^{-1}) in the temperature range 30–500 °C (heating rate = 3 °C min^{-1}). Powder XRD patterns of the compounds in different states were recorded by using Cu-Kα radiation (Bruker D8 Discover; 40 kV, 30 mA).

4.2.6 X-ray Crystallography

X-ray single crystal structural data for **1** and **2** were collected using a Bruker Smart-CCD diffractometer equipped with a normal focus, 2.4 kW sealed tube X-ray source with graphite monochromated Mo-Kα radiation (λ = 0.71073 Å) operating at 50 kV and 30 mA. The program SAINT[16] was used for integration of diffraction profiles and absorption correction was made using the SADABS[17] program. All of the structures were solved using SIR 92[18] and refined by a full matrix least square method using SHELXL-97. [19] All of the hydrogen atoms were geometrically fixed and placed in ideal positions. The potential solvent accessible area or void space was calculated using the PLATON[20] multipurpose crystallographic software. All crystallographic and structure refinement data for **1** and **2** are summarized in Table 1. Selected bond lengths and angles for **1** and **2** are given in **Tables 4–9** respectively.

4.2.7 Adsorption Study

The adsorption isotherms of CO_2 (195 K) and N_2 (77 K) using the dehydrated samples of **1** and **2** were measured by using a QUANTACHROME QUADRASORB-SI analyzer. In the sample tube adsorbent samples **1** and **2** (~100–150 mg) were placed which had been prepared at 353 and 393 K, respectively, under a 1×10^{-1} Pa vacuum for about 6 h prior to measurement of the isotherms. Helium gas (99.999% purity) at a certain pressure was introduced in the gas chamber and allowed to diffuse into the sample chamber by opening the valve. The amount of gas adsorbed was calculated readily from the pressure difference ($P_{cal} - P_e$), where P_{cal} is the calculated pressure with no gas adsorption and P_e is the observed equilibrium pressure. All operations were computer-controlled and automatic. The adsorption of different solvents like MeOH at 293 K and H2O and EtOH at 298 K was measured in the desolvated sample of **1** and **2** in the vapour state by using a BELSORP aqua- 3 analyzer. The samples of about ~100–150 mg were activated under similar conditions as mentioned earlier. The different solvent molecules used to generate the vapour were degassed fully by repeated evacuation. The dead volume was measured with helium gas. The adsorbate was placed into the sample tube, then the change of the pressure was monitored and the degree of adsorption was determined by the decrease in pressure at the equilibrium state. All operations were computer controlled and automatic.

4.2.8 Characterization

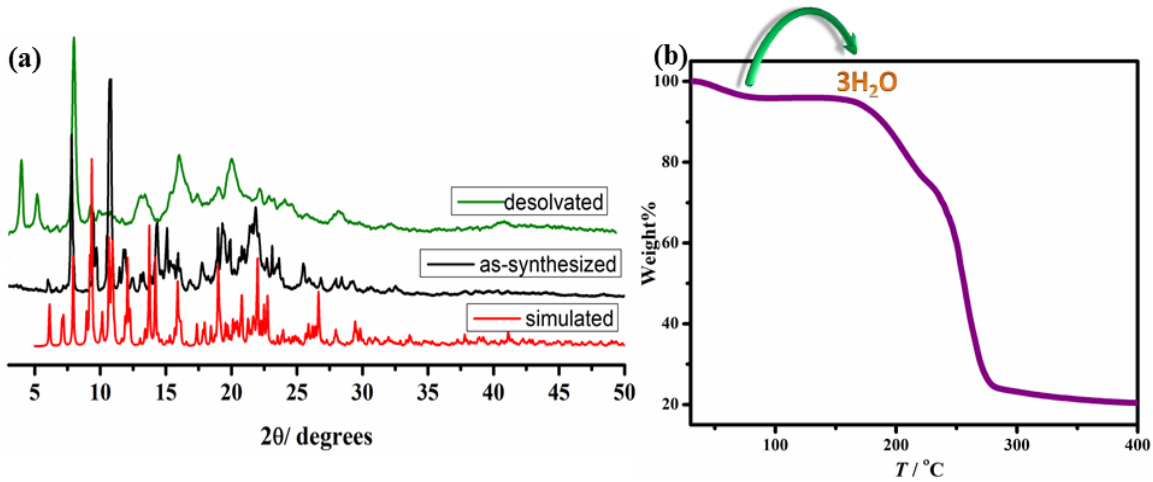

Fig.1(a) The change in the PXRD of **1** on being heated at 135°C. **(b)** TGA for **1**.

The thermogravimetric analysis (TGA) data of compound **1** shows an initial loss of ~4% corresponding to three guest water molecules (**Fig. 1(b)**). Subsequently there is a continuous weight loss beyond 150°C which may be attributed to the loss of the remaining two guest water molecules and the guest bpp molecule followed by the framework degradation. The two guest water molecules are released at a higher temperature probably due to hydrogen bonding with framework carboxylate oxygen atoms. The PXRD pattern of the as-synthesized compound matches perfectly with the simulated pattern, suggesting the phase purity (**Fig. 1(a)**). The framework on being desolvated undergoes structural changes, as evident from the PXRD pattern of the framework desolvated at 135°C under vacuum. On desolvation, almost all the peaks are broadened and the first two peaks in the as-synthesized pattern lose their intensity. The IR spectrum of compound **1** was also recorded (**Fig. 2**). Selected IR data (KBr, cm^{-1}) have been given in **Table 1**.

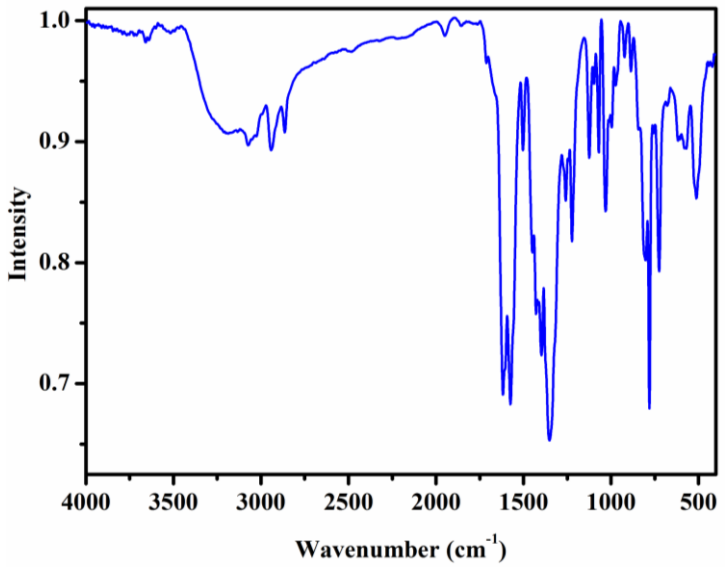

Fig. 2 IR spectrum of **1**.

Table 1: Principal Peaks in IR (**Fig. 2**).

Peak Position	**Nature**	**Vibration**
1568, 1618cm^{-1}	strong	C=O stretch
778cm^{-1}	strong	Aromatic C-H stretch
1358cm^{-1}	strong	C-N stretch

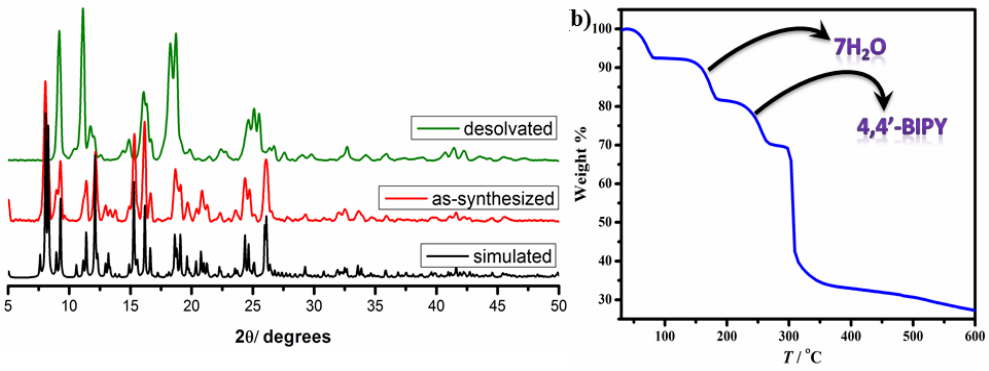

Fig. 3(a) PXRD pattern of **2** with increasing temperature **(b)** TGA for **2**.

The thermogravimetric analysis (TGA) data of **2** shows an initial loss of ~9% up to 100°C owing to the loss of 5 guest water molecules and one coordinated water molecule. Subsequently one more coordinated water molecule is lost at ~160°C (**Fig. 3(b)**). The subsequent ~13% loss around 240°C can be attributed to the loss of the guest bipyridine molecule. The desolvated framework degrades almost continuously after that. PXRD pattern of the as-synthesized compound **2** is in accordance with the simulated pattern. The structure of compound **2** shows changes with increasing the temperature, as evident from the desolvated PXRD pattern (**Fig. 3(a)**). This might be due to the removal of the coordinated water molecules and the guest bipy molecules, which interact with the framework via π-π stacking. The removal of the bipy molecule probably gives rise to another structural phase. In this framework, along with guest water molecules, there are coordinated water molecules and their removal results in UMS. Such change in the coordination sphere of Cu^{II} centre ensue structural change, as reflected from the PXRD pattern.The IR spectrum of compound **2** was also recorded (**Fig. 4**). Selected IR data (KBr, cm^{-1}) have been given in **Table 2**.

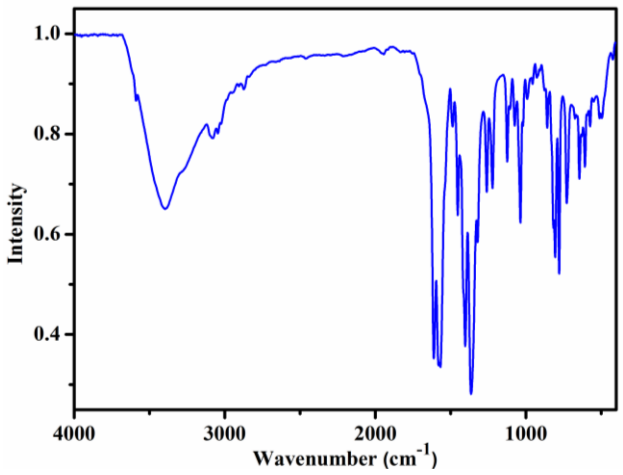

Fig. 4 IR spectrum of **2**.

Table 2: Principal peaks in the IR spectrum of **2** (**Fig. 4**)

Peak Position	Nature	Vibration
1570, 1616 cm^{-1}	strong	C=O stretch
782 cm^{-1}	strong	Aromatic C-H stretch
1265, 1354 cm^{-1}	strong	C-N stretch
3900 cm^{-1}	medium, broad	water

4.3 Results and Discussion

4.3.1 Crystal Structure Description

Single crystal X-ray diffraction data reveals that Compound 1 crystallizes in monoclinic $P2_1/c$ space group. The asymmetric unit contains two crystallographically independent penta coordinated Cu^{II} ions, which have a (4+1) square pyramidal geometry. The degree of deviation from ideal square pyramidal geometry has been calculated in terms of Addison parameter (ъ).[21] The value is 0.019 for Cu1, which is very small and suggests that the geometry to be square pyramidal rather than trigonal bipyramid. The coordination sphere of Cu1 is fulfilled by two oxygen atoms (O1 and O9) from tetracarboxylate ligand L1 and three nitrogen atoms (N1, N3 and N5) from three bispyridyl propane(bpp) ligands(**Fig. 5(a)**). The basal plane of Cu1 is occupied by N1 and N3 from two different bpp molecules along with O1 and O9 from L1. The apical position is occupied by N5 atom from another bpp ligand. Similarly, the penta coordination of Cu2 is fulfilled by two oxygen atoms (O4 and O6) from L1 and three nitrogen atoms (N2, N4 and N6) from bpp linker molecules. Here, the basal plane of Cu1 is occupied by N2 and N4 from two different bpp ligands along with O4 and O6 from L1(**Fig. 5(a)**). The ъ value is Cu2 is 0.13, suggesting the distortion from the ideal square pyramidal geometry. Cu1 and Cu2 are connected together by bpp ligand molecules to form a wavy chain (**Fig. 5(b)**). Two such chains originating from Cu1 are connected together by L1 till it terminates at Cu2 (**Fig. 5(c)**). Thus a 2D network with a cage like structure is formed, where no definite pore can be observed. However, there is the presence of a hydrophobic pocket along b direction. This pocket is lined by L1 along the *a* and *c* directions on one side and on the other side, it is lined by the bpp linker in the same directions. The aromatic rings of L1

and bpp molecule along the pocket make it hydrophobic in nature. The guest bpp molecules reside within this pocket and undergo weak π-π interaction with pyridyl ring of the bpp ligands (cg-cg distance 4.6 Å). The solvent accessible void is 2943.3 $Å^3$ (39.6% of the total cell volume) has been calculated using PLATON after removing the guest bpp and the water molecules. Almost all guest water molecules present in the framework are hydrogen bonded with the framework. Only the water molecule with O5w does not show any interaction with the framework. Also, among the other guest water molecules, O4w is hydrogen bonded to the framework nitrogen atom N8, and this H-bond is relatively weaker than those formed by the O atoms and the H-bond length is greater. Moreover, O3w is H-bonded with O4w. Hence removing both O4w and O3w is relatively easy. However, O2w is H-bonded with bonded with O2 and O8. O1w is H-bonded with O6 of the framework and the bond length is small (~2.2Å) hence the bond is very strong. The hydrogen bonding parameters of 1 have been summarized in **Table 6**.

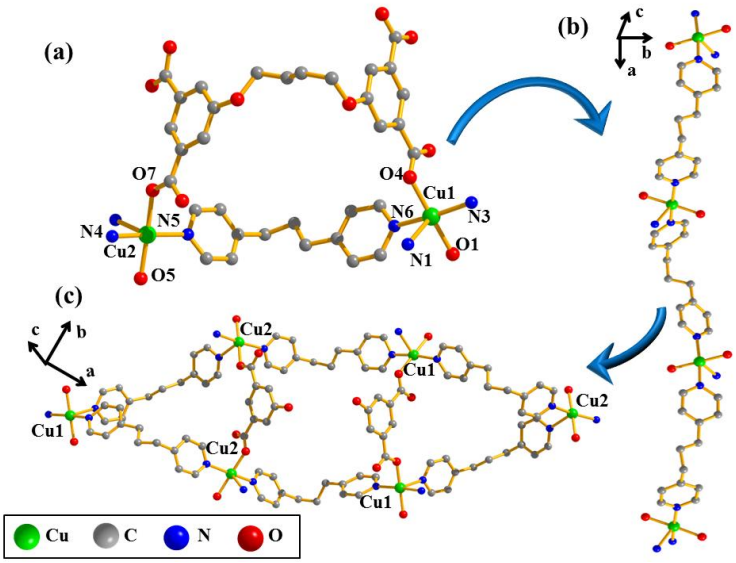

Fig. 5(a) Coordination sphere of Cu1 and Cu2 in compound **1**. **(b)** 1D wave in **1** formed by Cu centres linked with bpp molecules. **(c)** 2D network in **1**.

Compound **2** crystallizes in the *C*2/*c* monoclinic space group. Each asymmetric unit comprises two crystallographically independent penta-coordinated Cu^{II} centres, each of which assumes a distorted square pyramidal geometry, the degree of distortion being as low as 0.007 for Cu1 and 0.037 for Cu2. The penta coordination of Cu1 is fulfilled by two nitrogen atoms (N1 and N2) from two different bipy molecules, two oxygen atoms (O1 and O3) from tetracarboxylate ligand **L2**, and one oxygen (O7w) from a coordinated water molecule. Similarly, the penta coordination of Cu2 is satisfied by two nitrogen

atoms (N3 and N036) from two different bipy molecules, two oxygen atoms (O5 and O12) from L2, and one oxygen atom (O5w) from a coordinated water molecule. Cu1 and Cu2 bridged together by a bipy ligand molecule forming the 1D chain along the crystallographic *a* direction (**Fig. 6(a)**). These chains are connected together by L2 ligands along the *b* direction to form the 2D sheet on the *ab* plane (**Fig. 6(b)**). These sheets are further stacked together by L2 molecules to form a 3D framework with 2 fold interpenetration (**Fig. 6(c)**). Two 3D frameworks interpenetrate each other resulting in the 2-fold interpenetrated 3D framework. Along crystallographic *b* direction, the single nets of the 3D framework contain 1D pore channels with pore dimension 4.45 × 5.46 $Å^2$ (after removing the bpp molecules, the guest and the coordinated water molecules), which upon interpenetration reduces to smaller pore channel having pore dimension 1.93Å × 5.14 $Å^2$ and the pore channel is occupied by guest bipy and guest water molecules. All the guest water molecules, except O4w, are hydrogen bonded to the framework and the hydrogen bonding parameters have been summarized in **Table 9**. The pyridyl ring (containing N4 atom) of guest bipy molecules shares a π- π interaction (cg-cg distance 3.76 Å) with the pyridyl ring (containing N1 atom) of bipy linkers along the pore wall. As we have discussed earlier, both Cu1 and Cu2 are coordinated to water molecules and thus UMS could be generated after desolvation. The solvent accessible void is 5826.1 $Å^3$ (47.5% of the total cell volume) has been calculated using PLATON after removing the coordinated and as well as guest water molecules and the guest bipy molecules.

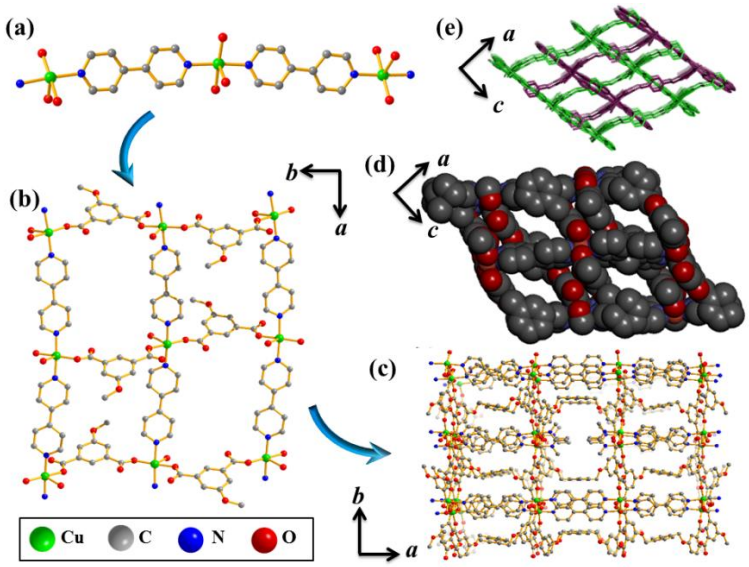

Fig. 6(a) 1D chain along crystallographic *a* direction in **2**. **(b)** 2D sheet along *ab* plane in **2**. **(c)** 3D framework in **1 (d)** Pore view of **2 (e)** 3D interpenetrated network of **2.**

Table 3. Crystal Data and Structure Refinement for compounds **1** and **2**

Parameter	**1**	**2**
Empirical formula	$C_{72}H_{72}Cu_2N_8O_{15}$	$C_{54}H_{46}Cu_2N_6O_{17}$
Formula weight	1416.4	1177.99
Crystal system	*Monoclinic*	*Monoclinic*
Space group	$P2_1/c$ (No.14)	$P2_1/c$ (No.15)
a, Å	23.6727(17)	44.8511(10)
b, Å	18.9130(13)	19.0460(4)
c, Å	17.6128(13)	14.7115(3)
β, deg	109.696(3)	102.380(1)
V, Å^3	7424.3	12274.8
Z	4	8
T, K	293	293
μ,mm^{-1}	0.640	0.761
D_{calcd},g/cm^3	1.258	1.264
F (000)	2912	4768
reflections [$I>2\sigma(I)$]	6050	6008
unique reflections	11104	9473
measured reflections	108306	81632
R_{int}	0.188	0.085
GOF on F^2	1.35	1.10
$R_1[I>2\sigma(I)]$[a]	0.1336	0.0815
$R_w[I>2\sigma(I)]$[b]	0.4117	0.2891

($R = \sum||F_o|-|F_c||/\sum|F_o|$,$R_w = [\sum\{w(F_o^2-F_c^2)^2\}/\sum\{w(F_o^2)^2\}]^{1/2}$)

Table 4. Selected bond distances (Å) for **1**.

Cu1 -O1	1.966(6)	Cu1-N1	2.043(10)
Cu1-N3	2.059(12)	Cu2-N6	2.349(12)
Cu2-O6	1.929(8)	Cu2-N2	2.042(10)
Cu2-N4	2.051(10)	Cu2-O4	1.952(8)
Cu1-O9	1.941(6)	Cu1 -N5	2.319(10)

Table 5. Selected bond angles (°) for **1**.

O1 -Cu1-N1	90.1(3)	O1 -Cu1-N3	89.5(3)
O4-Cu2 -N6	90.7(3)	O4-Cu2-N2	90.4(4)
O4-Cu2-O6	177.0(4)	O1-Cu1-N5	89.6(3)
O4-Cu2-N4	91.6(4)	O9-Cu1-N5	90.6(3)
N3-Cu1-N5	92.0(4)	O9-Cu1-N3	90.8(4)

Table 6. Hydrogen bond parameters (Å) for **1**.

O1w – O3	2.919	O4w –N8	2.971
O2w –O2	2.698	O3w –O4w	2.845
O2w –O8	2.645		

Table 7. Selected bond distances (Å) for **2**.

Cu1-O1	1.941(6)	Cu1-O3	1.946(6)
Cu1-O7W	2.250(6)	Cu2-N3	2.023(7)
Cu2-N036	2.006(9)	Cu2-O12	1.925(6)
Cu2-O5W	2.353(7)	Cu1-N1	2.026(6)
Cu2-O5	1.911(6)	Cu1-N2	2.042(7)

Table 8. Selected bond angles (°) for **2**.

O1-Cu1-O3	176.5(2)	O1-Cu1-O7W	88.3(2)
Cu2-N036 -C36	124.7(10)	O5-Cu2-N036	90.4(3)
O5-Cu2-O12	178.0(3)	O5-Cu2-O5W	91.3(3)
O7W-Cu1-N2	90.6(3)	Cu2-N3-C8	119.6(5)
N1-Cu1-N2	176.0(2)	Cu2-N3-C9	122.2(5)

Table 9. Hydrogen bond parameters (Å) for **2**.

O1w – O2	2.812	O3w –O13	2.773
O1w – O4	2.662	O3w –O6	2.795
O1w –O2w	2.711	O3w –O6w	2.769
O2w –O6	2.866	O5w –O6w	2.944

4.3.2 Gas and Solvent Vapour Adsorption

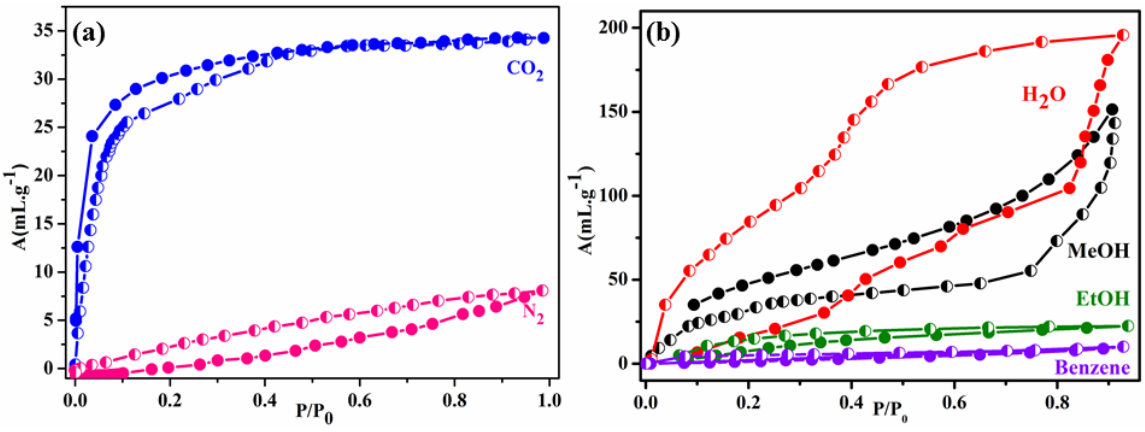

Fig.7(a) CO_2 adsorption isotherm of compound **1** at 195K. **(b)** Solvent adsorption isotherms of compound **1**.

Although compound **1** does not have a definite pore in any direction, the presence the hydrophobic pocket and electron rich aromatic benzene and pyridine rings along crystallographic *b* direction prompted us to check the adsorption behaviour of the desolvated framework (**1'**). At 195 K, **1'** adsorbs a reasonable amount (35 $mL.g^{-1}$) of CO_2, which can be attributed to the interaction of the CO_2 molecules with the free pendant carboxylate oxygen atoms that flank the pore surface (**Fig. 7a**).

1 is essentially hydrophobic in nature, owing to the π-electron density on the pore surface from the aromatic rings of the ligand. Hence it does not adsorb appreciable amounts of H_2O, ethanol or methanol at low pressure, reflecting that the interaction of these solvents is poor with the hydrophobic framework. The water adsorption curve (**Fig. 7b**) confirms the hydrophobic nature exhibiting low uptake at lower pressures. It shows a wide hysteresis, with the desorption curve following a separate path from the adsorption curve. Although no definite pore can be observed, the solvent accessible void space is 39.6%, hence at higher pressure of the adsorbate water molecules, there is a considerable amount of water uptake. The net water uptake is 195 $mL.g^{-1}$, with **1** adsorbing 2.04 moles of water at P/P_0 = 0.394 and 9.86 moles of water at P/P_0 = 0.928. The total uptake for methanol and ethanol are 151 and 22 $mL.g^{-1}$ respectively. The net adsorption amount decreases from water to methanol to ethanol as the kinetic diameter of the solvent molecule increases in that order. The kinetic diameter of water is 2.7 Å, which is 3.6 Å in MeOH and 4.5 Å in EtOH. At low pressures, till P/P_0 = 0.394, the adsorption of methanol is higher than that of water, since the polarity of ethanol is lower than that of water and methanol. However due to lesser size, the net uptake of water is much higher than MeOH. At P/P_0 = 0.928, each mole of **1** adsorbs only 7.62 moles of MeOH. In such cases, the hydrophobic MOF is expected to take up good amounts of non-polar solvents like benzene. However, in this case the pore dimensions of **1** is much smaller than the kinetic diameter of benzene (5.9 Å), hence it does not show appreciable benzene uptake (**Fig. 7b**).

In order to check the porous properties of compound **2**, N_2 adsorption isotherm of the desolvated framework (**2'**) was measured at 77 K. **2'** does not adsorb any N_2 gas, which is attributed to the high diffusion barrier as there could not be any interaction between inert N_2 gas (kinetic diameter: 3.65 Å) in the narrow pore channel of **2'** (1.93 × 5.14 $Å^2$) along *b* direction) (**Fig. 8(c)**). Moreover, the accessible void space in this framework is very small due to the two fold interpenetration. However, the desolvated framework **2'** shows high uptake of CO_2 uptake at 195 K and 273 K as well as at room temperature. This can be attributed to the presence of pendent carboxylate oxygen atoms on the pore surface. Also, the presence of unsaturated metal sites (UMS), i.e., penta co-ordinated Cu^{II} sites, along the pore further contributes to the enhanced adsorption. Also, the kinetic diameter of CO_2 is smaller (3.64 Å) and its high quadruple moment interacts with the π electron cloud of the aromatic rings on the pore surface. The uptake of CO_2 at 195 K is 127 $mL.g^{-1}$

with a step at high pressure in the adsorption isotherm (**Fig. 8(a)**). At lower pressures, **2'** shows steep uptake of CO_2, indicating its microporous nature. A step is observed at P/P_0 = 0.76 after which the adsorption increases again. This can be attributed to the flexible structure of the framework, which undergoes structural transformations at high pressure, there by facilitating higher adsorption. Till P/P_0 = 0.011, each mole of **2'** adsorbs 3.01moles, after which the isotherm saturates and the adsorption per mole is 4.23 moles at P/P_0 = 0.71. After this, the step at P/P_0 = 0.76 increases the adsorption and the net uptake is 5.10moles per mole of 2' at P/P_0 = 0.99. The desorption does not follow the same path as adsorption initially and we observe a hysteresis till P/P_0 = 0.55, below which both the curves converge. This further implies the flexibility of this system at higher pressures of CO_2 gas. The adsorption amount of CO_2 is 85 $mL.g^{-1}$ at 273 K and 65 $mL.g^{-1}$ at 298 K. **2** shows a type-I adsorption at 298 K where the adsorption and desorption curves do not coincide, exhibiting a narrow hysteretic profile. Owing to the flexible tetracarboxylate ligand as well as guest induced modification, the structure undergoes changes at high pressure as a result the step is formed in the adsorption isotherm. Under high pressure, the uptake amount of CO_2 is 60 $mL.g^{-1}$ at 298 K and the profile exhibits a wide hysteretic pathway.

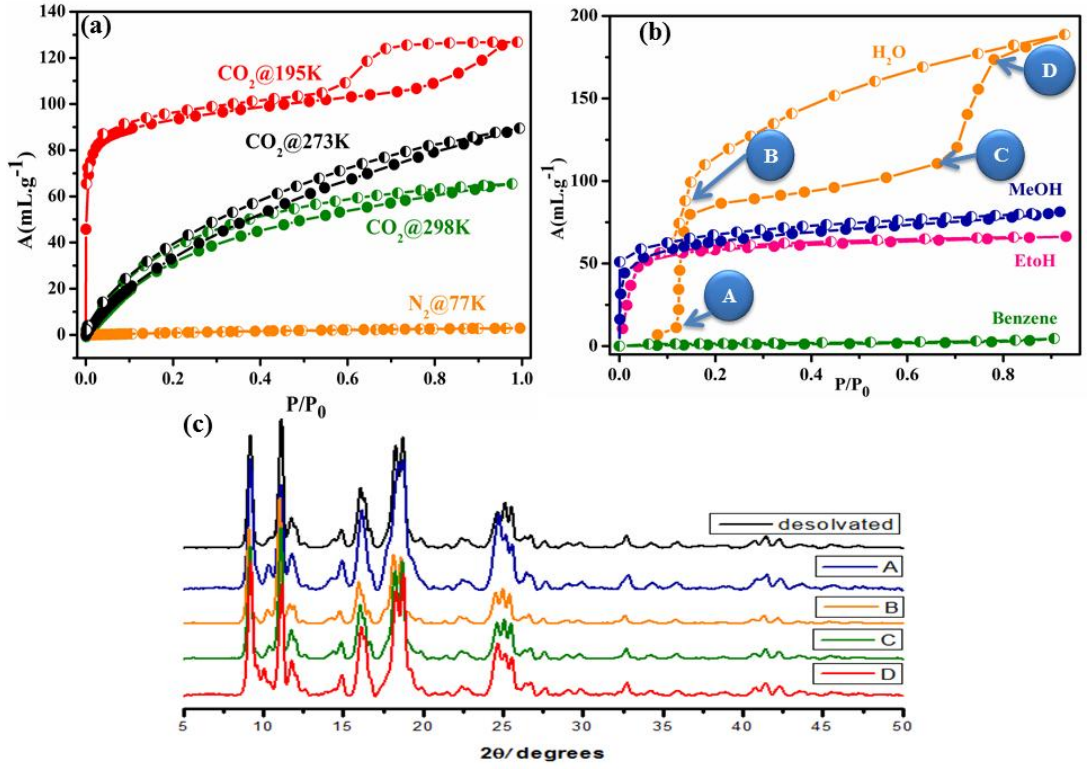

Fig.8(a) CO_2 adsorption isotherm of **2' (b)** Solvent adsorption isotherms of **2' (c)** N_2 adsorption isotherm of **2' (d)** PXRD pattern of **2'** at different stages of water adsorption

The adsorption profile was further analyzed by the Dubinin-Radushkevich equation[22] to realize the adsorbate-adsorbent interaction and the isosteric heat of adsorption ($q_{st,f}$) value for **2'** is found to be ~ 63.2 kJ. mol^{-1}, suggesting strong interaction of CO_2 with the framework.

The solvent adsorption profiles of **2** are quite interesting as well. **2'** adsorbs 188 mL.g^{-1} H_2O, and the adsorption isotherm shows a gated behaviour. In this case, the adsorption increases slowly till the gate opening pressure P/P_0 = 0.12. Beyond this pressure, the hydrophilic nature of the framework is reflected through the steep uptake till P/P_0 = 0.15 and the uptake amount is 3.21 moles/mole. After P/P_0 = 0.15, the curve somewhat saturates and adsorbs 4.84 moles/mole till P/P_0 = 0.70. Beyond this pressure, the second step appears and the adsorption isotherm again increases steeply, 6.97 moles/mole being the uptake amount till P/P_0 = 0.78. The curve again starts saturating at this point to decrease the uptake and the total uptake is 7.58 moles/mole at P/P_0 = 0.93 (**Fig. 8(b)**). As discussed in case of **1**, the adsorption amount decreases with the increasing kinetic diameter of the solvent. Hence, **2'** takes up 66 mL.g^{-1} MeOH and 81 mL.g^{-1} EtOH. In both cases, the adsorption profile is type-I in nature, which further confirms the microporous nature of **2**. **2'** adsorbs almost no benzene which further proves its hydrophilicity (**Fig. 8(b)**).

4.4 Conclusion

In conclusion, we report the room temperature pH dependent synthesis of two new MOFs with flexible tetracarboxylate ligands. Compound **1** has a 2D cage like structure, with no visible pore. However, there is the presence of a hydrophobic pocket, lined by aromatic rings from the ligand, owing to which **1'** adsorbs a reasonable amount of CO_2 at 195K. On the other hand, compound **2** constructed from L2, has a 3D framework with 2 fold interpenetration. Presence of polar carboxylate groups, UMS and flexible structure enable **2'** to adsorb excellent amounts of CO_2 both at room temperature as well as 195K. These results manifest the modulation of the porosity of a framework owing to the structural change brought about by ligand flexibility. Thus frameworks constructed from such tetracarboxylate ligands can be used as effective materials for CO_2 sequestration and separation by tuning flexibility and functionalities, which is currently being investigated in our lab.

4.5 References

1. S. Kitagawa, R. Kitaura and S.-i. Noro, *Angew. Chem. Int. Ed.*, 2004, **43**, 2334-2375.
2. (a) J.-R. Li, R. J. Kuppler and H.-C. Zhou, *Chem. Soc. Rev.*, 2009, **38**, 1477-1504; (b) M. P. Suh, H. J. Park, T. K. Prasad and D.-W. Lim, *Chem. Rev.*, 2012, **112**, 782-835; (c) K. Sumida, D. L. Rogow, J. A. Mason, T. M. McDonald, E. D. Bloch, Z. R. Herm, T.-H. Bae and J. R. Long, *Chem. Rev.*, 2012, **112**, 724-781.
3. J. Liu, L. Chen, H. Cui, J. Zhang, L. Zhang and C.-Y. Su, *Chem. Soc. Rev.*, 2014, **43**, 6011-6061.
4. S. Roy, A. Chakraborty and T. K. Maji, *Coord. Chem. Rev.*, 2014, **273–274**, 139-164.
5. Z. Hu, B. J. Deibert and J. Li, *Chem. Soc. Rev.*, 2014, **43**, 5815-5840.
6. S. Horike, S. Shimomura and S. Kitagawa, *Nat. Chem.*, 2009, **1**, 695-704.
7. Y. K. Park, S. B. Choi, H. Kim, K. Kim, B.-H. Won, K. Choi, J.-S. Choi, W.-S. Ahn, N. Won, S. Kim, D. H. Jung, S.-H. Choi, G.-H. Kim, S.-S. Cha, Y. H. Jhon, J. K. Yang and J. Kim, *Angew. Chem. Int. Ed.*, 2007, **46**, 8230-8233.
8. D.-m. Chen, W. Shi and P. Cheng, *Chem. Commun.*, 2015, **51**, 370-372.
9. (a) B. Liu, W.-P. Wu, L. Hou and Y.-Y. Wang, *Chem. Commun.*, 2014, **50**, 8731-8734; (b) M. O'Keeffe and O. M. Yaghi, *Chem. Rev.*, 2011, **112**, 675-702.
10. Z.-J. Lin, J. Lu, M. Hong and R. Cao, *Chem. Soc. Rev.*, 2014, **43**, 5867-5895.
11. A. Schneemann, V. Bon, I. Schwedler, I. Senkovska, S. Kaskel and R. A. Fischer, *Chem. Soc. Rev.*, 2014, **43**, 6062-6096.
12. (a) L. Qin, Z.-M. Ju, Z.-J. Wang, F.-D. Meng, H.-G. Zheng and J.-X. Chen, *Crystal Growth & Design*, 2014, **14**, 2742-2746; (b) R. Haldar and T. Maji, *J Chem Sci*, 2011, **123**, 883-890.
13. (a) P. Kanoo, R. Sambhu and T. K. Maji, *Inorg. Chem.*, 2010, **50**, 400-402; (b) B. Liu, Y. Li, L. Hou, G. Yang, Y.-Y. Wang and Q.-Z. Shi, *J. Mater. Chem. A*, 2013, **1**, 6535-6538.
14. R. Haldar, S. K. Reddy, V. M. Suresh, S. Mohapatra, S. Balasubramanian and T. K. Maji *Chem. Eur. J.*, 2014, **20**, 4347-4356.
15. (a) Y. Ling, Z.-X. Chen, F.-P. Zhai, Y.-M. Zhou, L.-H. Weng and D.-Y. Zhao, *Chem. Commun.*, 2011, **47**, 7197-7199; (b) X. Lin, J. Jia, X. Zhao, K. M. Thomas, A. J. Blake, G. S. Walker, N. R. Champness, P. Hubberstey and M. Schröder,

Angew. Chem. Int. Ed., 2006, **45**, 7358-7364; (c) L. H. Wee, C. Wiktor, S. Turner, W. Vanderlinden, N. Janssens, S. R. Bajpe, K. Houthoofd, G. Van Tendeloo, S. De Feyter, C. E. A. Kirschhock and J. A. Martens, *J. Am. Chem. Soc.*, 2012, **134**, 10911-10919; (d) Z. Pan, H. Zheng, T. Wang, Y. Song, Y. Li, Z. Guo and S. R. Batten, *Inorg. Chem.*, 2008, **47**, 9528-9536.

16. S. V. a. SMART (V 5.628), XPREP, SHELXTL; Bruker AXS Inc. Madison, Wisconsin, USA, 2004.
17. G. M. Sheldrick, *SADABS, Empirical Absorption Correction Program, University of Göttingen, Göttingen*, 1997.
18. A. Altomare, G. Cascarano, C. Giacovazzo and A. Guagliardi, *J. Appl. Crystallogr.*, 1993, **26**, 343-350.
19. G. M. Sheldrick, *SHELXL 97, Program for the Solution of Crystal Structure, University of Göttingen, Germany*, 1997.
20. A. Spek, *J. Appl. Crystallogr.*, 2003, **36**, 7-13.
21. A. W. Addison, T. N. Rao, J. Reedijk, J. van Rijn and G. C. Verschoor, *J. Chem. Soc., Dalton Trans.*, 1984, 1349-1356.
22. A. Kapoor, J. A. Ritter and R. T. Yang, *Langmuir*, 1989, **5**, 1118-1121.

Chapter 5

Anion Exchange and Iodine Capture in a Cationic Metal-organic Framework

Abstract

This chapter contains synthesis and characterization of a bi-metallic cationic metal-organic frameworks $[KCd_3(HIB)_6(H_2O)_3]\cdot(NO_3)\cdot 7H_2O$ (**1**) [HIB = 4-(1H-imidazole-1-yl) benzoate) (**1**). Framework **1** is a 3D porous positively charged framework and the voids are occupied by guest water molecules and a nitrate anion to compensate the positive charge of the framework. Removal of coordinated water molecule from Cd^{II} center creates an unsaturated metal site (UMS) and upon removal of all the guest molecules framework remains intact. Although **1** does not possess sufficient void space, the desolvated framework shows selective gated CO_2 adsorption at 195 K. The affinity for water was also verified through steep uptake profile of water vapour. Further, this anionic framework was found to be efficient for anion exchange with azide, thiocyanate and dicyanamide anions. Strong and efficient encapsulation of iodine vapour in form of I^{3-} could also be achived using this anionic framework.

5.1 Introduction

Metal-organic frameworks (MOFs)[1] are an exciting range of materials which have received immense attention owing to their multi-faceted properties, e.g., gas storage,[2] catalysis,[3] luminescence,[4] sensing,[5] optoelectronics[6] and drug delivery.[7] The properties of MOFs can be tuned by playing with diverse labile metal ions and multi-dentate organic ligands. Moreover, rich host-guest dependant behaviour is observed in MOFs with a range of counter ions or solvent molecules in their cavities. MOFs are generally neutral compounds in nature, unlike certain other porous materials like zeolites,[8] where extra-framework cations are commonly present. Such inorganic porous solids like zeolites with negative frameworks are widely used for cation exchange. However, there is a pressing need for the development of new materials with positive frameworks for selective anion exchange and separation or storage and delivery.[9] MOFs provide a hope in this direction, where tuning the stoichiometric ratio appropriately can lead to the formation of ionic MOFs, where the framework itself is cationic/ anionic and the net charge on the framework necessitates the presence of extra-framework counter ions.[10] In the vast MOF library, although several anionic MOFs are reported, there are only a few permanently porous MOFs with positive frameworks.[8c, 11] Anion exchange in cationic MOFs has been used for certain specific applications, e.g., water pollutant removal,[10, 12] drug delivery,[13] tunable emission,[14] selective dye encapsulation[9, 11b] and structural dynamism.[14]

Iodine along with its various radioactive isotopes has diverse applications e.g., monitoring long living environmental contaminants (I^{129}), imaging thyroid glands (I^{123}), radiation for cancer treatment therapy (I^{131}), gamma emitting protein tag (I^{125}), etc. Besides, it has also been used in catalysis, animal feed and water disinfection. However, iodine released from nuclear plants is extremely health hazardous and there is a growing concern regarding the capture and removal of iodine from such industrial waste.[15] Also, the various forms of iodine, i.e., I_2, methyl iodide (CH_3I), iodate (IO_3^-) and iodide(I^-) have received great attention from researchers. Polyiodides, e.g., triiodide (I_3^-), pentaiodide (I_5^-) and septaiodide (I_7^-) are commonly found in aqueous and organic solvents.[16] Among the various porous materials, zeolites have been observed to be one of the most effective materials for iodine capture. Zeolites have high stability and particularly silver metallated frameworks show high iodine sorption capacity. But the relatively low porosity of zeolites restricts high sorption and storage capacities and efficiency in case of nuclear accidents.[17] Unlike these zeolitic materials, MOFs show very high surface areas coupled

with a wide possibility of framework functionalization. Recently, iodine capture and storage has also been added to the list of diverse applications of MOFs.[15-18]. It has also been observed that the capture of I_2 in the framework results in cooperative electrical conductivity, thereby enhancing the electrical conductivity of the framework.[15, 18b]

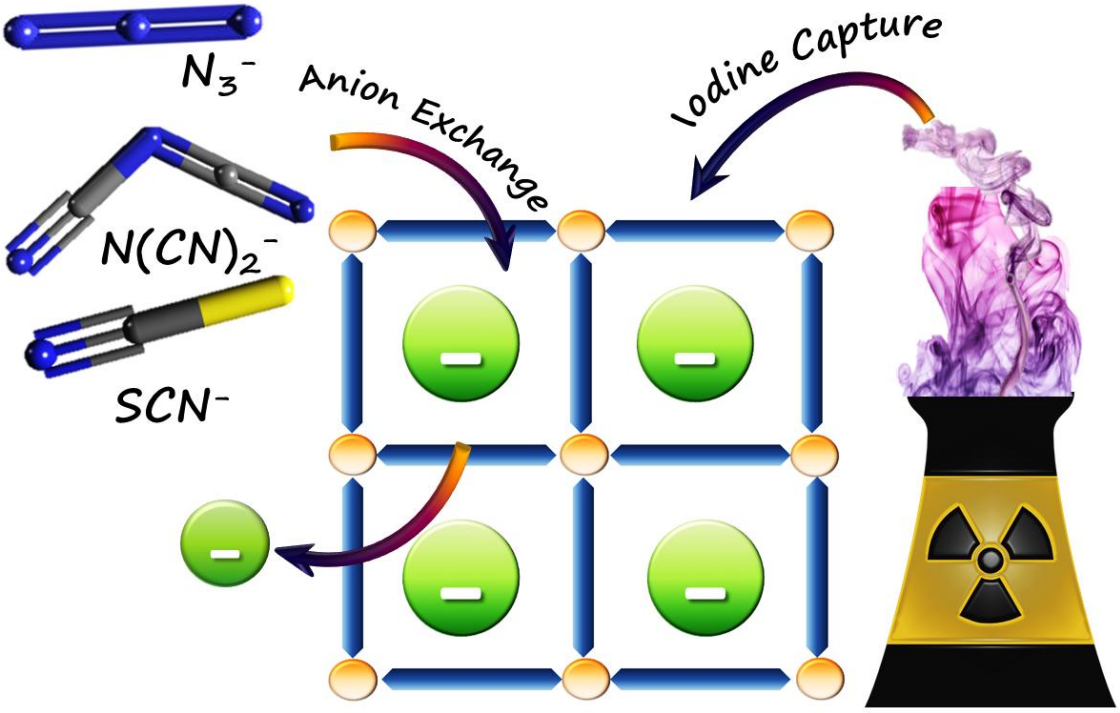

Fig. 1 A scheme representing the applications of **1**.

This chapter describes the synthesis and selective adsorption properties of a porous cationic MOF $[KCd_3(HIB)_6(H_2O)_3]\cdot(NO_3)\cdot 7H_2O$ (**1**). The overall framework neutrality in **1** is maintained by nitrate anions residing within its pore channels. The framework does not have pores in any definite direction, however it shows a selective uptake of CO_2 over N_2. The nitrate anions of **1** maybe exchanged with anions like azide (N_3^-), thiocyanate (SCN^-) and dicyanamide ($N(CN)_2^-$). Also **1** shows iodine capturing properties, which can be used for several applications (**Fig. 1**).

5.2 Experimental Section

5.2.1 Materials

All the reagents and solvent were used as obtained from commercial supplies without any further purification. Imidazole, Ethyl-4-bromo benzoate and all the metal salts were procured from Sigma Aldrich Co.

5.2.2 Synthesis of 4-(1H-imidazole-1-yl)-ethyl ester (HIEE)

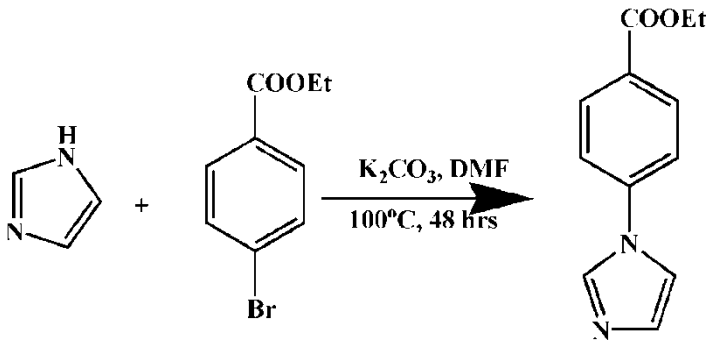

Scheme 1 Synthesis of 4-(1H-imidazole-1-yl)-ethyl ester (HIEE)

300 mg imidazole, 0.64 mL Ethyl-4-bromo benzoate, 830 mg K_2CO_3 and 40 mL DMF were taken in a round bottomed flask. It was heated at 100°C for 48 hrs. The solution was cooled and poured in 200 mL cold water and filtered. It was then extracted in ethyl acetate and dried under vacuum.

5.2.3 Synthesis of 4-(1H-imidazole-1-yl) benzoic acid (HIBA)

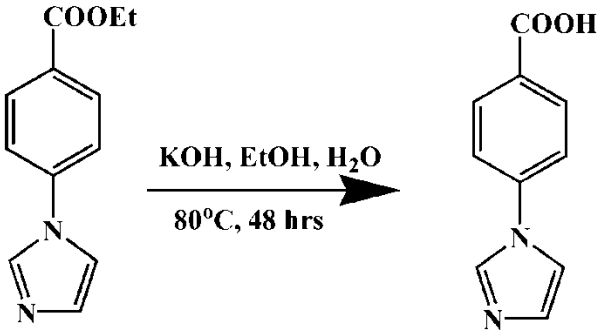

Scheme 2 Synthesis of 4-(1H-imidazole-1-yl)-benzoic acid (HIBA)

1 gm HIEE, 1.12 gm KOH, 40 mL ethanol and 40mL distilled water were taken together in a round bottomed flask. It was stirred at 80°C for 48 hrs. The resultant mixture was filtered and the filtrate was treated with 30mL 6(N) HCl at 0°C with constant stirring. The white precipitate was filtered and washed with distilled water repeatedly.

5.2.4 Synthesis of $[KCd_3(HIB)_6(H_2O)_3]\cdot(NO_3)\cdot 7H_2O$ (1)

0.154 gm $Cd(NO_3)_2$, 0.188 gm HIBA and 10 ml 0.1 (M) KOH were taken in a Teflon bomb and stirred for 15 mins. It was kept in an autoclave at 180°C for 7 days. After 7 days, the autoclave was taken out and cooled. The resultant white crystals were filtered

and dried. Yield: 72% with respect to Cd^{II}. Anal. calcd. for $C_{60}H_{56}Cd_3KO_{25}N_{13}$: C 41.524; H 3.522; N 10.492%. Found: C 41.26; H 3.45; N 10.27%.

5.2.5 Preparation of A⁻@1'

For preparing the different metal ion exchanged compounds, **1** is activated at 110°C under high vacuum overnight before immersing it in the respective anion solutions. 50 mg of activated **1**(**1'**) is immersed in 10ml 0.01M A^- (where A is any anion) solutions in water for 7 days and the solution is changed daily within these 7 days. For I_2 exchange, **1'** is immersed for 7 days in a 10 ml 0.01 M solution of I_2 in methanol.

5.2.6 Physical Measurements

The elemental analysis was carried out using a Thermo Fischer Flash 2000 Elemental Analyzer. Thermogravimetric analysis (TGA) was carried out (Mettler Toledo) in nitrogen atmosphere (flow rate = 50 ml min^{-1}) in the temperature range 30 – 550 °C (heating rate = 3°C min-1). Powder XRD pattern was recorded by using Cu-Kα radiation (Bruker D8 Discover; 40 kV, 30 MA). Electronic absorption spectra were recorded on a Perkin Elmer Lambda 750 UV-VIS-NIR Spectrometer and emission spectra were recorded on Perkin Elmer Ls 55 Luminescence Spectrometer. Solid state UV spectrum was recorded in reflectance mode. IR spectra of the compounds were recorded on a Bruker IFS 66v/S spectrophotometer using the KBr pellets in the region 4000−400 cm^{-1}. Inductively Coupled Plasma-Optical Emission Spectroscopy (ICP-OES) measurements were recorded on Perkin Elmer Optima 7000dv ICP-OES.

5.2.7 Crystallography

A suitable single crystal of compound 1 was mounted on a thin glass fibre with commercially available super glue. X-ray single crystal structural data were collected on a Bruker Smart-CCD diffractometer equipped with a normal focus, 2.4 kW sealed tube X-ray source with graphite monochromated Mo-Kα radiation (λ = 0.71073 Å) operating at 50 kV and 30 mA. The program SAINT[19] was used for the integration of diffraction profiles and absorption correction was made with SADABS[20] program. All the structures were solved by SIR 92[21] and refined by full matrix least square method using SHELXL.[22] All the hydrogen atoms were fixed by HFIX and placed in ideal positions.

5.2.8 Preparation of Sample for Adsorption

Adsorption isotherms of CO_2 at 195 K and N_2 at 77 K were recorded with the dehydrated sample using QUANTACHROME QUADRASORB-SI analyzer. To prepare the dehydrated sample of **1** (**1'**) approximately 100 mg of sample was taken in a sample holder and degassed at 110ºC under 10^{-1} pa vacuum for about 12 hrs prior to the measurements. Dead volume of the sample cell was measured using helium gas of 99.999% purity. The amount of gas adsorbed was calculated from the pressure difference ($P_{cal} - P_e$), where P_{cal} is the calculated pressure with no gas adsorption and P_e is the observed equilibrium pressure. All the operations were computer-controlled and automatic.

5.2.9 Characterization

Phase purity was checked using PXRD and the as-synthesized PXRD pattern matches perfectly with the simulated PXRD pattern (**Fig. 2**). Also the framework does not show appreciable change in the PXRD patter upon desolvation. The IR spectrum was also recorded (**Fig. 3**).

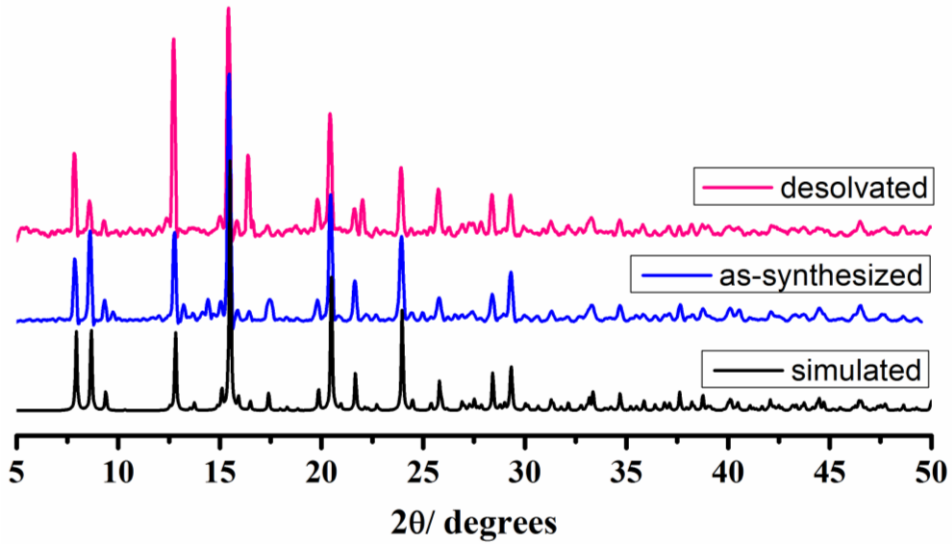

Fig. 2: The simulated and as-synthesized PXRD pattern of **1.**

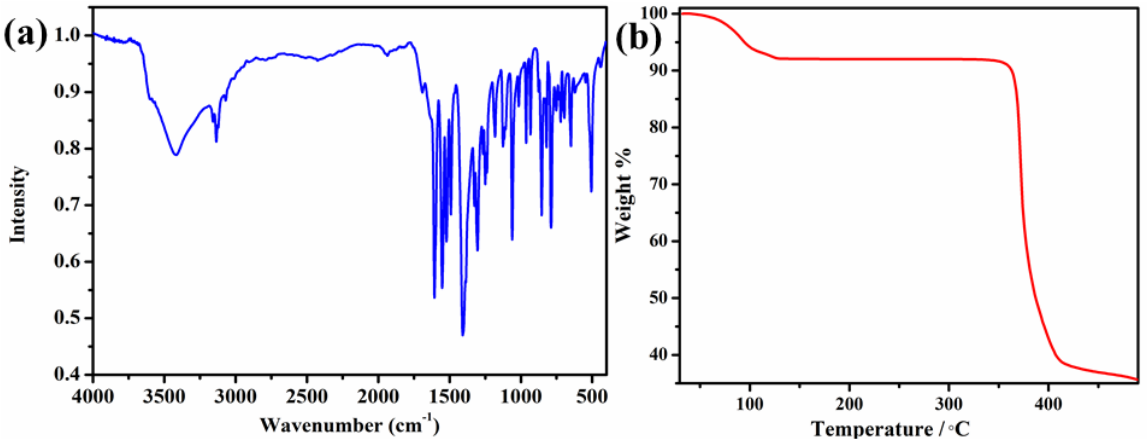

Fig. 3(a) FT-IR spectrum of **1 (b)** TGA for **1**.

Table 1: Principal peaks in the IR spectrum of **1** (**Fig. 3**).

Peak Position	Nature	Vibration
1400, 1604 cm^{-1}	Strong	Aromatic C-C (in ring) stretch
1547 cm^{-1}	Strong	N-O asymmetric stretch
1304 cm^{-1}	Strong	C-O stretch (carboxylic acid)
1065 cm^{-1}	Strong	C-N stretch
3130 cm^{-1}	Weak	Aromatic C-H stretch

According to thermogravimetric analysis (TGA), the framework of **1** experiences an initial weight loss of 6% corresponding to 6 guest water molecules till 100°C. One more guest water and the three water molecules coordinated to the three Cd^{II} centers is lost at 120°C. After that, the desolvated framework remains stable till 330°C, beyond which the framework degrades continuously (**Fig. 3(a)**).

5.3 Results and Discussion

5.3.1 Structural Description

Single crystal X-ray diffraction analysis reveals that compound 1 crystallizes in trigonal R132 space group. Each asymmetric unit comprises a hepta coordinated Cd^{II} centre having distorted pentagonal bipyramidal geometry and a hexa coordinated K^{I} centre. The hepta coordination of the Cd^{II} centre is filled by O2 and O3_a on one side and O4_a and O5 from two different ligand (HIB) molecules and these occupy the basal

position of the pentagonal bipyramid(**Fig. 5(a)**). The fifth basal position is occupied by a water molecule coordinated to the Cd1 center. The apical positions are occupied by N1 and N3 from two different ligand molecules. The O3_a and O4_a attached to Cd1 is further coordinates K1 weakly. K1 fulfils its hexa-coordination with O3_a, O3_b, O3_c, O4_a, O4_b and O4_c from different ligands (**Fig. 4(a)**). Two CD1 centres are bridged together by a HIB molecule and this forms the 1D chain roughly along the *c* direction (**Fig. 4(b)**). The dicarboxylate oxygens O3 and O4 from HIB further coordinate K1 atom in all direction, thus building up the 3D network (**Fig. 4(c)**). The pore channels of the 3D network contain three guest water molecules. Also the pore channels along the *a*-direction contain guest nitrate anions that maintain the overall framework neutrality. The solvent accessible void is 1368.0 $Å^3$ (13.6% of the total cell volume) has been calculated using PLATON after removing the guest and coordinated water molecules.

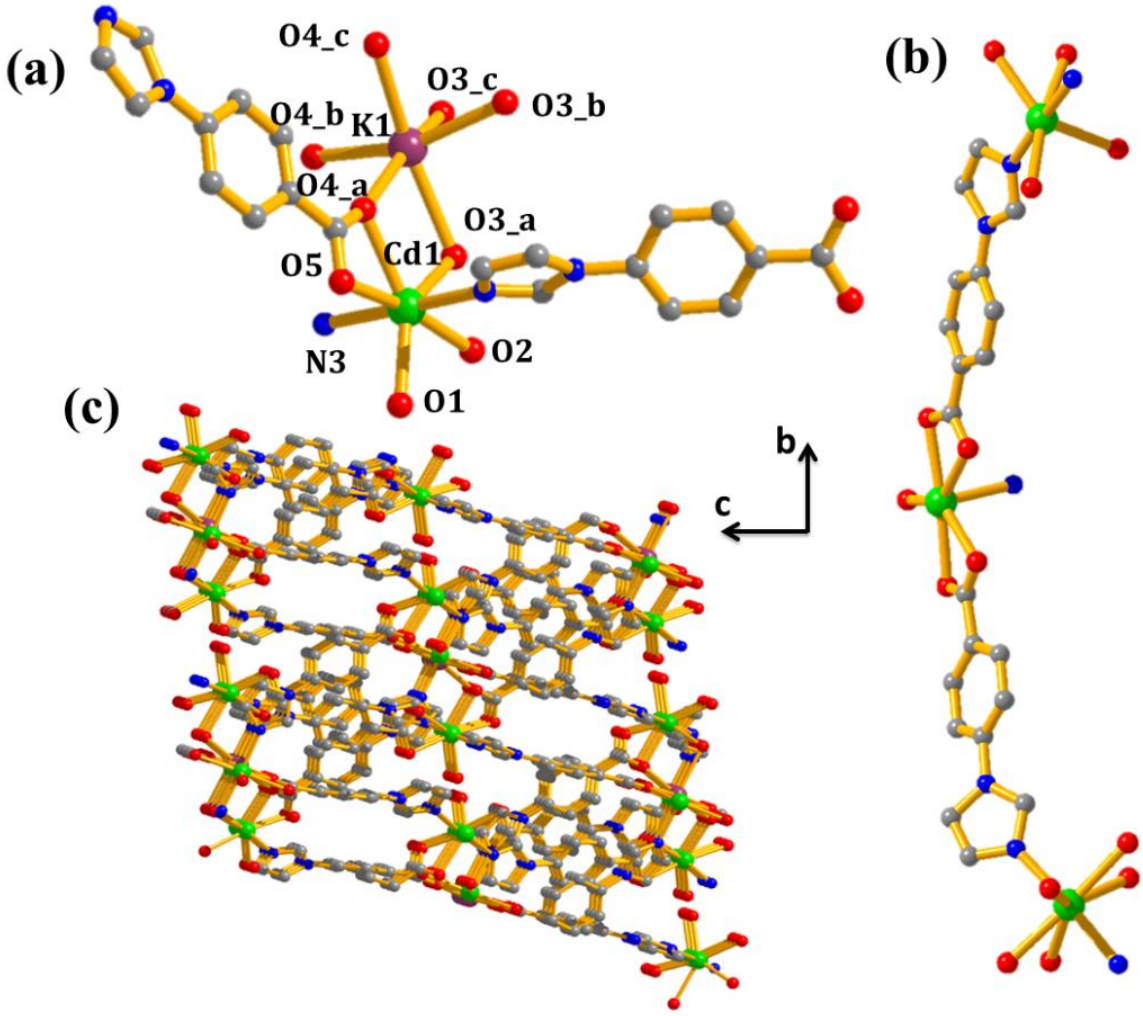

Fig. 4(a) Asymmetric unit of **1 (b)** 1D chain of **1** in the crystallographic *c* direction **(c)** 3D network of **1**.

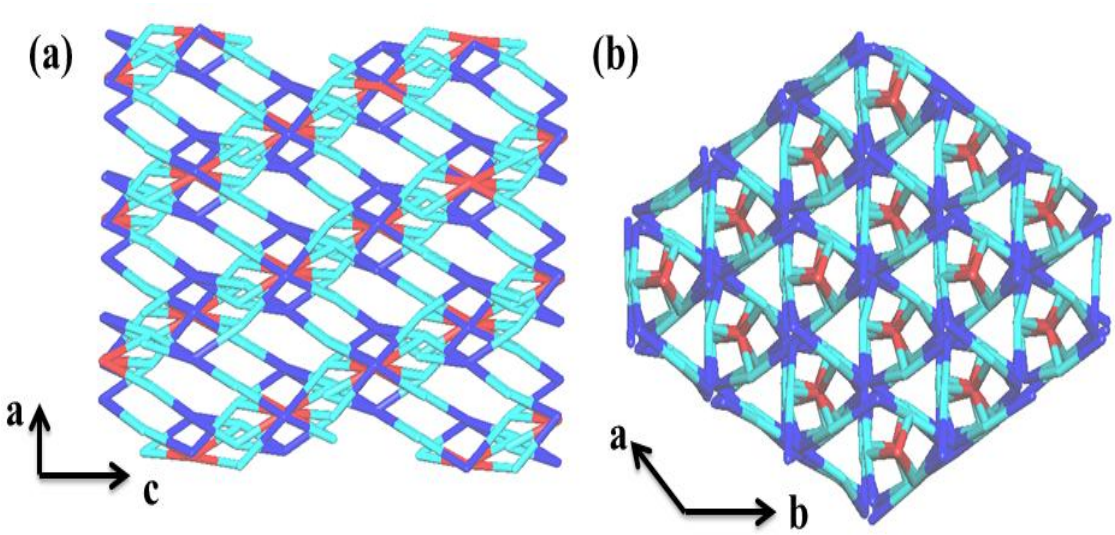

Fig. 5 Topological figures of **1 (a)** in the crystallographic *b*-direction and **(c)** the crystallographic *c*-direction**.**

Topological analysis of **1** by TOPOS 4.051 suggests the formation of a 3 nodal 3, 4, 6-connected net with Schläfli symbol $\{4;8;10\}6\{4;8^4;10\}3\{4^3;8^9;10^3\}$. **Fig. 5** shows the view of the nets along crystallographic *b* and *c*-directions.

Table 2: Crystal Data and Structure Refinement $[KCd_3(HIB)_6(H_2O)_3]\cdot(NO_3)\cdot 7H_2O$ (**1**)

Parameter	1
Empirical formula	$C_{60}H_{56}Cd_3KO_{25}N_{13}$
Formula weight	1721·41
Crystal system	Trigonal
Space group	*R*32 (No.155)
a, Å	13.7989(3)
b, Å	13.7989(3)
c, Å	61.118(5)
α, β, deg	90
γ, deg	120
V, Å^3	10078.3(8)
Z	6
T, K	293
μ,mm^{-1}	1.094
D_{calcd},g/cm^3	1.702
F (000)	5136
reflections [$I>2\sigma(I)$]	3464
unique reflections	5105
measured reflections	39455
R_{int}	0.107
GOF on F^2	1.03
$R_1[I>2\sigma(I)]$[a]	0.0490
$R_w[I>2\sigma(I)]$[b]	0.1087

($R = \sum||F_o|-|F_c||/\sum|F_o|$,$R_w= [\sum\{w(F_o^2-F_c^2)^2\}/\sum\{w(F_o^2)^2\}]^{1/2}$)

Table 3: Selected bond distances (Å) for **1.**

Cd1-O1	2.368(5)	Cd1 -N1	2.306(6)
Cd1 -N3	2.306(7)	Cd1-O4	2.484(4)
Cd1-O2	2.443(5)	Cd1 -O5	2.389(4)
Cd1-O3	2.438(6)	K1-O4_a	2.664(6)
K1-O4_b	2.664(6)	K1-O4_c	2.664(6)
K1-O3_a	2.743(5)	K1 -O3_b	2.743(6)

Table 4: Selected bond angles (°) of Compound **1.**

O1-Cd1-N1	91.0(2)	O3_c-K1 -O4_b	100.7(2)
O1 -Cd1-N3	88.1(2)	O3_a-K1-O4_b	73.58(15)
N1 -Cd1 -N3	176.43(19)	O1-Cd1-O4	141.30(17)
O1-Cd1-O3	135.96(18)	O1-Cd1-O5	87.75(19)
O1-Cd1-O2	82.53(19)	O3_b -K1-O4_c	73.58(14)

5.3.2 Framework Stability and Adsorption properties

Although no definite pore can be observed in **1** in any particular direction, the presence of a pocket lined by aromatic benzene and imidazole along the crystallographic *a*-direction prompted us to check the adsorption properties of **1'**. Although **1'** does not show any N_2 uptake, it shows a total uptake of 90 $mL.g^{-1}$ of CO_2 (**Fig. 6(a)**). This is surprising since the void space in the framework is 13.6% very less. The CO_2 adsorption profile at 195K shows an initial step at P/P_0 = 0.1. The adsorption profile has a second step at P/P_0 = 0.65 beyond which the CO_2 adsorption shows a steep increase. The desorption curve forms a wide hysteresis with the adsorption curve, indicating that once adsorbed, CO_2 is strongly bound with the framework. From the steps at higher temperature, it can be speculated that structural changes occur in the framework at higher pressures. Also, the strong interaction with the framework gives rise to the assumption that CO_2 molecules might be interacting with the unsaturated metal sites. However, further studies are to be carried out before drawing any conclusion. At room temperature, the net CO_2 uptake by **1'** is 22 $mL.g^{-1}$.

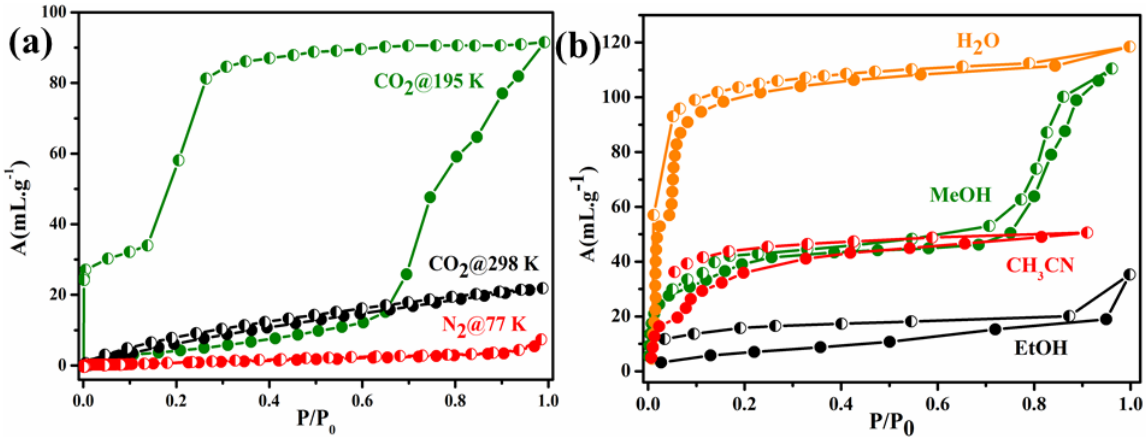

Fig. 6(a) CO_2 and N_2 adsorption isotherms of **1' (b)** Solvent vapour adsorption isotherms of **1'**

The pocket present in 1 is hydrophilic in nature as evident from the H_2O adsorption isotherm. The adsorption profile shows a steep uptake at low pressures, which implies its hydrophilic nature. At P/P_0 = 0.84, a step is observed, which increases the water adsorption. The net water uptake is 118 $mL.g^{-1}$. The hydrophilic nature of **1** is also evident from the methanol, ethanol and acetonitrile uptake. The adsorption profiles of both methanol and ethanol show steps at high pressures, similar to the water adsorption isotherm. The net uptake is 110 $mL.g^{-1}$ for methanol, 50 $mL.g^{-1}$ for acetonitrile and 35 $mL.g^{-1}$ for ethanol (**Fig. 6(b)**). The uptake amount is in accordance with the kinetic diameter of the respective solvents, the higher the kinetic diameter, lower the uptake amount.

5.3.3 Encapsulation of Anions

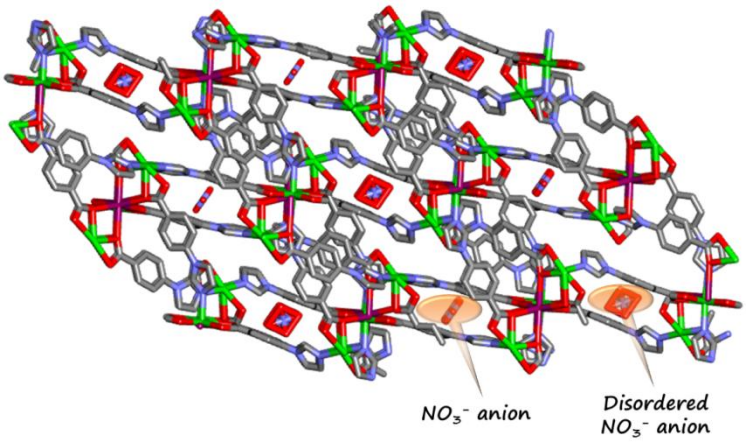

Fig. 7 Nitrate anions residing in the pores of **1**.

The nitrate anions present within the framework as guests can be exchanged with other anions to suit specific applications (**Fig. 7**). For this purpose, the nitrate anion was exchanged with azide (N_3^-), dicyanamide ($N(CN)_2^-$) and thiocyanate (SCN^-) anions, by immersing **1'** in the sodium salt solution of the respective anions. The integrity of the framework is maintained even on exchange with these anions, as evident from the PXRD patterns (**Fig. 8(a)**). The encapsulation of the respective anions is ensured by the presence of the characteristic anion peaks in the IR spectrum of the exchanged samples (**Fig. 8(b)**).

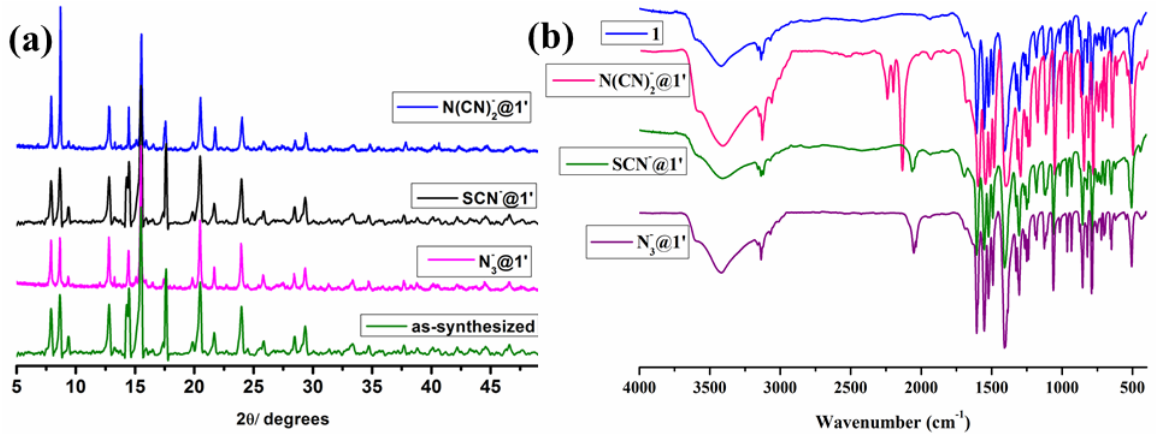

Fig. 4 PXRD patterns of the anion exchanged samples **(b)** FT-IR spectra of anion encapsulated samples.

Table 5: Principal peaks of the anion exchanged samples (**Fig. 8(b)**)

Sample Name	Peak Position	Vibration
$N(CN)_2^-$@1'	2252 cm^{-1}	C-N stretch
	2145 cm^{-1}	N=C=N stretch
SCN^-@1'	2061 cm^{-1}	SCN^- stretch
N_3^-@1'	2052 cm^{-1}	N=N=N stretch

5.3.4 I_2 Capture

From the properties of the framework, we speculated that iodine can be captured by it. The I_2 loaded framework is expected to show enhanced conductivity. For this purpose, **1'** was immersed in a methanol solution of I_2 and it was seen that the white sample turns brown gradually.

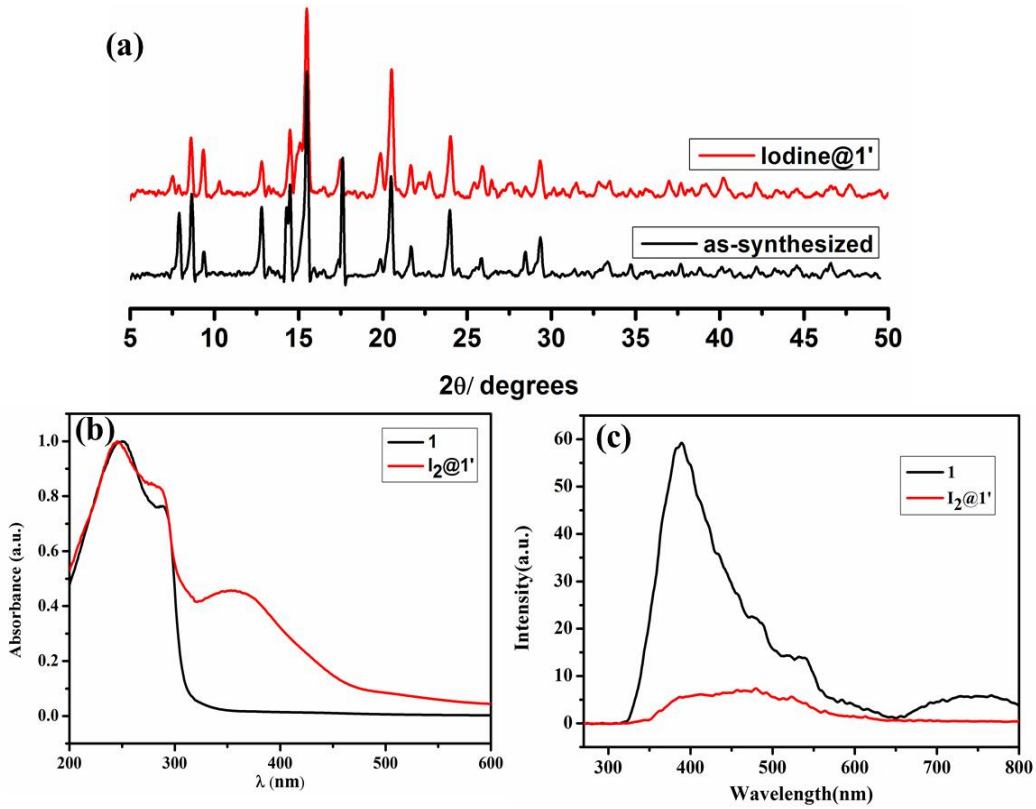

Fig. 5(a) PXRD of iodine encapsulated sample **(b)** UV spectra of **1** and **I_2@1' (c)** Emission spectra of **1** and **I_2@1'**.

The framework maintained its structural integrity with very slight changes in the PXRD patterns (**Fig. 9(a)**). The sample thus prepared was analysed using UV-vis spectroscopy and the UV spectrum of **I_2@1'** showed the appearance of a new band at 350nm, which implies the incorporation of I_2 in the framework. The band at 350nm specifically confirms the presence of triodide (I_3^-) in the framework (**Fig. 9(b)**). The emission spectroscopy showed that the characteristic blue emission of **1** is quenched by the encapsulation of I_2 and **I_2@1'** does not show any emission (**Fig. 9(c)**).

In order to ascertain whether the I_2 encapsulation is reversible or not, I_2 release by the framework was also studied. For this purpose, a few crystals of **I_2@1'** were taken in a cuvette filled with methanol. It was homogenized from time to time and the UV spectra were recorded after definite time intervals (**Fig. 10(a)**). It was seen that although I_2 is released steadily by the framework, there is no peak at 350 nm, which implies that I_3^- is tightly bound to the framework and is not released easily. From here, it can be speculated that the tri-iodide species has replaced the NO_3^- anion in the framework and hence has become an integral part of the framework. The I_2 release by the framework is essentially a zero order reaction, as observed by studying the reaction kinetics (**Fig. 10(b)**). The release

of I_2 in methanol increases gradually with time which implies that the release process is governed mainly by the host-guest interaction[18b]. **I_2@1'** is expected to show greater conductivity than **1** owing to the incorporation of I_3^- in the framework and this study is to be done in future.

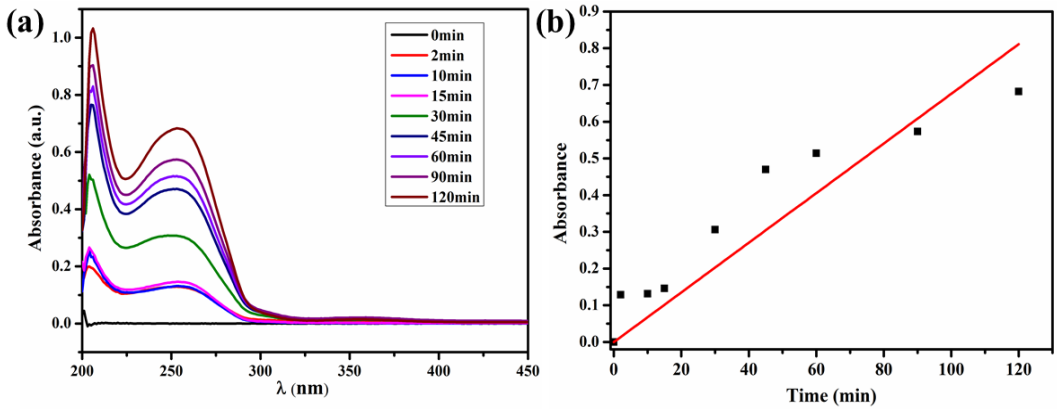

Fig. 6(a) I_2 release by **I_2@1'**. **(b)** Adsorbance maxima vs time plot for I_2 release.

5.4 Conclusion

In conclusion, **1** is a unique bimetallic cationic framework with nitrate anions residing in its pores. Although **1** does not have any appreciable pore channel, it shows a good selective CO_2 uptake over N_2. This holds the possibility for future studies, where it is to be investigated whether **1** undergoes pressure or guest induced structural changes during adsorption. Also it can be speculated that the relatively higher adsorption capacity is due to the interaction of adsorbate molecules with the nitrate anion. This nitrate anion can be successfully exchanged with a handful of anions like azide, thiocyanate and dicyanamide anions. The framework integrity is maintained even after these exchanges. Also, **1** is capable of capturing I_2 reversibly and the release of iodine is dependant mainly on the host-guest interaction of the framework. However, it is seen that during I_2 capture, tri-iodide is exchanged with the nitrate anions.

5.5 References

1. (a) S. Kitagawa, R. Kitaura and S.-i. Noro, *Angew. Chem. Int. Ed.*, 2004, **43**, 2334-2375; (b) O. M. Yaghi, M. O'Keeffe, N. W. Ockwig, H. K. Chae, M. Eddaoudi and J. Kim, *Nature*, 2003, **423**, 705-714.
2. (a) M. P. Suh, H. J. Park, T. K. Prasad and D.-W. Lim, *Chem. Rev.*, 2012, **112**, 782-835; (b) K. Sumida, D. L. Rogow, J. A. Mason, T. M. McDonald, E. D. Bloch, Z. R. Herm, T.-H. Bae and J. R. Long, *Chem. Rev.*, 2012, **112**, 724-781.
3. J. Liu, L. Chen, H. Cui, J. Zhang, L. Zhang and C.-Y. Su, *Chem. Soc. Rev.*, 2014, **43**, 6011-6061.
4. (a) J. An, C. M. Shade, D. A. Chengelis-Czegan, S. Petoud and N. L. Rosi, *J. Am. Chem. Soc.*, 2011, **133**, 1220-1223; (b) Y. Cui, Y. Yue, G. Qian and B. Chen, *Chem. Rev.*, 2012, **112**, 1126-1162; (c) S. Roy, A. Chakraborty and T. K. Maji, *Coord. Chem. Rev.*, 2014, **273–274**, 139-164.
5. (a) L. E. Kreno, K. Leong, O. K. Farha, M. Allendorf, R. P. Van Duyne and J. T. Hupp, *Chem. Rev.*, 2012, **112**, 1105-1125; (b) R. Haldar, R. Matsuda, S. Kitagawa, S. J. George and T. K. Maji, *Angew. Chem.*, 2014, **126**, 11966-11971.
6. V. Stavila, A. A. Talin and M. D. Allendorf, *Chem. Soc. Rev.*, 2014, **43**, 5994-6010.
7. (a) H. Su, F. Sun, J. Jia, H. He, A. Wang and G. Zhu, *Chem. Commun.*, 2015, **51**, 5774-5777; (b) J. An, S. J. Geib and N. L. Rosi, *J. Am. Chem. Soc.*, 2009, **131**, 8376-8377.
8. (a) G. Calzaferri, C. Leiggener, S. Glaus, D. Schurch and K. i. Kuge, *Chem. Soc. Rev.*, 2003, **32**, 29-37; (b) K. Moller and T. Bein, *Chem. Soc. Rev.*, 2013, **42**, 3689-3707; (c) S. R. J. Oliver, *Chem. Soc. Rev.*, 2009, **38**, 1868-1881.
9. X. Zhao, X. Bu, T. Wu, S.-T. Zheng, L. Wang and P. Feng, *Nat. Commun.*, 2013, **4**.
10. H. Fei, D. L. Rogow and S. R. J. Oliver, *J. Am. Chem. Soc.*, 2010, **132**, 7202-7209.
11. (a) A. Schoedel, L. Wojtas, S. P. Kelley, R. D. Rogers, M. Eddaoudi and M. J. Zaworotko, *Angew. Chem. Int. Ed.*, 2011, **50**, 11421-11424; (b) G. Nickerl, A. Notzon, M. Heitbaum, I. Senkovska, F. Glorius and S. Kaskel, *Crystal Growth & Design*, 2013, **13**, 198-203.
12. A. Nalaparaju and J. Jiang, *J. Phys. Chem. C*, 2012, **116**, 6925-6931.

13. Q. Hu, J. Yu, M. Liu, A. Liu, Z. Dou and Y. Yang, *J. Med. Chem.*, 2014, **57**, 5679-5685.

14. B. Manna, A. K. Chaudhari, B. Joarder, A. Karmakar and S. K. Ghosh, *Angew. Chem.*, 2013, **125**, 1032-1036.

15. A. K. Chaudhari, S. Mukherjee, S. S. Nagarkar, B. Joarder and S. K. Ghosh, *CrystEngComm*, 2013, **15**, 9465-9471.

16. L. Fu, Y. Liu, M. Pan, X.-J. Kuang, C. Yan, K. Li, S.-C. Wei and C.-Y. Su, *J. Mater. Chem. A*, 2013, **1**, 8575-8580.

17. C. Falaise, C. Volkringer, J. Facqueur, T. Bousquet, L. Gasnot and T. Loiseau, *Chem. Commun.*, 2013, **49**, 10320-10322.

18. (a) J. T. Hughes, D. F. Sava, T. M. Nenoff and A. Navrotsky, *J. Am. Chem. Soc.*, 2013, **135**, 16256-16259; (b) M.-H. Zeng, Q.-X. Wang, Y.-X. Tan, S. Hu, H.-X. Zhao, L.-S. Long and M. Kurmoo, *J. Am. Chem. Soc.*, 2010, **132**, 2561-2563.

19. S. V. a. SMART (V 5.628), XPREP, SHELXTL; Bruker AXS Inc. Madison, Wisconsin, USA, 2004.

20. G. M. Sheldrick, *SADABS, Empirical Absorption Correction Program, University of Göttingen, Göttingen*, 1997.

21. A. Altomare, G. Cascarano, C. Giacovazzo and A. Guagliardi, *J. Appl. Crystallogr.*, 1993, **26**, 343-350.

22. G. M. Sheldrick, *SHELXL 97, Program for the Solution of Crystal Structure, University of Göttingen, Germany*, 1997.

List of Publications

1. A bimodal anionic MOF: turn-off sensing for Cu^{II} and specific sensitization of Eu^{III}, Sohini Bhattacharyya, Anindita Chakraborty, Kolleboyina Jayaramulu, Arpan Hazra and Tapas Kumar Maji, *Chem. Commun.*, 2014, **50**, 13567.

2. Tetracarboxylate Ligand Based Flexible Frameworks with Selective CO_2 and Solvent Adsorption Properties, Sohini Bhattacharyya, Anindita Chakraborty, and Tapas Kumar Maji, submitted.